Spring 2019

Biochar and other properties resulting from the gasification and combustion of biomass with different components

Tejasvi Sharma
University of Iowa

BIOCHAR AND OTHER PROPERTIES RESULTING FROM THE GASIFICATION AND COMBUSTION OF BIOMASS WITH DIFFERENT COMPONENTS

by

Tejasvi Sharma

A thesis submitted in partial fulfillment
of the requirements for the Doctor of Philosophy
degree in Mechanical Engineering in the
Graduate College of
The University of Iowa

May 2019

Thesis Supervisor: Associate Professor Albert Ratner

Graduate College
The University of Iowa
Iowa City, Iowa

CERTIFICATE OF APPROVAL

_____

PH.D. THESIS

_____

This is to certify that the Ph.D. thesis of

Tejasvi Sharma

has been approved by the Examining Committee for
the thesis requirement for the Doctor of Philosophy degree
in Mechanical Engineering at the May 2019 Graduation.

Thesis Committee: _____
Albert Ratner, Thesis Supervisor

_____
H.S Udaykumar

_____
James Buchholz

_____
Gregory H. LeFevre

_____
Casey Harwood

ACKNOWLEDGEMENTS

I am very thankful for Professor Ratner, who has supported, guided, and mentored me ever since I was an undergraduate lab assistant. I am very grateful to be part of your team.

I am thankful for the support that my parents and my brother have given me. Thank you for believing in me.

Lastly, I would like to thank my lab teammates: Guiyan Zang, Jianan Zhang, Gurjap Singh, and the rest of the combustion lab mates for their support and collaboration.

ABSTRACT

Gasification is a process that converts organic carbonaceous materials at high temperatures into a fuel gas primarily containing carbon monoxide (CO), hydrogen (H_2), methane (CH_4), and carbon dioxide (CO_2). Gasification has three main byproducts: syngas, heat, and char. This thesis explores the characteristics of biochar created from the downdraft gasification of corn, soybeans, wood pellets, and refuse derived fuel (RDF). The goal of this thesis is to better understand how gasification influences the biochar and syngas byproducts so as to help model simulations and to understand how better-quality syngas and biochar can be produced through this process. Ultimate and proximate analysis, BET surface area analyses, and SEM X-ray analysis were obtained on the biochar. It was found that wood biochar was the most porous char with a high carbon content, while RDF char had the lowest porosity with the lowest carbon content. Three of the four biochars, excluding RDF, had a significant phosphorus content, while the RDF biochar had a high concentration of aluminum. X-ray analysis of the biochar shows mineral localization on the char surface and how that relates to local porosity. The syngas content from different biomasses was also tested. It was found that, in agreement with previous studies, biomass with high amounts of cellulose led to high amounts of CO, while fuel with high lignin content led to high amounts of hydrogen. To better understand equilibrium chemistry gasification, examination of syngas, char, and tar content from the gasification of miscanthus briquettes in a double stage downdraft gasifier was carried out. The results show that the optimum equivalence ratio at which miscanthus briquettes can be gasified is 0.35, with peak CO and H_2 content at 20.29% CO and 18.68% H_2, respectively; with a resulting syngas heating value of 5.5 MJ/Nm^3. The process yields significantly higher energy content syngas and higher porosity biochar, indicating that the more uniform process created in the equilibrium environment yields significant product improvements.

PUBLIC ABSTRACT

Gasification is a process in which fuel such as wood is burned at high temperatures with a small amount of air. It results in three main byproducts: syngas, heat, and char. The syngas, which is primarily composed of hydrogen and carbon monoxide, can be inserted into a boiler to produce energy, while the char can be used to enhance soil fertility. The goal of this thesis is to understand how better syngas and biochar quality can be produced and how the gasification process influences its production. This thesis explores the characteristics of biochar from a downdraft gasifier at the University of Iowa from corn, soybeans, wood pellets, and refuse derived fuel (RDF). Several tests were carried out on the different resulting biochars. The analysis included analyzing their carbon, hydrogen and moisture contents and studying their surface areas. Through SEM X-ray analysis, minerals such as potassium, chlorine, and iron were located and examined. It was found that wood biochar was the most porous char with a high amount of carbon content, while RDF char had the lowest porosity with the lowest carbon content. Some studies have shown that more porous char may hold more nutrients in the soil. Three of the four biochar's, excluding RDF, also showed significant phosphorus and potassium content which is known be found in fertilizers. The RDF biochar showed a high concentration of aluminum. This thesis also explores in detail where these minerals are located on the char surface and their relationship with porosity. The syngas content from different biomass components was also tested. Biomass, such as wood or paper, is known to be made up of three major components: hemicellulose, cellulose, and lignin. It was found that, in agreement with previous studies, biomass with a high amount of cellulose led to high amounts of CO production, while fuel with high lignin content led to high amounts of hydrogen production. Finally, this thesis also explores the syngas, char, and tar content from burning miscanthus briquettes in a downdraft gasifier with two air inlets. The optimum condition at which miscanthus

briquettes can be burned was found to be 20.29% CO and 18.68% H_2, which yielded the maximum syngas heating value content of 5.5 MJ/Nm^3.

TABLE OF CONTENTS

LIST OF TABLES

LIST OF FIGURES

1. INTRODUCTION

1.1 Motivation

Today, 85% of the world's energy demand is supplied using conventional fossil fuel, which releases 56.6% of anthropogenic greenhouse gas emissions [1]. The development of renewable energy has been the focus of attention for several decades, because of its promise of energy independence and sustainability. Biomass gasification in addition to other renewable energy technologies, is one of the possible routes through which carbon-neutral energy can be produced. Gasification is a process that converts organic carbonaceous materials at high temperatures into a fuel gas, heat and biochar. The produced gas contains primarily carbon monoxide (CO), hydrogen (H_2), methane (CH_4), and carbon dioxide (CO_2) [2][3]. The mixture of CO and H_2 is primarily known as syngas (synthesis gas). There has been an extensive amount of research which has looked into the production of these gases. However, there are not many studies that look into the produced biochar from gasification. Today, most of the biochar studied is as a result of pyrolysis, where there is a total absence of air. Gasification falls between two spectrums. On the one end, there is slow pyrolysis, where in the presence of no air, and char production is the main product, but with minimal gas production. On the other end is incineration, where fuel is combusted with 100% required oxygen to release maximum heat but producing little or no char. This thesis looks into the intermediate state, where the goal is the production of high quality syngas with significant biochar.

The application of gasification can be found in multiple projects around the world, ranging from large industrial-scale projects (energy output in MW) to small-scale projects (in kW). Some examples of large-scale projects include the Harboøre and Güssing power plants in Denmark and Austria respectively [4]. Examples of small-scale downdraft gasifier commercial manufacturers

include ALL Power Labs, Entrade (both located in California), and Ankur gasifiers (based in India). According to the International Energy Agency (IEA), there are a total of 141 gasification plants (114 operational, 14 on hold and 13 under construction). Out of the 141 plants which produce syngas as their end product, 106 of the 141 are used for power production (about 356 MW electric power and 185 MW thermal power), 24 are for liquid fuel production, seven are used for gaseous fuel, and eight for chemical production as end product [5][3].

Biomass utilization has an advantage as it is less dependent on the location and climate. Biomass in most regions is storable and transportable. This especially true for rural areas which depend on biomass for essential activities such as cooking and heating. Waste biomass in most areas are readily available and can be found useful at a relatively low price. This makes biomass an attractive source of fuel. There are several techniques currently used to convert biomass to energy. These include landfill, incineration and anaerobic digestion to name a few. Biomass gasification, however, has a higher potential when compared to these techniques. Biomass gasification can accept a broader range of input fuels and can produce multiple products. The gas emission from biomass gasification is also cleaner than the gas from incineration as it requires significant investment in gas cleaning and combustion process control as incineration flue gases may contain particulate matter, heavy metals, dioxins, furans, Sulphur dioxide, and hydraulic acid.

Biochar, one of the products of gasification, has numerous benefits: it increases net carbon sequestration, decreases N_2O emissions from the soil, and increases soil fertilizer intake [6]. The surface area of the biochar is a critical component, as it traps spores and bacteria [7], which can allow increases in nutrient absorption by plants. One study found the surface areas of biochar vary from 7–50 m^2/g in a fluidized bed gasifier [8], while another discovered surface areas of up to 64 m^2/g in a downdraft gasifier [9]. Studies conducted by Qian et al. [10] show that the surface area

increases with an increase in Equivalence ratio. However, there are not many papers that study the metal and mineral content of biochar from gasification, which is one of the core focus of this thesis.

The Produced gases, with high concentrations of CO and H_2 from the gasifier, can be fed into internal combustion engines for power production [11–12]. The syngas from the gasifier can also be used for other purposes, such as producing chemical products, especially when it contains a high percentage of CO_2 and CH_4 [13]. Several prior studies have been done which look into effects biomass content on syngas. In addition to exploring the some of the syngas content of different biomasses, the main area of interest and discovery deals with the biochar results from the downdraft gasifier, which form this gasifier have never been explored before.

There are several objectives of this thesis. The goal of this thesis is to understand how syngas composition and biochar quality are affected by the changes in the gasification process. There are several specific questions that will be addressed. These are: (1) does the presence of a wider thermo-equilibrium zone in a gasifier affect the syngas composition particularly from biomasses with different components (lignin, hemicellulose, and cellulose). (2) For a wide range of materials, what is the pattern of mineral residue in the biochar and does that follow a trend and can that be quantified. (3) Is there an equivalence ratio at which syngas composition is optimized and how does that affect the biochar.

Chapter 1 briefly discuss the history of Biomass gasification thus far and how it has been used previously. Chapter 2 gives an overview of previous studies done on biomass gasification, syngas content and biochar research from gasification. Chapter 3 discusses the setup of the downdraft gasifiers Iowa (one stage downdraft gasifier) and that in the University of Brazil in Itajuba (second stage downdraft gasifier), and the equipment in both facilities. Chapter 4 and 5 discuss the syngas and biochar results from Iowa's gasifier respectively. The biochar results address their surface

areas, their mineral content and x-ray analysis, also show how minerals are located on biochar. Chapter 6 discusses the syngas, biochar and tar content from the double stage downdraft gasifier situated in the University of Brazil.

1.2 Biomass and History

Gasification is a technology that has existed since the early 1600s. Syngas has evolved from being previously known as a "town gas" for industrial lighting to an advanced, multi-product, carbon-based technology. Currently this syngas can be burnt in a boiler to produce steam and electricity. The syngas can also be converted to other carbon-based fuels such as diesel and jet fuel to name a few [2].

Gasification first became commercially available in 1800 for heating and lighting. As electricity and natural gas evolved, this "town gas" use declined, and gasification development was put on hold. Throughout history, gasification has been revisited whenever there has been limited access to natural gas, oil, or petroleum products. This scarcity was usually due to high prices or too little or no access to those resources.

Today, gasification technology is used for producing electricity, synthetic natural gas, liquid fuels, or chemical products from coal, biomass, or other carbon-containing materials [2]

Below is a brief summary of gasification history, including its discovery and earliest experimentation [2][4]:

- 1609: Jan Baptista Van Helmont (a Belgian chemist and physician) discovered that gas could be produced from heating wood or coal. Following this discovery, several others aid in developing and refining the gasification process.

- 1669: Thomas Shirley performs various experiments with carbonated hydrogen (now called methane).

- Late 1600s: John Clayton experiments with capturing gas produced from coal.

- 1788: Robert Gardner becomes the first to obtain a patent dealing with gasification.

• 1791: John Barber receives the first patent in which "producer gas" was used to drive an internal combustion engine.

• 1798: Biomass gasification is first conceived when Philippe Lebon led efforts to gasify wood.

Interestingly, “town gas” from gasification of coal was demonstrated to the British royalty in 1733, but at that time scientists saw no use for it. It wasn’t until William Murdoch used coal gas (“town gas”) to light the main building of the Soho Foundry and publicly displayed it in 1802 and astonished the local public that gasification took traction. In 1804, Friedrich Winzer of Germany was among the first to patent coal-gas lighting.

By 1823, several towns and cities throughout Britain were gas lit, and by 1959 gas lighting had spread throughout Britain. Gas lighting came to the United States in 1816, with Baltimore being the first city to implement it. This rapidly spread across the eastern United States, with Boston implementing it in 1821, New York in 1823, and Philadelphia in 1841.

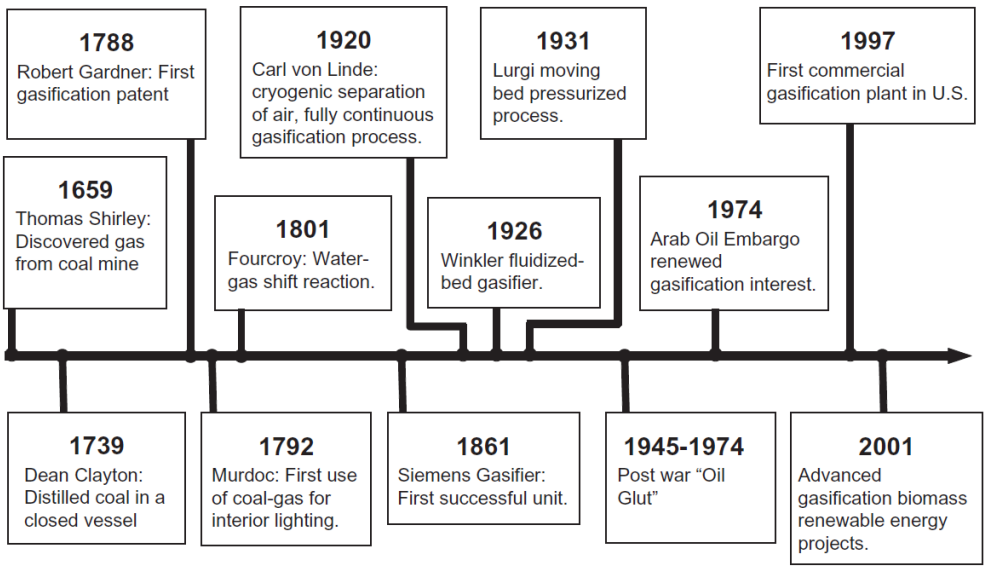

Figure 1.1: Historic trends in gasification [3]

1850-1940:

During this period, gas was primarily made from coal. It was mainly used for lighting and heating homes and helped the industrial revolution by extending the working hours in factories, especially during the winter. Gasification continued to play a significant role until the 1900s when Thomas Edison forced it out of the interior gas market. The gas from then on was mostly used for heating and cooking.

In 1926, major commercial gasification technologies rose. The main ones were the Winkler's fluidized bed in 1926, Lurgi's pressurized moving bed gasifier in 1931, and Koppers-Totzek's entrained gasifier. Once natural gas was discovered, the need for gasification of coal or biomass declined.

1940 – 1975

During this period, gasification was used in two main fields as synthetic fuels: the internal combustion engine and the chemical synthesis into oil and other process chemicals. During World War II, when Germany lost most of its oil refineries and its crude oil supply significantly reduced, it turned to gasification and started producing synthesized oil from coal-gasification using the Fischer-Tropsh process and the Bergius process. By the time the war ended, Germany had 12 coal hydrogenation plants and nine Fischer-Tropsch Plants.

Meanwhile, in the rest of Europe in that period, biomass and coal gasification was used in cars and trucks. It is estimated that more than a million small gasifiers were built mainly for transportation. Once the war ended, the Middle East became one of the largest oil suppliers, which reduced the need for gasification for transportation and chemical production. Even though there was plenty of natural gas in the 1950s (which reduced biomass and coal gasification), syngas production from natural gas and naphtha by steam continued to increase.

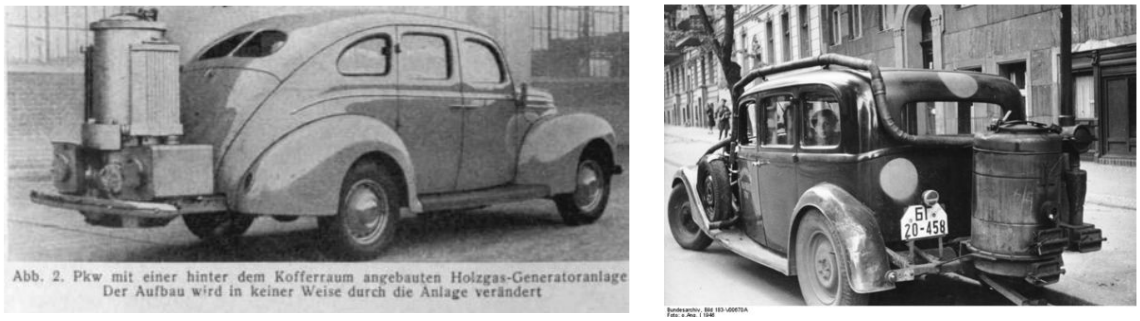

Figure 1.2: Gasifier cars used during World War II [15]

1975 – 2000

On October 15, 1973, members of the organization of petroleum exporting countries shocked the western world by banning oil exports to the United States and other western countries, which relied heavily on oil from the Middle East. As such, the impacted countries had to move towards alternatives such as gasification to reduce their dependence on imported oil.

Eventually, with reduced prices in oil, interest in gasification fell, but several governments realized the need for a cleaner environment and gave support to the development of integrated gasification combined cycle (IGCC) power plants.

Post 2000

Several factors, such as global warming, instability in some oil-producing countries, and the quest to become energy dependent, have led to a renewed momentum in gasification. Biomass gasification is seen as one of the most attractive choices for the conversion of carbon-neutral biomass into gas (and also as a replacement).

Gasification Market

Gasification produces three main byproducts: syngas, heat, and biochar. The syngas from gasification can be used for electricity production, chemicals, transportation fuels such as diesel and gasoline, and other gaseous fuels such as synthetic natural gas.

As of 2014, about 60% of all gasification-produced syngas was used to form chemicals, 24% to produce liquid transportation fuels and 8% to produce power, and gaseous fuels. China, which is the leader in producing chemicals and fertilizers, is expected to double its production.

The U.S market primarily uses syngas to produce liquid fuels from coal and biomass. However, as of now, the U.S is forecasting only a small increase in liquid fuels from syngas in 2035: 19.9 million barrels per day, up from 19.2 million barrels per day produced in 2010. There is also a government regulation (known as EISA 2007) [16] that mandates that by 2022, 36 billion gallons of biofuels be produced from biomass to liquid diesel transportation fuel. About 2-3 % of the 36 billion is expected to be biomass to liquid fuel. The U.S. Energy Information Administration predicts that biomass to liquid fuel technology will replace about 2.5 million gallons of petroleum by 2022.

2. LITERATURE REVIEW

2.1 Gasification Process

The gasification process is the conversion of solid or liquid feedstock into a useful and convenient gaseous fuel that can be burned to release energy, or used for the production of value-added chemicals [3]. Gasification and combustion are very similar to one another, but they have an essential difference. Gasification packs energy into chemical bonds in the product gas, while combustion breaks those bonds to produce energy. The biomass gasification process includes the following processes [3, 18] [17]:

Drying

All biomasses have a certain amount of moisture present in them. For example, freshly cut wood has a moisture content varying from 30 to 60%. It is calculated that every kilogram of moisture in biomass wastes a minimum of 2242 KJ of energy from the gasifier [3]. That energy cannot be recovered. For this reason, most biomasses need to be pre-dried before being inserted into a gasifier. An acceptable amount of moisture in biomasses for insertion into a gasifier ranges from 10 to 20% [3]. In the drying zone in the gasifier, at above 100 °C, loosely bound water present in the biomass is irreversibly removed. This leads to the low-molecular-weight extractives starting to volatize until the temperature of the system reaches 200 °C [3].

Pyrolysis/thermal decomposition

Pyrolysis occurs at temperatures of about 350 °C [14]. It involves the thermal breakdown of larger hydrocarbon molecules of biomass into smaller gas molecules with no significant chemical reactions occurring with air or any other gasification medium (for example, nitrogen) [7]. The output of this process is biochar (which is mostly made up of carbon), gas (CO, CO_2, H_2, H_20, CH_4), and tar vapor [19]. The tar is formed through the condensation of condensable vapor produced in the process. There are two types of pyrolysis: slow and fast pyrolysis. Slow pyrolysis is the slow heating of biomass with no oxygen present usually at low temperatures (around 300 degrees Celsius), while fast pyrolysis involves burning the biomass with no oxygen at high temperatures (around 500 degrees Celsius) and this lasts for a short period time.

Combustion

The outputs from the pyrolysis pass through the combustion zone. The temperature in this zone ranges from 800 to 900 °C [20].

Basic reactions:

$$C + O_2 \rightarrow CO_2$$

$$4H + O_2 \rightarrow 2H_2O$$

Gasification of decomposed products. (Char gasification)

This stage is also called the reduction zone [22]. The char produced from pyrolysis is not usually pure carbon, and usually contains some amount of hydrocarbons, consisting of hydrogen and oxygen [19]. Char gasification is an important process, and this zone involves several reactions between char and the gasification medium.

$$Char + O_2 \rightarrow CO_2 + CO$$

$$Char + CO_2 \rightarrow CO$$

$$Char + H_2O \rightarrow CH_4 + CO$$

$$Char + H_2 \rightarrow CH_4$$

The reduction zone can also be interpreted as the zone where the "producer gas" is produced [20]. This is done by using the following two endothermic equations:

Boudouard reaction:

$$C + CO_2 \rightarrow 2CO$$

Water gas reaction:

$$C + H_2O \rightarrow H_2 + CO$$

Gasification reactions are generally endothermic in nature, but some of them can be exothermic as well [19].

There are no sharp boundaries between the drying, pyrolysis, combustion and reductions zones, and they overlap often. The input fuel has to pass through all the above-mentioned zones so as to be completely converted [20].

2.2 Types of Gasifiers

There are mainly three categories of gasifiers: fixed bed, fluidized bed, and entrained flow bed [19, 22]. Fixed bed gasifiers (updraft and downdraft) are usually used for smaller units (<10 MW), fluidized bed (5- 10 MW) and entrained flow are used for large capacity units (1000MW) [18]. Some examples of companies that use gasification as a source of energy include Sasol, based in South Africa, and several plants in Germany that convert municipal waste to syngas for generating electricity [23][30].

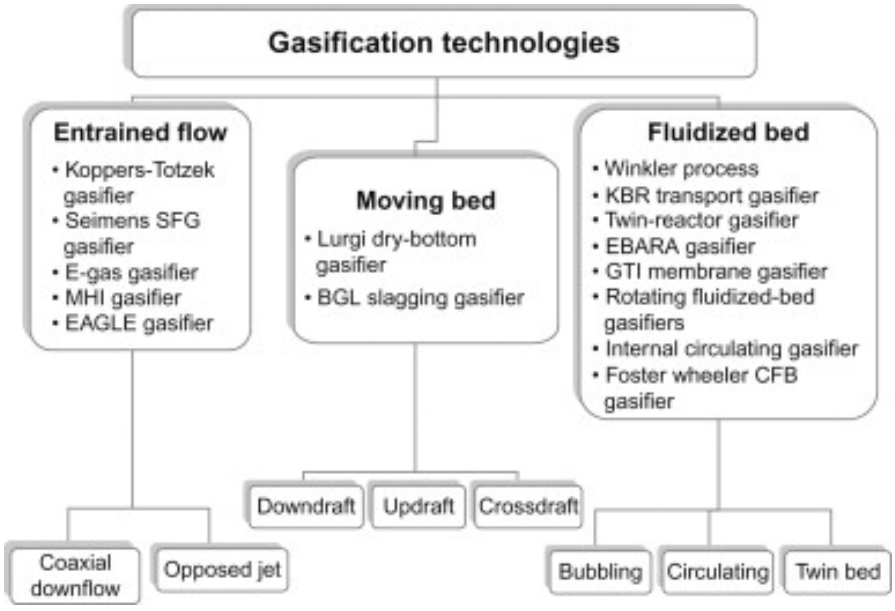

Figure 2.1: Gasifier Technologies

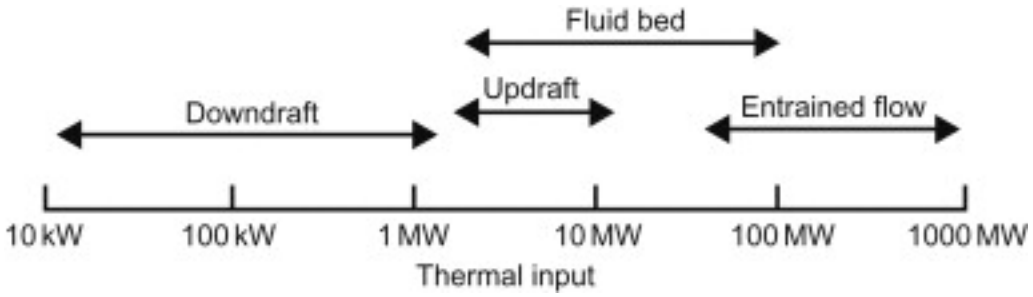

Figure 2.2: Range of applicability for biomass gasifiers [19]

Fixed bed gasifiers can be relatively easy to manufacture at a cheaper price than other types of gasifiers. For this reason, large numbers of small-scale gasifiers are used around the world.

There are three types of fixed bed gasifiers: updraft, downdraft, and cross-draft.

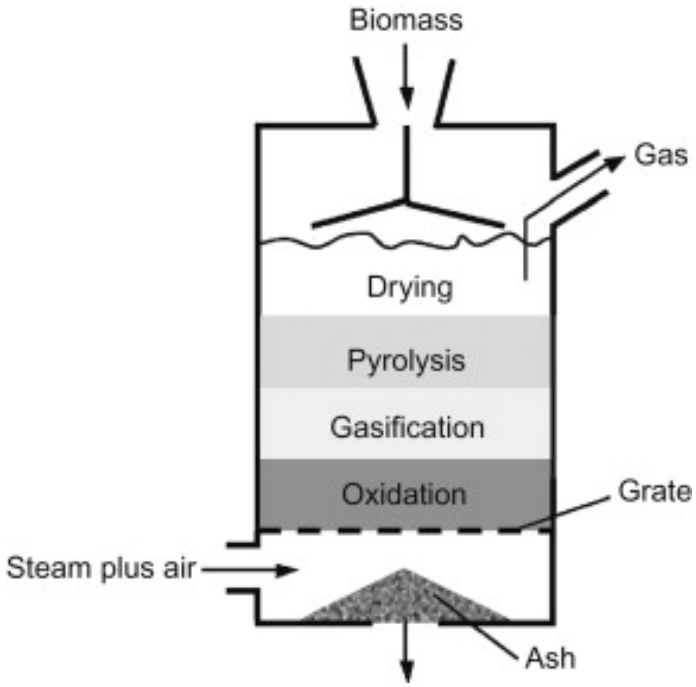

Figure 2.3: Schematic of an updraft gasifier [19]

An updraft gasifier, used since the early part of World War II, is widely used for coal gasification and non-volatile fuel (fuel that does not readily evaporate); but it produces tar at a higher rate (30-150 lb./Nm^3). High tar content in gases leads to clogging in engines and as such lower amounts are always preferred [2]. In this system, air enters the gasifier from below the grate and flows through the bed to produce a combustible gas [19]. Moisture from the biomass is removed in the drying zone, followed by pyrolysis zone, and then moves into the reduction and combustion zone, where the char is broken down. Due to high production, fluffy biomasses are unsuitable for use in an updraft gasifier [22]. An example of a company that currently uses an updraft gasifier is SASOL, based in South Africa. SASOL produces 170000 barrel/day of Fischer-Tropsch liquid fuel [18].

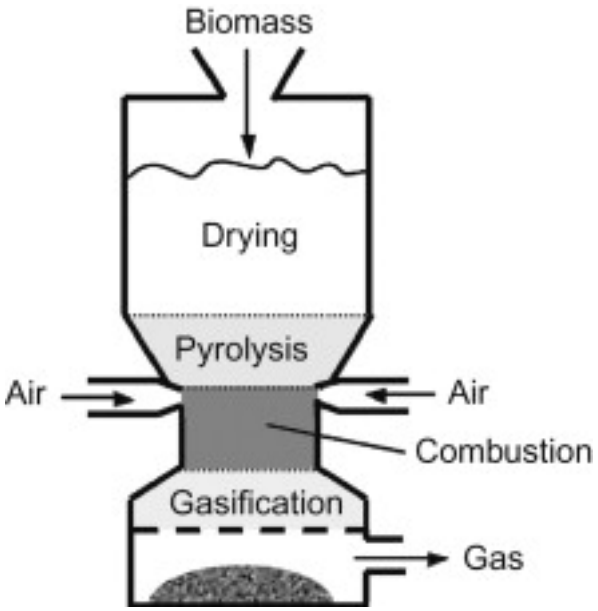

Figure 2.4: Schematic of a downdraft gasifier [17]

In a downdraft gasifier, air enters the gasifier at a certain level above the top. The product gas flows out from the bottom. This gas passes through a high-temperature zone, which provides favorable conditions for thermal tar decomposition (cracking) to occur. For this reason, a downdraft gasifier produces very little tar, since most of it is thermally cracked down at the reduction zone [19, 24, 22]. Higher amounts of tar have been observed in systems that gasify at a temperature of under 700 °C [25]. Downdraft gasifiers work well with biomasses that contain low moisture content [26].The gas from a downdraft is clean and can work well with internal combustion engines. The biomass in a downdraft gasifier passes through several zones. In the first zone, the biomass is dried. It then passes through a pyrolysis zone, which is the second zone, where little or no air is present. Most of the tar, ash, and pyrolyzed char is produced in the third and fourth zones and consists of hot ash and unreacted charcoal, which cracks any tar present [19].

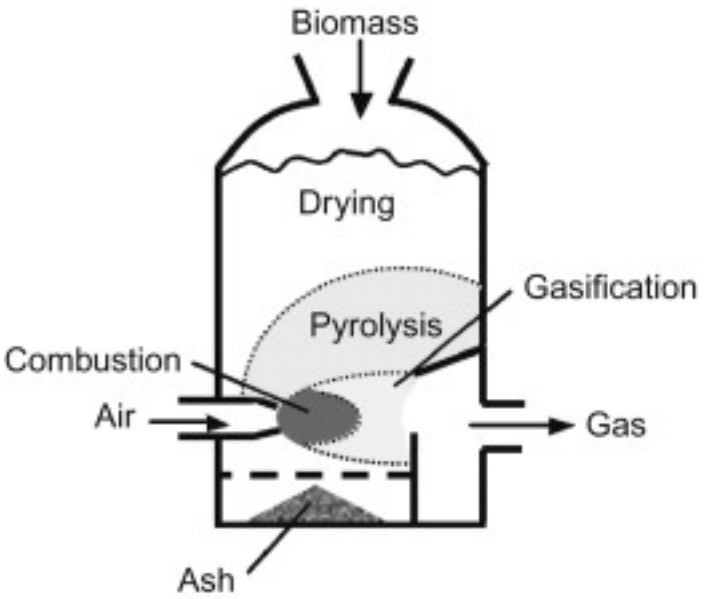

Figure 2 5: Schematic of a cross-draft gasifier [18]

In a cross-draft gasifier, fuel is fed from the top, and the air is inserted from the sides using a nozzle. This type of gasifier is primarily used for gasifying charcoal with little ash content. Cross-draft gasifiers can be light, small, and able to handle biomasses with high moisture.

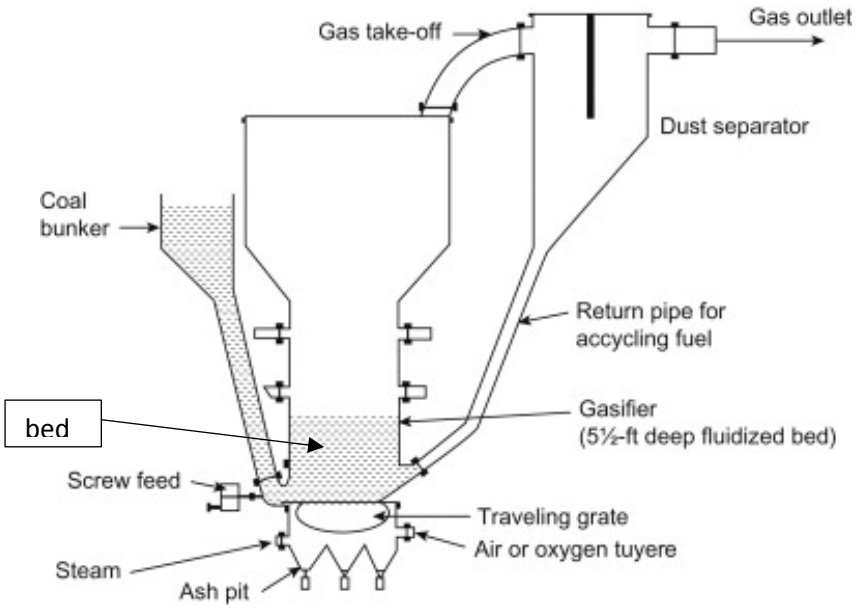

Figure 2.6: Sketch of the original bubbling fluidized bed Gasifier [18]

A fluidized bed gasifier contains a bed, which is used to heat the biomasses with a gasifying agent [22]. This bed is made up of sand or ash and acts as a heat transfer medium [18]. In contrast to the fluidized bed gasifier, no distinct zones exist, and such gasification and occur. Several catalysts, such as carbonates, limestone, calcium chloride, and inorganic salts, can be used to increase the efficiency of a fluidized bed gasifier. Biomass entering a fluidized bed needs to be crushed to less than 10mm in diameter. Examples of fluidized bed plants in the US are the 15-MW project at McNeil Generation Station in Burlington (Vermont), and 5-MW project in Paia (Hawaii) [27].

2.3 Factors Affecting Gasification

There are a number of factors that affect gasification reactions. Some of these include: temperature, pressure, height of the reactor bed, the fluidization velocity, the equivalence ratio, the air to steam ratio, and the characteristics of the fuel [28].

Temperature

An increase in temperature in a gasifier increases the formation of combustible gases and decreases the yield of char and liquids [28]. This was observed by Scott et al., when trying maple sawdust. Voloch et al. also observed this when they were testing corn cobs in 1983 [28]. It was found that the calorific value of biomass producer gas increased steadily up to 700 °C, and then reduced [28]. Surgrant suspects that the increase in temperature was most likely due to increased concentrations of CO, H_2, and hydrocarbon gases in the gas mixture. The decrease in temperature, observed by Sadakata, could also be from the thermal decomposition of the hydrocarbons present [28]. A downdraft gasifier, such as the one used at Iowa, has a gas exiting temperature of approximately 700 °C, but its peak gasification temperature at the throat is about 1000 °C. This corresponds correspond to results obtained by Basu [19]. The syngas exit temperature from a downdraft gasifier may range from 600 to 1200 °C.

Bed pressure

An increase in pressure in a gasifier leads to a rise in char gasification. The higher the pressure have shown to lead high char surface area [18] [29]. Higher bed pressure also leads to a higher production of methane [28].

Bed height

An increase in bed height increases the residence time, and also leads to an increase in gas yield. This was shown by Sadakar et al. [28] when their gasifier efficiency increased by raising their bed height. Font et al. saw an increase in their gas components (H_2, CO_2, CO, CH_4, and C_2H_2) as a result of increased residence time due to the increase in bed height [28].

Equivalence ratio

The equivalence ratio (ER) has a significant impact on the performance of gasifiers because it affects the bed temperature, its thermal efficiency, and the quality of the gas evolved from the gasifier [28]. The equivalence ratio is defined as the ratio of the actual air-fuel ratio to the stoichiometric air-fuel ratio [19, 21].

$$Equivalence\ ratio = ((\frac{m_{fuel}}{m_{oxidizer}})/(\frac{m_{fuel}}{m_{oxidizer}})_{stoichometric}) \quad (2.1)$$

Some studies show that downdraft gasifiers give their best yield at an equivalence ratio of about 0.25 [19]. It has been observed that low equivalence ratio values led to low char formation [19]. High equivalence ratios of more than 0.4 tend to produces combustion gases that are composed of CO_2 and H_2O, rather than the desirable CO and H_2 [19]. High equivalence ratios also increase the rate of syngas production, while lower ratios lead to lower energy content and more tar production [19].

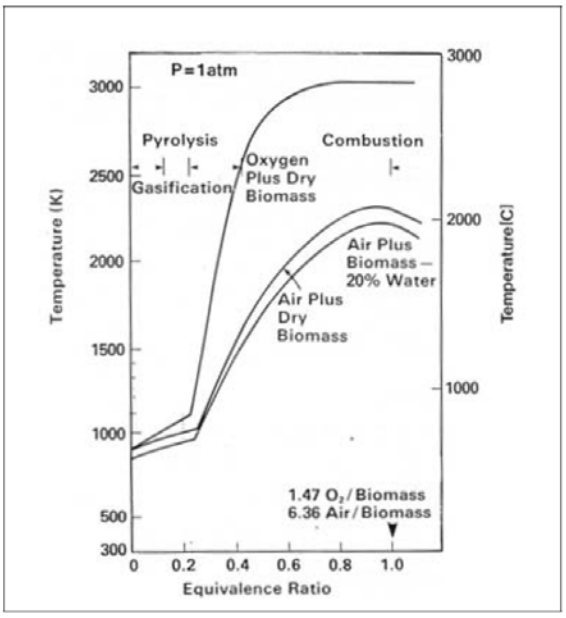

Figure 2.7 Temperature versus equivalence ratio for a gasifier

Fluidized velocity

Fluidization is a processing technique, which employs a suspension of a small solid particle in a stream of fluid (usually gas) so that the solid particle may come in contact with the fluid [18]. The higher the fluidization velocity, the higher the bed temperature, and the lower the produced gas heating value due to the increased amounts of oxygen and nitrogen in the system [28].

Characteristics of fuel (Moisture content, size of the feed material)

The moisture content of the fuel affects the reaction temperature. This is because part of the energy from the system is required to evaporate the water present in the fuel. Studies done by Elliot and Sea Lock [28] in 1985 suggest that the temperature of the gasifier decreased when fuel with higher moisture content is fed into the system, and also has an effect on the production gases [18].

The size of the fuel also affects the amount of tar and char produced—a rough fuel texture leads to increased production in char and lower production of tar [28]. Lu et al [19] showed that fuel

with small particle sizes improved the gasifier's efficiency. This has not yet been generally accepted because other authors, such as Mettanant et al., did not find the same results under similar experimental conditions [19].

2.4 Biomass

2.4.1 Types of biomass

Biomass refers to organic materials derived from plants or animals [20]. The official definition used by the United Nations Frame Work Convention on Climate Change defines it as below.

'*Non-fossilized and biodegradable organic material originating from plants, animals and micro-organisms. This shall also include products, by-products, residues and waste from agriculture, forestry and related industries as well as the non-fossilized and biodegradable organic fractions of industrial and municipal wastes*' [20]

Biomass is formed from the constant interaction of CO_2, air, water, soil, and sunlight (for plants and animals). Once an organism loses life, microorganisms break the biomass into elementary constituent parts, such as H_2O and CO_2.

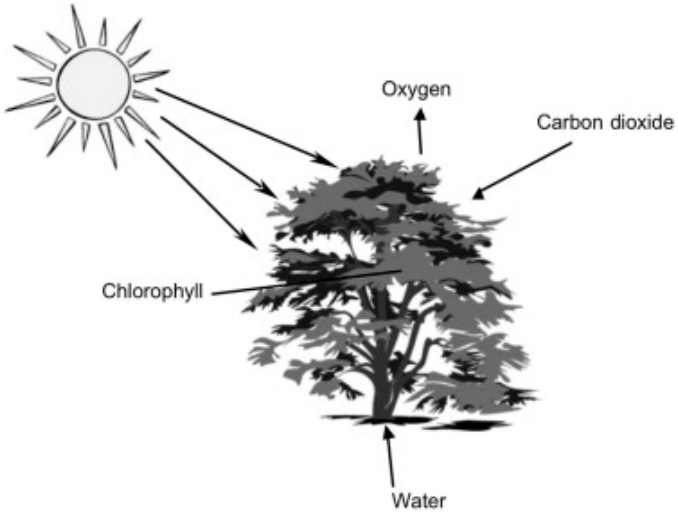

Figure 2.8: Biomass growth through photosynthesis [2]

$$Living\ plant + CO_2 + H_2O + Sunlight \rightarrow (CH_mO_n) + O_2 - 480kj/mol$$

Where (CH_mO_n) represents glucose

Common sources of biomasses are [31], and can be seen in Figure 2.9:

- Agricultural: Food grain, corn stalks, seed hulls, nutshells
- Forest: Trees, wood waste, wood
- Municipal: sewage sludge, refuse–derived waste (RDF), food waste
- Energy crops: switch grass, poplars, willows
- Biological: Animal waste, aquatic species, biological waste
- There are two main sources of biomass: purpose-grown energy crops and waste [31].
- Virgin biomass includes wood, plants, and leaves (ligno-cellulose) Waste includes solid and liquid wastes, MSW (municipal solid waste), sewage, animal and human waste, and gases derived from land fills

Figure 2.9: Sources of biomass [4]

2.4.2 Biomass components

Lignocellulosic Biomass:

Biomass is composed mainly of lignocellulose, which is comprised of three primary constituents: cellulose, hemicellulose, and lignin.

Cellulose:

This is a common organic compound found on earth, as it is the primary structural component of Biomass. For example, its amount can vary from up to 90% in cotton to 33% in other plants (in weight). Cellulose (also represented C6H10O5) has a crystalline structure and is made of many glucose molecules. This structure provides high strength to terrestrial biomasses.

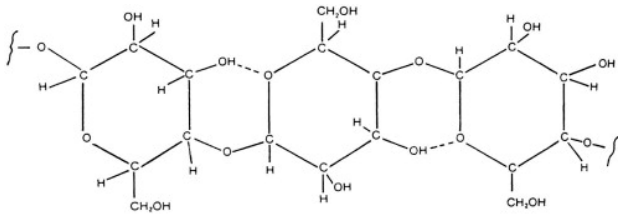

Figure 2.10: Molecular structure of Cellulose [2]

Hemicellulose:

Compared to cellulose, which has a firm structure, hemicellulose ($C_5H_8O_4$) has a random, amorphous structure with much less strength. Hemicellulose contains pure sugar residues, such as d-xylose, glucose, I-arabinose, d-glucuronic acid, and d-mannose.

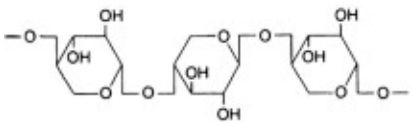

Figure 2.11: Structure of Hemicellulose [2]

Lignin:

Lignin is an internal part of the secondary cell wall of plants and is one of the most abundant polymers (after cellulose). It is primarily made up of the 3D polymers: 4- propynyl phenol, 4-propenyl-2methoxy phenol, and 4-propenyl-2.5 dimethoxy phenol [2].

Lignin acts as a cementing agent for cellulose fibers (holding them together). It is mostly composed of the benzene ring and is highly insoluble. Softwood, for example, can contain up to 35% lignin (dry weight).

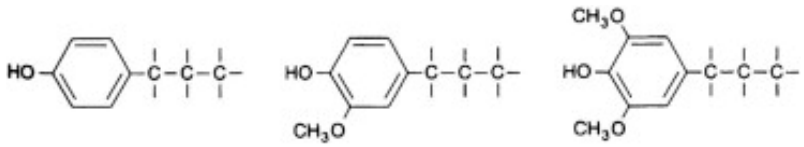

Figure 2.12: Structural units of lignin [2]

Some examples of how hemicellulose, cellulose, and lignin vary on selected biomasses can be seen below.

Table 2.1: Hemicellulose, cellulose, and lignin composition in selected biomass [17]

Lignocellulosic residues	Hemicellulose (%)	Cellulose (%)	Lignin (%)	Ash (%)	Reference
Nut shells	25–30	25–30	30–40	NA	[9]
Corn cobs	35	45	15	1.36	
Paper	0	85–99	0–15	1.1–3.9	
Rice Straw	24	32.1	18	NA	
Sorted Refuse	20	60	20	NA	
Leaves	80–85	15–20	0	NA	
Cotton seeds hair	5–20	80–95	0	NA	
Waste paper from chemical pulps	10–20	60–70	5–10	NA	
Primary wastewater solids	NA	8–15	24–29	NA	
Sugar cane bagasse	27–32	32–44	19–24	4.5–9	
Barley straw	24–29	31–34	14–15	5–7	

2.5 Gasification and pyrolysis of biomass components

Here, we review some studies on the gasification of biomass regarding the three components (Hemicellulose, cellulose, and lignin), and the methods used.

Studies done by Shen and Gu [32] were able to obtain crystalline cellulose, lignin and hemicellulose. They heated the three components separately. A sample of about 3-5 g of each is tested once at a time at different rates. Their pyrolysis unit is composed of a feeding system, pyrolysis system, carbon filter, vapor–condensers, and gas storage (Figure 2.13). The reactor is made of a quartz tube (diameter of 15mm, length 1200 mm, and thickness 2mm). The sample is heated using a carbonium heater which uses a power of 8 KW.

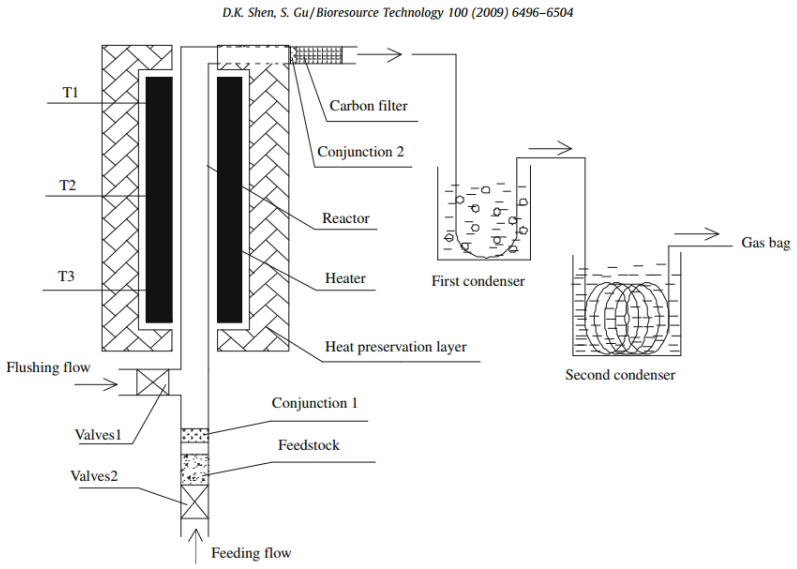

Figure 2.13: Pyrolysis Apparatus used by Shen and Gu [32]

Once the system reaches the desired temperature, a flushing flow gas is initially passed through for a minute to purge any oxygen present. From there, Valve 1 is closed, and Valve 2 is opened. The stream of mixed products and char residues is then separated. The carrier gas (nitrogen) is

collected in sample bags [33]. The table 2.2-2.4 summarizes their findings from all three components [32, 33, and 34]

Table 2.2: Syngas composition of Lignin

Gas composition (wt.%)	475 °C	575 °C	650 °C	700 °C	775 °C	825 °C
CO	4.79	5.02	5.84	7.23	8.67	10.65
CO_2	7.37	8.55	10.34	11.08	11.53	11.74
CH_4	1.58	1.73	2.14	3.31	4.52	5.86
H_2	0.13	0.18	0.27	0.42	0.58	0.71

Table 2.3: Syngas composition of Hemicellulose

Compounds (wt%)	425 °C	475 °C	510 °C	570 °C	625 °C	690 °C
CO	5.35	5.23	6.02	6.93	9.24	13.33
CO_2	25.01	24.54	25.61	25.78	24.79	22.87
H_2	1.08	1.60	2.35	2.49	3.29	3.34
C_xH_y	0.81	0.96	1.09	1.15	1.70	2.56

Table 2.4 Syngas composition of cellulose

Compounds (wt%)	420 °C	470 °C	530 °C	580 °C	630 °C	730 °C
CO	11.1	13.8	14.5	15.2	16.4	20.2
CO_2	8.6	9.8	10.1	9.6	9.6	9.5
H_2	1.2	1.6	1.9	2.3	3.0	3.2
C_xH_y	0.2	0.3	0.3	0.4	0.5	0.7

They found the highest CO production from Cellulose was at 630 and 730 degrees Celsius. Their highest Hydrogen component was from cellulose.

Comparing all of the three results, we can observe that the highest content of CO at a similar temperature range appears to be from cellulose, followed by hemicellulose, and then lignin. The highest H_2 content appears to be from cellulose, followed by lignin, and then by hemicellulose [35]. Although the studies mentioned above looked into cellulose, hemicellulose, and lignin on an individual basis, some studies have looked into the pyrolysis of all three components in small scale.

Authors Yang et al. [36] also carried out a similar experiment using a thermogravimetric analyzer (NETZSCH STA 409C, Germany). They measured the evolved syngas by using a Fourier transform infrared (FTIR) spectroscopy. They found that the pyrolysis of hemicellulose occurred in between 220 and 315 degrees Celsius, while that of cellulose occurred between 315 and 400 degrees and lignin pyrolysis required higher temperatures ranging from 160 to 900 degrees. In this study Yang et al. [36] heated the material to 900 degrees, using nitrogen as a carrier gas and the following syngas results were obtained:

Table 2.5: Gas product from Hemicellulose, Cellulose, and Lignin [36]

Sample	Gas product yield					
	H_2	CO	CH_4	CO_2	C_2H_4	C_2H_6
Hemicellulose	8.75	5.37	1.57	9.72	0.05	0.37
Cellulose	5.48	9.91	1.84	6.58	0.08	0.17
Lignin	20.84	8.46	3.98	7.81	0.03	0.42

This study, in comparison to studies done by Shen et al., shows that the highest amount of CO was produced from cellulose while the highest amount of H_2 obtained was obtained from Lignin, followed by hemicellulose, and then by Cellulose.

Other studies such as that from Toshiaki et al. [37] looked into steam gasification of Lignin, Cellulose, and Hemicellulose. They used a small scale downdraft gasifier to investigate the syngas content from Cellulose, Xylan, and Lignin. They also looked into Japanese oak and Japanese red pine. The Japanese oak was composed of 45.21% wt. Cellulose, 27.96% wt. Hemicellulose, and 20.20 % wt. Lignin while the Japanese red pine was composed of 44.9% wt. Lignin, and 46.6% wt. for both the Cellulose and Hemicellulose content. Figure 14 [37] shows the schematic of the system that was used.

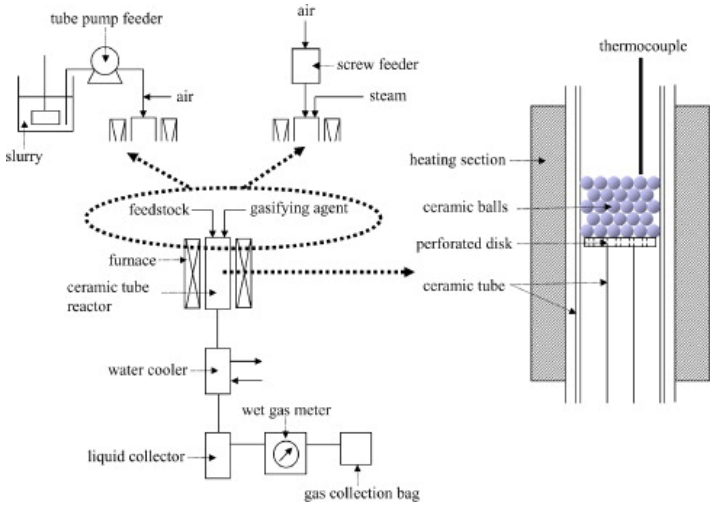

Figure 2.14: Steam gasification Experimental setup of Lignin [37]

The setup was made of a ceramic reactor (450mm long, and 20 mm diameter), temperature controller, gas meter, and gas collection bag. The temperatures tested ranged from 1073 to 1273 degrees kelvin (800 – 1000 degrees Celsius) at atmospheric temperature. The syngas results obtained can be seen in the table below:

Table 2.6: Product gas composition in the air-steam gasification

Feedstock	Gasification conversion (% C basis)	CO	CO_2	H_2	CH_4	C_2H_4
Cellulose	97.9	35.5	27.0	28.7	6.5	0.7
Xylan (also hemicellulose)	92.2	24.8	35.6	32.4	5.2	1.0
Lignin	52.8	25.8	35.7	32.1	5.0	0.6
Japanese oak	88.1	39.9	23.4	22.0	10.4	3.1
Japanese red pine bark wood	70.3	25.6	34.7	31.0	5.5	2.5

With steam gasification, it appears that the highest syngas content was from Cellulose, followed by Lignin, and then by Xylan. The highest content of Hydrogen appeared to be from Xylan, which was very close to Lignin. Interestingly, Japanese red pine, which contained the highest amount of Lignin, produced a higher CO and higher H_2 suggesting that high amount of lignin leads to increased Hydrogen production.

A list of different fuels and components can be seen in the appendix section.

2.6 Conversion of syngas to bio power

We have been approached by companies which will be using downdraft gasifiers, such as the one located at the University of Iowa main Power Plant, to produce electricity in developing countries. For this reason, this part of my thesis looks at methods through which the syngas from our gasifier could be used to generate electricity.

Boiler

The syngas that comes out from a gasifier usually has a temperature of around 700 °C. This means that gas can be fed directly into a boiler without the need for a heat exchanger [38]. A boiler, such as the one at the University of Iowa Oakdale Utility Power Plant, can burn natural gas to produce heat, which can be used to convert water to steam. Syngas can be co-fired with natural gas to burn in a boiler. Figure 2.15 shows an example of a Hurst gas boiler, similar to the one located at the university of Iowa Oakdale power plant.

Figure 2.15: Schematic of a Hurst Boiler- series 200 [39]

Gas engines

A gas engine is an internal combustion engine, which runs on gas fuel. Usually, a wide range of gases can be used with gas engines, but depending on the gas composition, engine backfiring may occur. Due to the rising use of gasification technologies, companies, such as Clarck Energy, produce gas turbines costumed especially for syngas. Companies, such as General Electric (GE), are following the same trend, and work in collaboration with other companies, such as Clarck Energy. An example of a syngas engine is the GE Lenbacker Type-2 Engine, which can produce an electric output of up to 330 Kilowatt-electric (KWe) [40].

Figure 2.16: The GE's Jenbacker Type-2 Syngas Engine [40]

Gas Turbine

A gas turbine expands hot gases that are produced by burning fuel. In this case, the fuel is syngas. These gases can also work with natural gas, and can supply enough energy to generate up to 510 MW of electricity. An example of such a gas turbine is the GE E-class turbine [40]. Table 2.8 shows the Tar limit tolerable per application. Large amounts of tar from syngas have led to clogging and even damage in the long run. As seen in table 28 IC engines tend to be best suited for gas that contains a large amount of tar compared to gas turbines. Tars from different gasifiers range between 0- 100g/Nm^3 [56].

Figure 2.17: The GE E-class Syngas Turbine [41]

Table 2.8: Application limits of tar and particulates in biomass gas [4]

Application	Particulate (g/Nm^3)	Particulate (g/Nm^3)
Direct combustion	No limit specified	No limit specified
Syngas production	0.02	0.1
Gas turbine	0.1-120	0.05-5
IC engine	30	50-100
Pipeline transport	-	50-500 for compressor
Fuel cell	-	<1.0

2.7 Gasification technology versus other waste management technology

Gasification is currently seen as one of the best solutions to get rid of waste, and at the same time, produce electricity. We shall be comparing gasification with other technologies used in trash management and the possible advantages of using incineration.

Incineration

Incineration is defined as "the act of burning something completely, reducing it to ashes" [42]. Incinerators operate at atmospheric pressure and temperature [43]. In an incinerator unit, feedstock, waste material, is directly burnt by using large amounts of air. What remains from this process is ash that has to be treated before been deposited in the landfill. A considerable drawback of Incineration is that it also emits harmful gases, such as sulfur dioxide, nitrogen dioxide, and fine particulates [34].

Anaerobic digestion

Anaerobic digestion is defined as the microbial decomposition of organic matter into methane, carbon dioxide, inorganic nutrients, and compost. This is done in an oxygen-depleted environment, and in the presence of the hydrogen gas [44]. There are many countries, including Germany, Denmark, and the UK, that are investing in using anaerobic digesters. These digesters are sealed and contain heated tanks, which provide a suitable environment for naturally occurring anaerobic bacteria to grow, multiply, and convert manure into biogas and a low order effluent. The biogas can be used to replace natural gas. The main drawbacks of this process are that the digestion system is costly, and the digester requires a periodic cleaning [45, 46].

Thermal hydrolysis

Thermal hydrolysis is a two-stage process that uses pressure-cooking, followed by rapid decompression. Here, sludge from waste can be heated to a temperature ranging from 150 to 200 °C with a pressure range in between 6 and 25 bar [47]. This process is usually combined with anaerobic digestion. The pressure and temperature in thermal hydrolysis get rid of any pathogens that can be used as a precursor to anaerobic digestion. An example of a thermal hydrolysis plant in the District of Colombia Water and Sewer Authority (DC Water), which started operation in 2014.

Plasma gasification

Here, very high temperatures are used to gasify biomass hydrocarbons. This process can also be called plasma pyrolysis because it takes place in an oxygen-starved environment. Here, an inert gas is passed through two electrodes, causing an electric arc to be produced. The temperature generated by this arc is usually around 13,000 °C and can go up to 18000 °C. The main advantage of using plasma gasification is that it's insensitive to the quality of feedstock that is inserted into this system [19].

2.7 Biochar

Definitions

- Char: Solid decomposition product of a natural or synthetic organic material.
- Charcoal: A 'Char' obtained from the pyrolysis of wood and some related natural organic materials. (Note: Charcoal has highly reactive inner surfaces and low sulfur content).
- Activated Carbon: A porous material.

(Note: Activated carbon has a high surface area and relatively high concentration of functional groups at its surface.)

- Biochar: "Biochar can be defined as a carbon-rich product obtained when biomass, such as wood, manure or leaves is heated in a closed container with little or no air." [48]

The very first observation though not very scientific on biochar appears to have been done in the mid-1800 by Tumble who shared his observations of the effect of charcoal on the farm which lived in. He mentioned that he had observed his farms with coal dust to have increased vegetation relatively quickly. Further detailed research was then found in 1915 when some the effects of biochar was studied on seedling growth. In 1927, the national keeper mentioned that 'charcoal acts as a sponge in the soil, absorbing and retaining water, gases, and solutions'. Other researchers such as Liebig in 1878 [48] have mentioned that in places such as China, the locals would burn waste biomass covered with soil for days until the soil turned black which led to reported increase in soil productivity. Although early interest in biochar was productive, global attention did not catch on until the past years. [48]

Today there are four complementary and often synergetic objectives as to why biochar may be applied for environmental management. These are soil improvement, waste management, and climate change mitigation and energy production [48].

Characteristics of Biochar

- Surface area.

Surface area is an important factor as it influences the soil fertility. The capacity to store water and plant nutrients in the soil is partly related to the surface area. Some experimental studies have shown that the surface area of biochar can improve soil structure or aeration in soils. [48]

- Biochar Macro porosity

Biochar have mostly been assessed mainly for their role as adsorbents. In the past, Macropores (>50nm in diameter) were considered to be significant due to their pores for transport of adsorbate molecules. However, a recent discovery has shown that macropores are relevant to vital soil functions such as aeration and hydrology. [48]

- Particle-size distribution system.

The particle sizes of the biochar resulting from the pyrolysis are highly dependent on the original material. The resulting biochar likely shrinks due to the heating process and most studies have shown their size to smaller than that of the initial feedstock. Studies have shown that as the pyrolysis temperature increases from 200c to 1000c, the linear shrinkage of the particles was demonstrated to increase from 2 to 20 per of peat biochar. Other studies have also shown the effect of pressure on sizes of biochar produced. Cetin et al [61][48] showed that increasing the pyrolysis pressure from atmospheric pressure to 5, 10 and 20 bars leads to the formation of larger biochar particles. The authors accounted for this swelling as well as the formation of particle clusters as a result of melting and fusion of the particles.

- Entrained minerals

Feedstock and process conditions control the amount of distribution of mineral matter in biochar. During thermal degradation potassium and chlorine ions are known to be highly mobile and will start to vaporize at relatively low temperatures. Calcium is mainly located in the cell walls as silica or as opal phytoliths. Both Ca, and Si are released during degradation at much higher temperatures than K and CL. Magnesium is ionically and covalently bonded with organic molecules and only vaporizes at high temperatures. Phosphorus and sulfur are associated with complex organic compounds within the cell and are relatively stable at low degradation temperatures. Other elements such as iron and Manganese (Mn) exist in some organic and inorganic forms in the biomass and are largely retained during biochar formation. [48]

Little work have been carried out to understand the stability of heavy metals in biochar [48]. Biochar especially those from chicken manure and activated carbon are known to absorb heavy metals. There are also not many publications on the distribution of minerals within different types of biochar [48]. In some biochar, K and Ca are distributed throughout the surface. Minerals in biochar may include sylvite (KCL), Quartz (SiO_2), amorphous silica, calcite ($CaCO_3$), hydroxyapatite ($Ca_{10}(PO_4)_6(OH)_2$), and other minor phases such as Calcium phosphates, anhydrite ($CaSO_4$), various nitrates and oxides and hydroxides of Ca, Mg, aluminum (Al) , Titanium (Ti), Mn, Zinc (Zn) or Iron Fe. [48]

Crystalline silica as it has been found in some biochars and may pose high level of respiratory risk while amorphous silica on the other hand is known to contain and protect plant carbon from degradation.

Morphologies and distribution patterns of mineral on some biochars are shown below. Figure 3.5 shows that some mineral phases consist of more than one mineral type. Figure 3.6 shows that there

is a large variety of mineral content even within each particle and shows both metal and non-metals in the end grain of wood biochar. Figures 3.7 to 3.9 shows how a verity of minerals can differ between different biochars. [48]

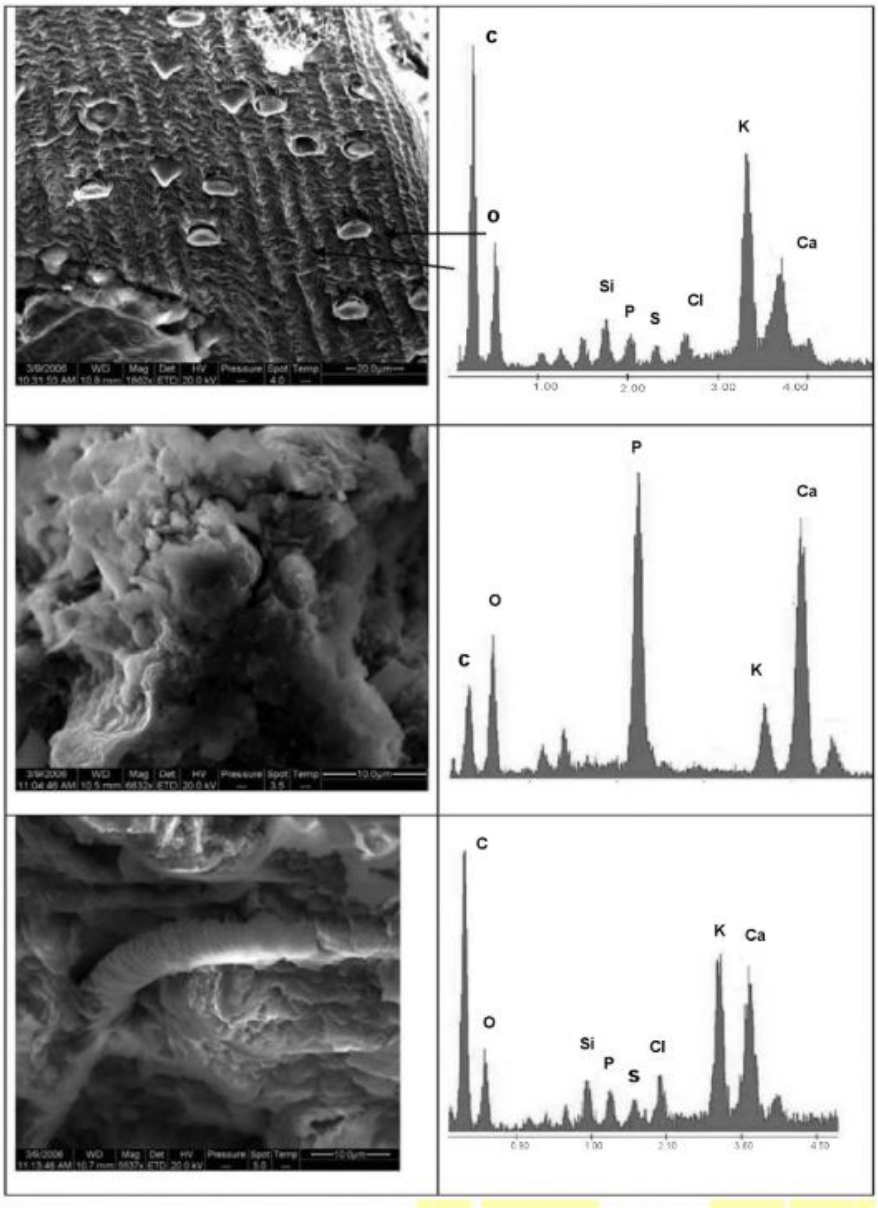

Figure 2.18: Scannning electric microscopy (SEM) micrographs of different mineral phases in chicken manure biochar (produces at 450 celcius for 0.5 hrs) and their energy-dispersive X-ray spectroscopy (EDS) spectra

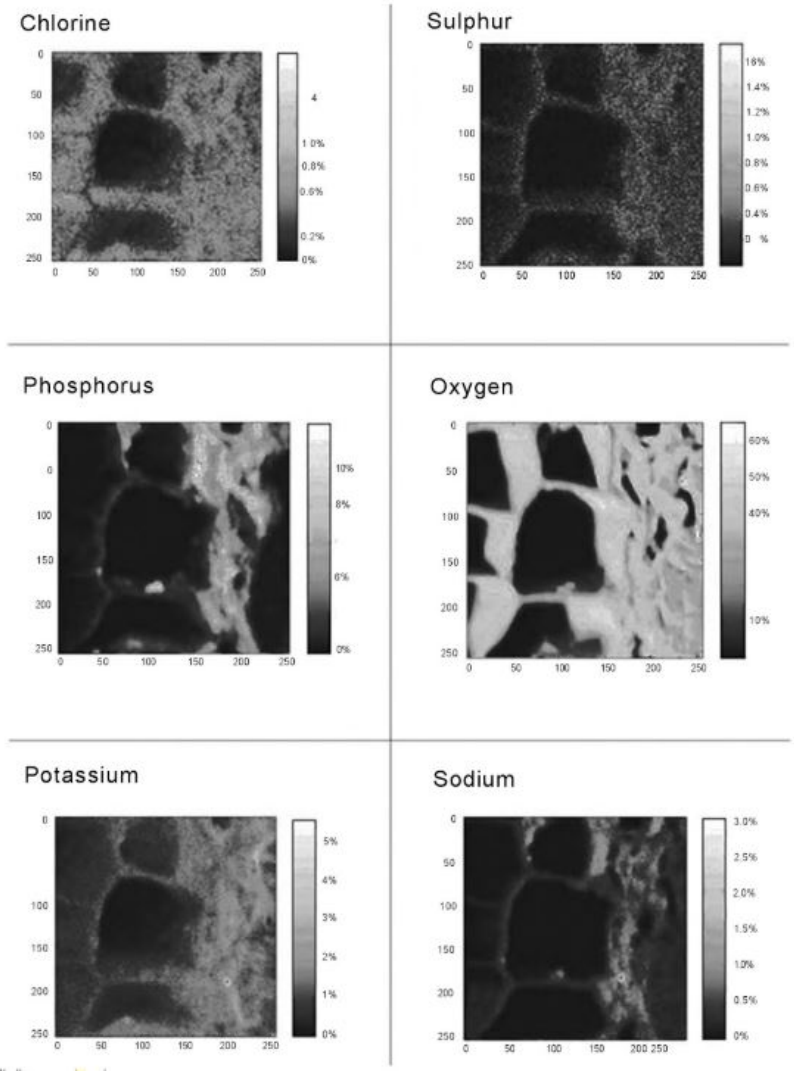

Figure 2.19: Distribution of non- C elements on the surface of wood biochar (produced at 450C of 0.5 Hrs.) determined by microprobe analysis.

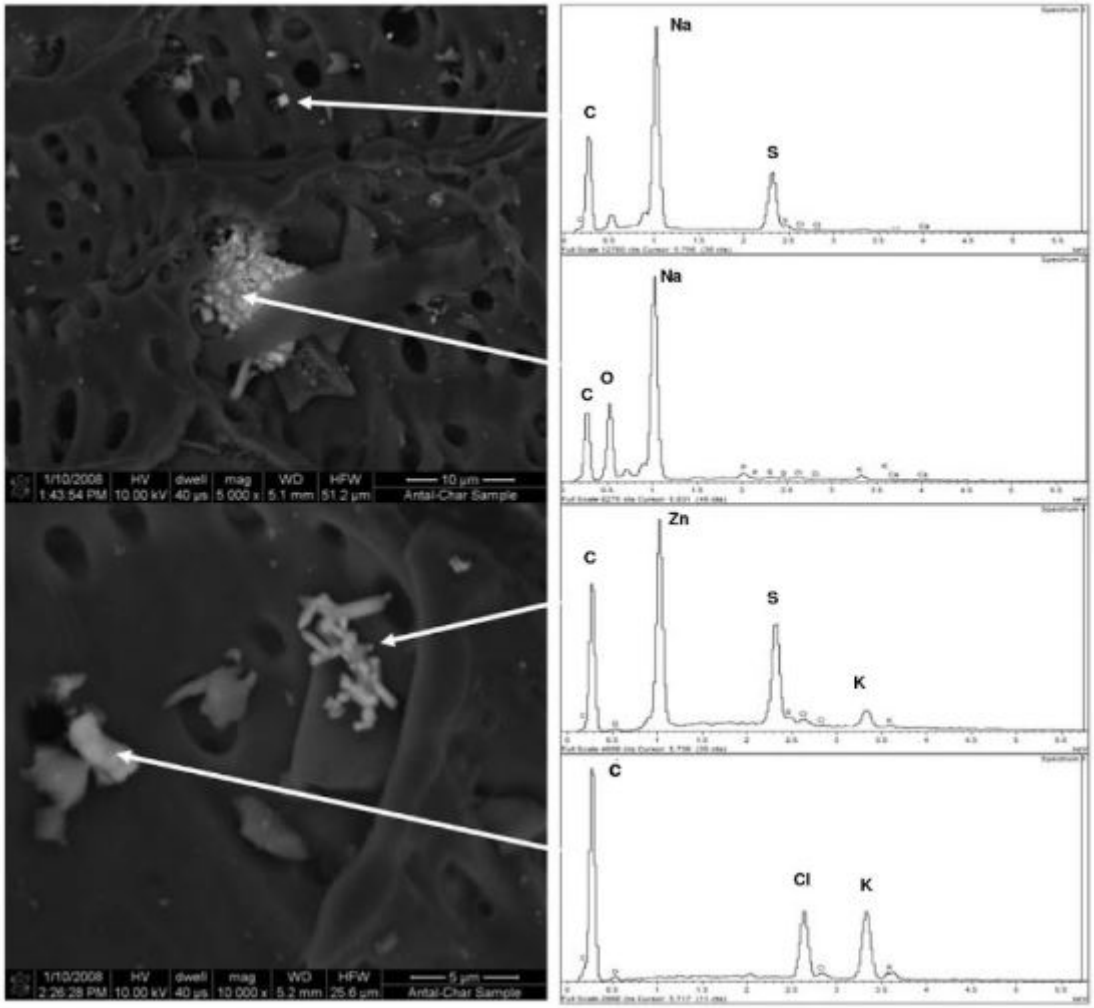

Figure 2.20: SEM micrographs and associated EDS spectra for mineral phases in maize-cob biochar prepared by flash pyrolysis: Probable minerals include Na2S, Na2O or Na2CO3, ZnS and KCL [48].

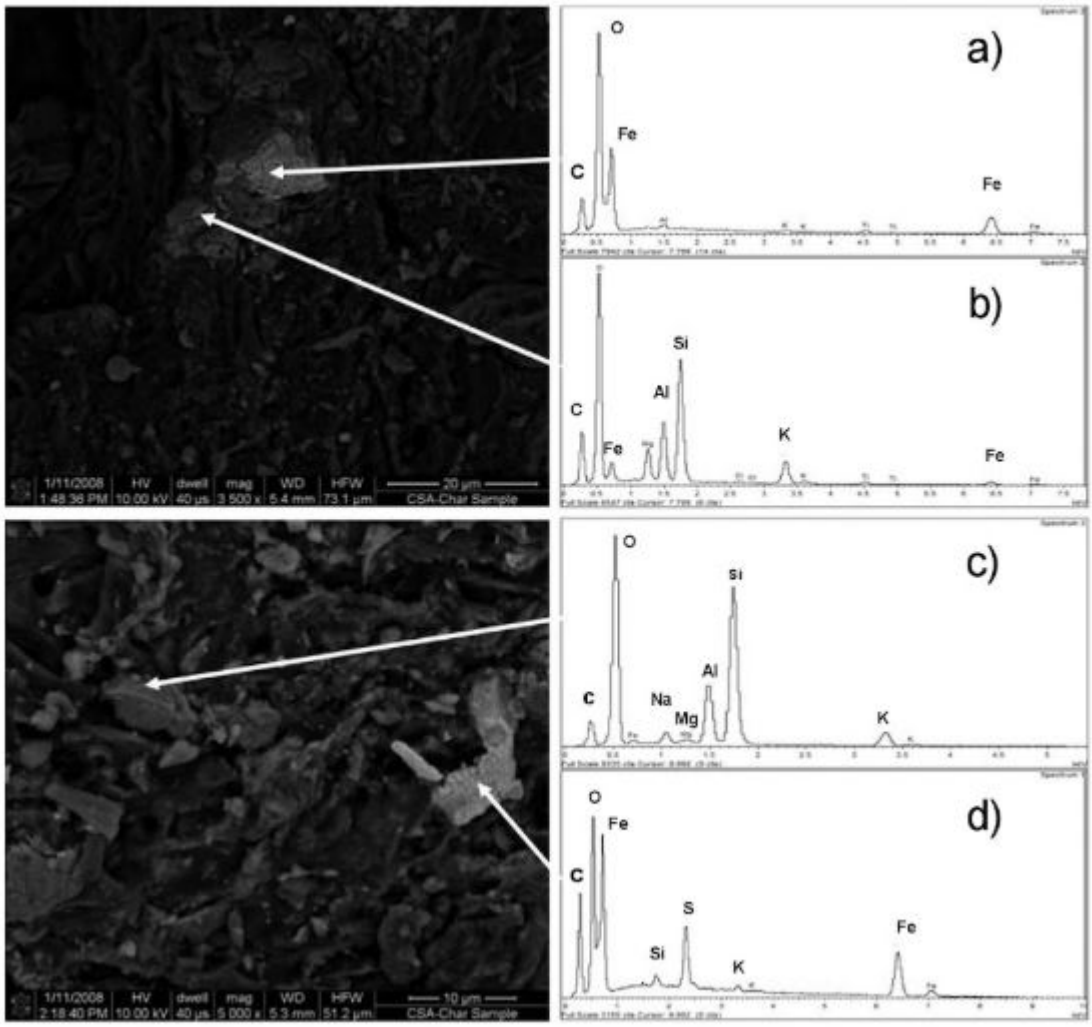

Figure 2.21: SEM micrographs and associated EDS spectra for mineral phases in while oak biochar prepared by fast pyrolysis [48].

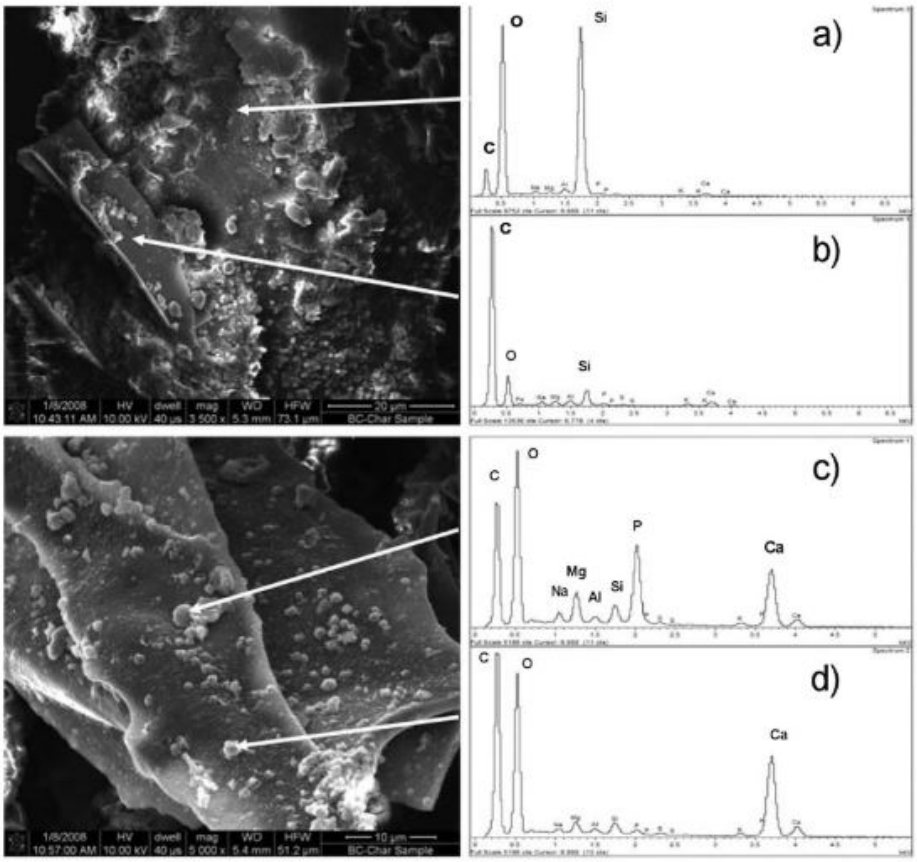

Figure 2.22: SEM micrographs and associated EDS spectra for mineral phases in poplar wood biochar from a combustion facility [48].

Potential benefits of Bio char

The following benefited have been cited from the P. Basu's textbook [4] [51]

Biochar is useful for the following reasons

1. Sequesters carbon and thereby minimizes climate change
2. Leads to negative carbon emission
3. Displaces carbon-positive fossil fuel
4. Reduces nutrient losses in soils
5. Reduces fertilizer use

6. Enhances marginal soil productivity
7. Increases sustainable food production
8. Improves water retention, aeration, and tilth
9. Higher cation exchange capacity (CEC)
10. Improves water quality by reducing contaminated runoff and nutrient loss.
11. Soil remediation
12. Reversal of desertification on massive scales and can work in tandem with reforestation
13. A better alternative to slash and burn agriculture residues.
14. Decreases nitrous oxide and methane emissions from solids.
15. Leads to net primary production
16. Generates carbon offsets and increased on-farm profitability for the company.

3. EQUIPMENT AND EXPERIMENTAL CONFIGURATION

3.1 Single stage gasification system and experimental configuration (Iowa)

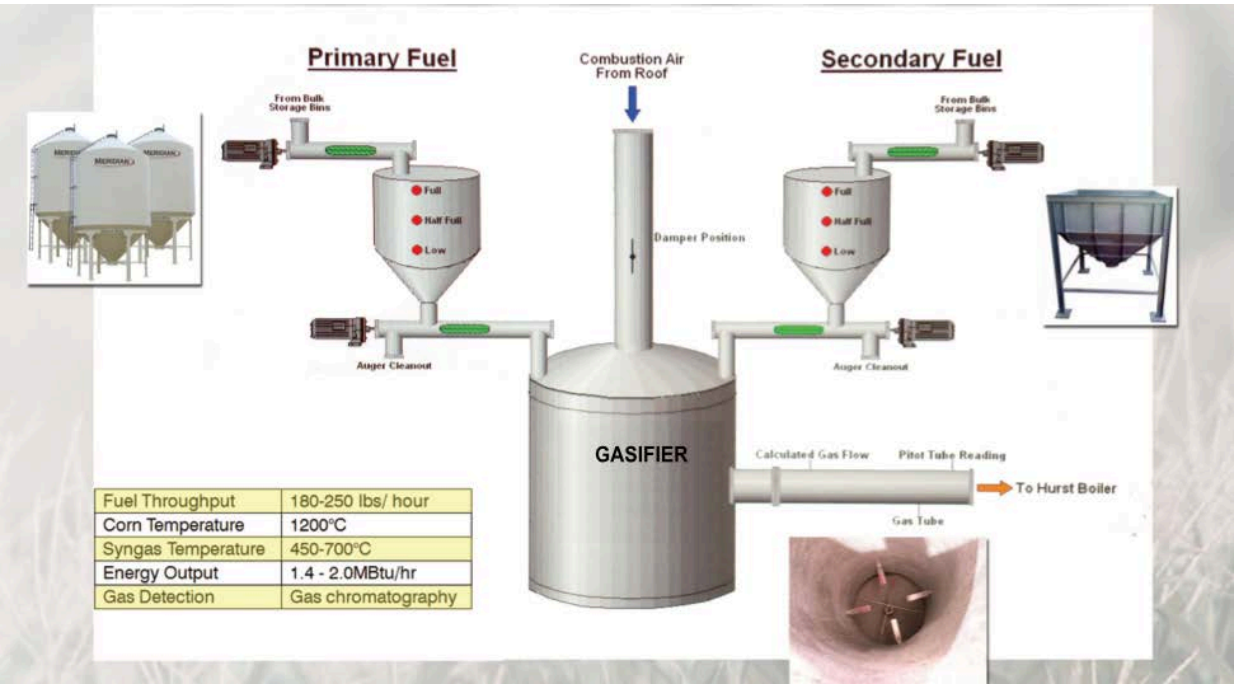

Figure 3.1: Oakdale pilot scale gasifier setup

The primary and secondary fuels are located externally from the main gasifier. Fuel from the primary and secondary bins are transported to a metering bin, using a spiral connected to a motor. This process is automated, and the operator can control the amount of fuel carried from both bins, using a control panel, located next to the gasifier. As such, the amount of fuel in the metering bin is carefully measured and monitored before inserting the fuel into the gasifier. Once the gasifier is running and has attained a steady state, most of the syngas produced from the gasifier exit into a boiler. At steady state, part of this syngas is collected for testing purposes by either using a probe or an outlet, located on the pipe that connects the gasifier to the boiler. Once syngas is collected, it is passed through a tar filtering system, and its gas components are tested, using gas

chromatography (GC). Our pilot-scale gasifier at Oakdale is made up of several essential parts. These are:

Primary and secondary fuel storage

One of the advantages of our pilot scale gasifier is its ability to combine two or more different types of biomasses at the same time. Our first bin (in Figure 32) is filled with corn and can hold up to three tons of corn kernels. The primary fuel bin is connected to a dust collector.

There are two secondary bins (as shown in Figure 33). Each of them contains a grid to allow biomasses of up to 2x2 inches diameter to go through. The size of the fuel plays a critical role. A size of up to 2x2 inches can easily be carried from the bins to the gasifier, using spirals. Spirals (example in the figure below) were chosen specifically for this task because they can easily transport biomasses of different sizes and densities from one location to another without getting clogged.

Figure 3.2: Auger spirals

Figure 3.3 Primary Fuel Bin

Figure 3.4: Secondary Fuel Bin

Primary and secondary Metering bin

To assure that the biomass entering the gasifier is metered, the biomasses are temporarily stored in a primary and secondary bin. Each of these bins can withhold a weight of 250 to 300 lbs. per biomass material type. These metering bins are located on the top of the gasifier.

Gasifier

Our pilot-scale gasifier is a downdraft gasifier. In a common downdraft gasifier design, air is inserted into a gasifier from the sides, but in our system, air is inserted from the top. As such, fuel and air "co-flow" in the same direction. There is a damper on the top of the gasifier that is used to control the amount of airflow entering the system. Our pilot-scale gasifier has an outer diameter of 45.5 in., is 101.5 inches tall, and is made up of mild steel [49]. Inside of it, there is a fire tube and an adjustable turntable. The turntable, as seen in Figure 34, rotates one revolution every four minutes, and is used to assure an even temperature at the bottom of the fire tube. On the sides of the gasifier, there are four fingers, which are used to mix the fuel inside of the gasifier, and also to maintain an even temperature. The syngas produced goes into a boiler, where it is combusted. The driving force on this syngas is the boiler's blower, which creates a vacuum, causing a draft of air into and through the gasifiers [49]. There are two thermocouples mounted on the gasifier. One thermocouple is on the pipe that transports the syngas into the boiler, and the second is on the top of the gasifier.

Figure 3.5: Outer view of the gasifier in Oakdale

Figure 3.6: View inside of the gasifier (bottom view-left, and top view-right)

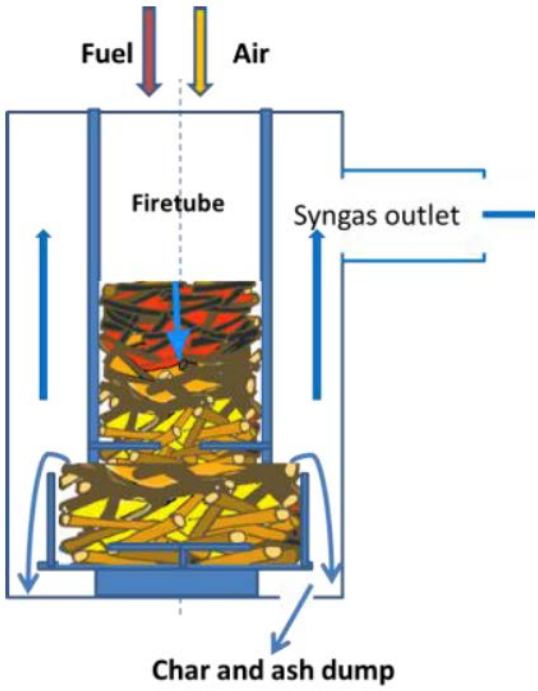

Figure 3.7: Schematic of the UI downdraft gasifier

When the biomass enters the system from the top, it passes through a drying zone, pyrolysis zone, combustion zone, and a reduction zone. The char produced from the gasifier falls through the bottom of the gasifier, and is transported to the storage bin using an auger, driven by a motor. Further details on the gasifier are listed in Appendix 1.

Probe

To more accurately study the different temperature variations in the layers produced in the gasifier, a K-type thermocouple is inserted at the tip of the probe. This probe is 60 in. long, and can be moved to different heights within the gasifier. The bottom of the probe has two holes that can be used to absorb in the syngas at the different zones using a pump.

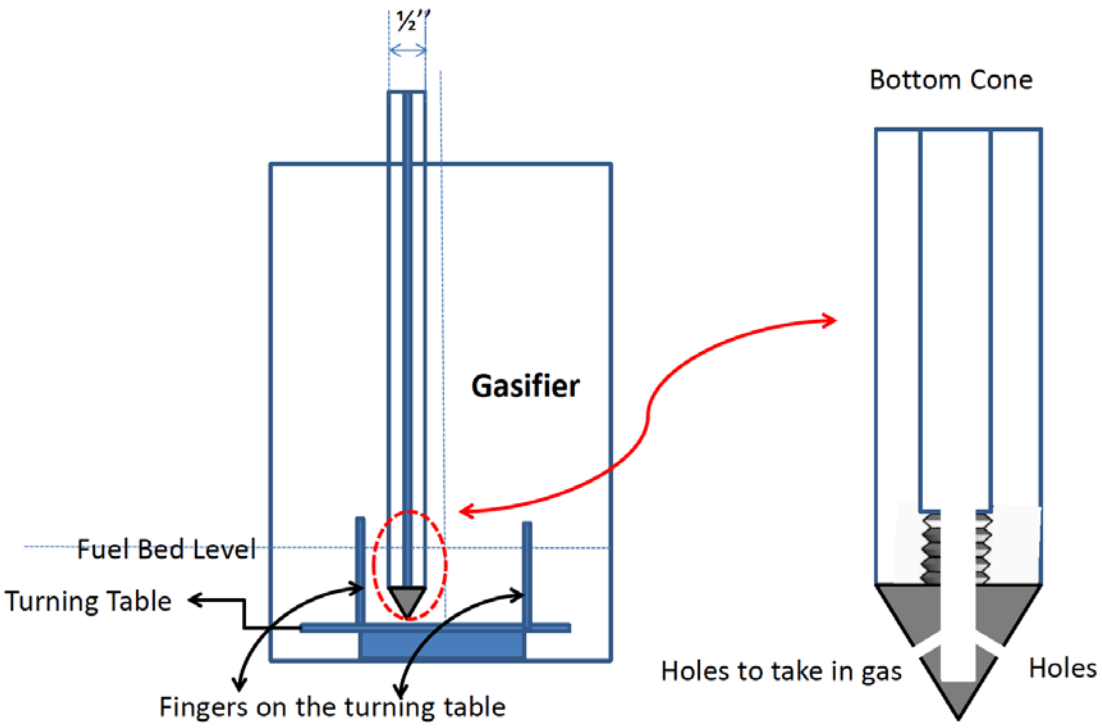

Figure 3.8: Schematic of the probe

Burner

A burner is located at the top of the gasifier. It runs on natural gas, and is used during the first six minutes of operation to heat the system. The burner can be controlled using a control panel, or used manually.

Pump

A pump is used to suck the syngas produced from the gasifier. This gas passes through a filtering system, where impurities, such as tar, are removed. The cleaned gas is collected in gasbags, or can be directly connected to a gas chromatography.

A detailed list of equipment and their dimensions can be seen in Appendix 1.

Tar removal system

One of the byproducts of gasification is tar. For the syngas to work directly in equipment, such as gas turbines and the combustion engine, it is essential to reduce the tar level present. The syngas from the gasifier is extracted using a probe, and its flow is controlled using a flow meter. This helps assure a stable flow. The syngas is then passed through six sets of impingers, five of which contain approximately 100 ml of isopropanol each, and the sixth one is left empty. The fifth and sixth impingers are placed in an ice bath of temperatures of about -20 °C. This is done to assure that any condensable gas-containing tar and moisture is condensed. The flow rate is kept at 60 cfm for about three minutes.

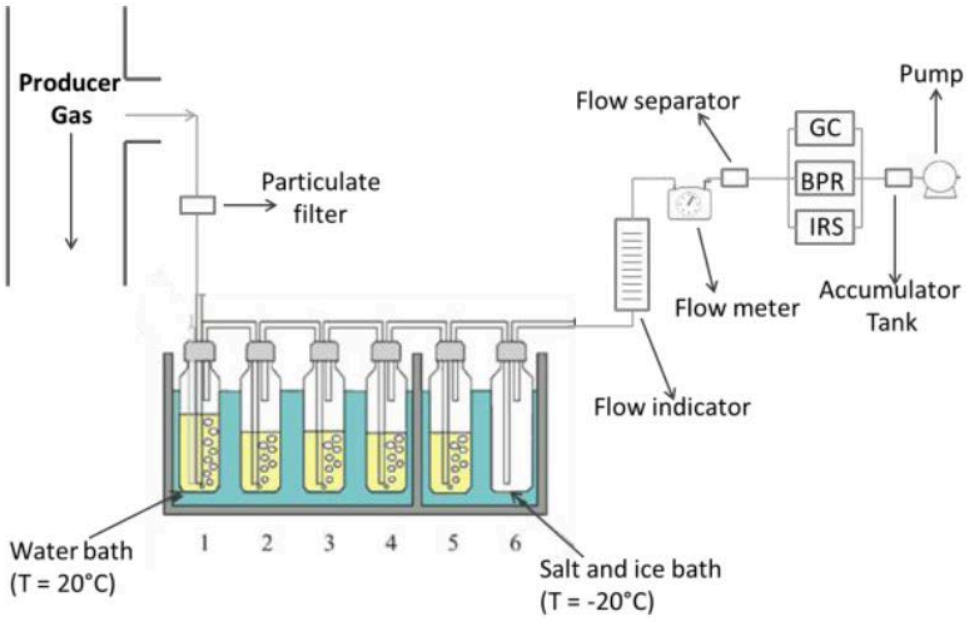

Figure 3.9: Tar collection system

Gas Chromatography machine

The gas chromatography (GC) machine in our lab is an Agilent 490 micro GC. This GC is made up of four columns, but we currently use two for testing purposes. The first column uses Argon as a carrier gas and can measure major gases, such as He, H_2, O_2, N_2, CH_4, and CO. The second column uses helium as a carrier gas, and measures CO_2 and various CxHy compounds (such as C_2H_4, C_2H_6).

The clean gas that goes through the tar mentioned above collection system is fed into the GC. The GC absorbs the sample gas for 30 seconds, and analyzes the different gas components present—the sample gas's thermal conductivity is matched with the thermal conductivities of the carrier gases (helium and argon). Calibration of the GC is necessary if the gas peaks are unaligned (therefore are in accurate). The inaccuracy in a GC's results may usually be due to moisture content. When the GC is not used for at least two days, the "bakeout mode" setting is used to remove any moisture contents present in the GC.

Experimental procedure

Before starting the experiments, the following steps should be taken:

1) A physical check must be done. The operator, using a ladder, should inspect the top of the gasifier. The operator should make sure that all wires are connected, and also be made sure that no external objects, such as a wrench or screwdriver, is present on the top of the gasifier because injuries may occur as a result.

2) The natural gas line connected to the burner should be checked. For safety reasons, the Oakdale Power Plant engineers sometimes close the natural gas line. It is essential to make sure it's open when running the burner connected to the gasifier.

3) It should be made sure that the gate at the bottom of the primary fuel bin is open. This is especially important during the winter season. Due to freezing condition, the moisture present in the biomass (corn) tends to solidify. This causes the motor that enables the fuel to move from the storage bin to the gasifier to be stuck. To avoid this, the gate at the bottom of the bin is closed during non-operating hours.

4) Before starting the gasifier, the operator should ask for permission from the power plant engineers to run it and should request a negative pressure of 0.3 WC from the boiler. This negative pressure takes care of moving the syngas from the gasifier to the boiler.

5) Most of the operations on the gasifier are done using a control panel. There are mainly four steps that have to be followed. These include: start-up mode, steady-state mode, burn down mode, and shut down mode.

The start-up mode begins with the following actions on the control panel:

1. Start long char/ash auger motor (to a receptacle outside the building)
2. Start airlock motor
3. Start short char/ash auger motor (under gasifier)
4. Start gasifier turntable motor.

5. The slide gate between the boiler and the gasifier should be open. This is very important in order to reduce any chances of overheating and internal pressure accumulation from happening.

These settings are found on the right side of the panel, as seen in Figure 3.10.

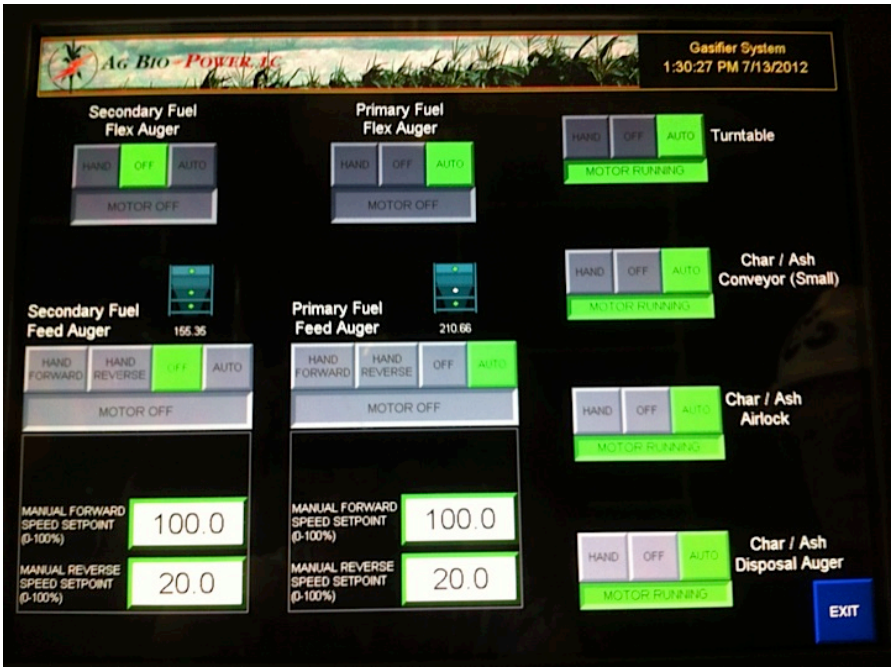

Figure 3.10: Screen shot of the control panel

From there, the fuel is loaded into the primary bin, and its level is monitored. The temporary bin can store up to 300 lbs. of fuel. Using the start-up mode, on the control panel, the damper is opened to 100%. The airflow is monitored. About 50 lbs. of primary fuel (corn) is inserted in the gasifier. The airflow entering the gasifier is monitored.

Once the gasifier is loaded with fuel—about 50 to 100 lbs to start with, the burner is turned on for 600 seconds or 10 minutes. The burner may run for a couple of times until a temperature of above 400 °F is reached. The temperature of the gasifier is closely monitored to ensure the proper

functioning of the burner. If no temperature increase is noticed within the first two minutes of running the burner, the burner is reset, by using both the control panel and manually. The syngas flow is also closely monitored throughout the process.

About 20 lbs. of fuel or more is inserted until a steady-state operation is achieved, as shown in Figure 40. The temperature in a gasifier is controlled using the amount of fuel inserted, and the damper.

It takes approximately 90 minutes to two hours to reach steady state, depending on the moisture content of the fuel. During this period, the char bin is checked a number of times to assure a smooth flow of fuel within the system. At steady state, fuel is inserted when a temperature decrease is observed, as shown in Figure 40.

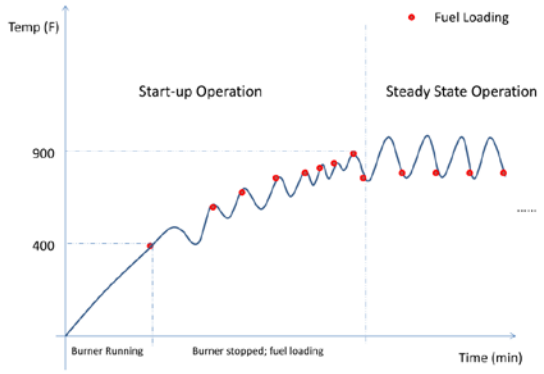

Figure 3.11: Start-up and steady state fuel loading

Once steady state is achieved, gas samples are collected, both from the probe and from the gasifier outlet. These outlets can be switched using a flow valve.

To collect the gas, one of the operators needs to climb to the top of the gasifier and adjust the height of the probe. As such, different temperatures and different gas samples can be obtained

within the different zones of the gasifier. The controller needs to make sure to stop the turning table, located at the bottom of the gasifier. This is done to avoid breaking the rotating fingers, situated at the bottom of the gasifier. Once the ideal location of the probe is set, the gas is extracted using a pump. The gas flows through a flow meter, where the flow rate is adjusted and stabilized. The gas is then circulated through a set of impingers, containing isopropanol, to remove any tar and impurities present in the gas. The clean gas, from the impingers, is then flowed through gas chromatography, where the composition of the gas is analyzed. These measurements are repeated two times at different probe locations.

After running the system for some hours at steady state, the following steps are taken to shut down the gasifier.

No fuel is loaded into the system, and the temperature drop is monitored. Once the temperature falls below 500 °F, the air damper is slowly opened. When the temperature falls down to 350 °F, the slide gate, linking the gasifier to the boiler, is closed, and the auger, transporting the char from the bottom of the gasifier, is run for another thirty minutes. The turntable, ash auger (short), ash airlock, and ash auger (long) are closed in this order. The main red switch, located under the control panel, is pulled to shut off the system [49].

Although the gasifier may work smoothly, some problems were encountered when running the gasifier. Here are some of those problems, and the steps that we took to solve them.

One of the problems we face with the pilot scale gasifier is overheating. After many trials and errors, we realized that the chute, connecting the bottom of the gasifier to the char auger, caused char to be stuck. This was because the chute was narrow and bent. This refrained the smooth flow of char, which led to high temperatures.

Material used

The primary material used for one stage gasifier was corn, wood pellets and refused derived waste (RDF). The ultimate and proximate analysis table can be seen below: Corn grains were used due to their high availability, while wood pellets were used because of uniformity. Refused derived waste pellets are currently been tested by the University of Iowa main power plant to replace coal. RDF is composed of 35% plastic which is used as a binder and rest is a mixture of cardboard and paper. From table 5.1 and 5.2, we can see that the amount of fixed carbon of corn, soybeans, and wood is similar while that of RDF is the lowest. The amount of Sulphur content in all fuels is less the 0.5%. Figure 3.11 shows the physical structure of the fuel.

Figure 3.12: Fuel used for testing – Corn, soybeans, wood pellets and RDF

Table 3.1: Proximate analysis of fuel

	Corn grain	*Soybeans	Wood pellets	Refused derived waste (RDF) Pellet
Volatile Matter	66.63	82.40	74	63.71
Fixed Carbon	17.15	13.27	16.6	7.53
Ash	1.4	4.34	0.43	28.71
Total	100%	100%	100%	100%
HHV	8500 btu/lb	10160 btu/lb	13900 btu/lb	8759 btu/lb

Table 3.2: Ultimate analysis of fuel

	Corn grain	*Soybeans	Wood pellets	Refused derived waste (RDF) Pellet
Carbon	40.07	64.77	47.52	43.28
Hydrogen	7.1	7.79	6.5	14.40
Nitrogen	1.4	7.64	0.05	1.09
Sulfur	0.17	0.32	0.1	0.19
Oxygen	50.5	15.15	42.0	12.32
Total	100%	100%	100%	100%

*Soy beans were used for char testing only

3.2 Double stage gasification system and experimental configuration (Brazil)

The downdraft gasifier used in this experiment (seen in Figure 3.13 and 3.14) was designed and manufactured by Termoquip Renewable Energy, based in Campinas, São Paulo, Brazil. The gasifier is made of carbon steel material, and has a height of 1.06 m and an inner diameter of 0.3 m. This gasifier was primarily built to test wood and other carbonaceous materials to produce tar amounts of less than 35 mg/Nm^3, and to limit particulate matter to less than 10 mg/Nm^3 [50,19,3].

There are 6 K-type thermocouples placed on the inner wall of the gasifier. The approximate sensitivity of the thermocouples is 41 μV/°C. These thermocouples have been strategically placed on the inner wall of the reactor to avoid any interference with the flow of the biomass.

Two vibration devices were installed: one at the top of the gasifier and the other at the bottom. This was done to ensure a homogenous distribution of the biomass within the system. The vibration device located at the bottom of the gasifier helps to discharge the ash produced. The cleaning system attached to the gasifier is comprised of a cyclone, a heat exchanger, and a bag that contains filters. A floating-drum gas storage recipient which absorbs the pressure variation in the producer gas is installed to maintain pressure throughout the gasifier [3][52].

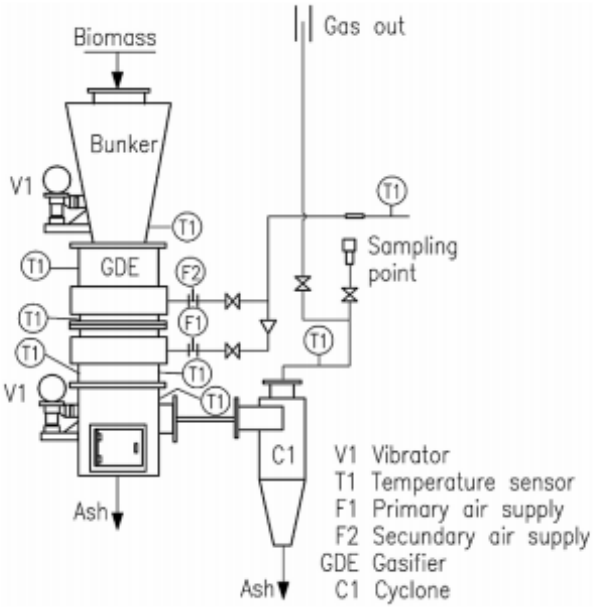

Figure 3.13: Gasification system flow diagram

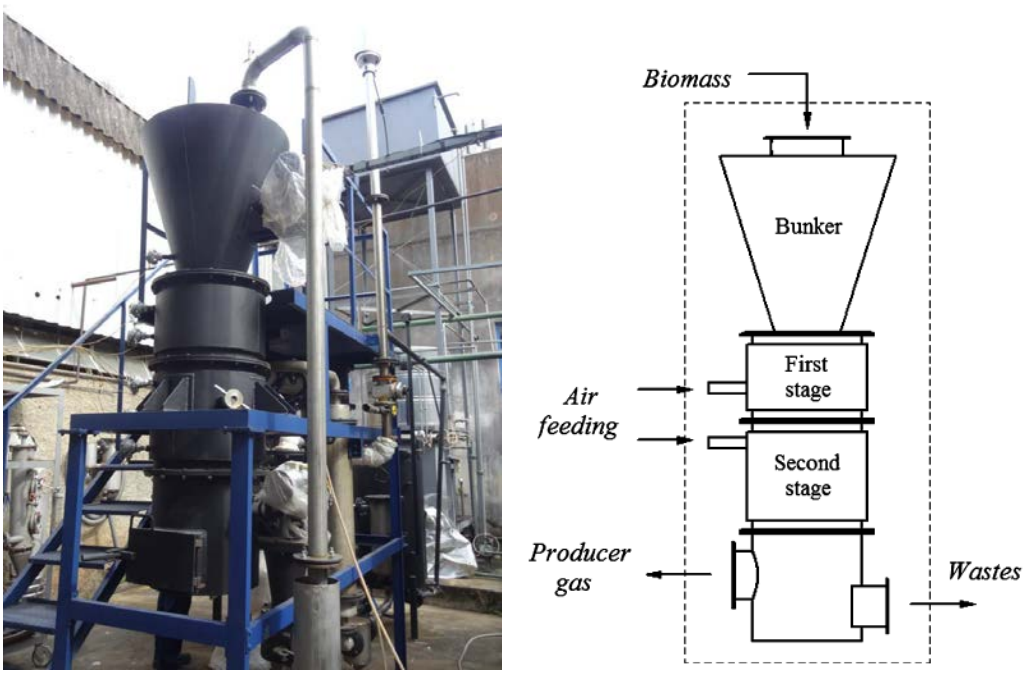

Figure 3.14. (a)Downdraft Gasifier and (b) schematic

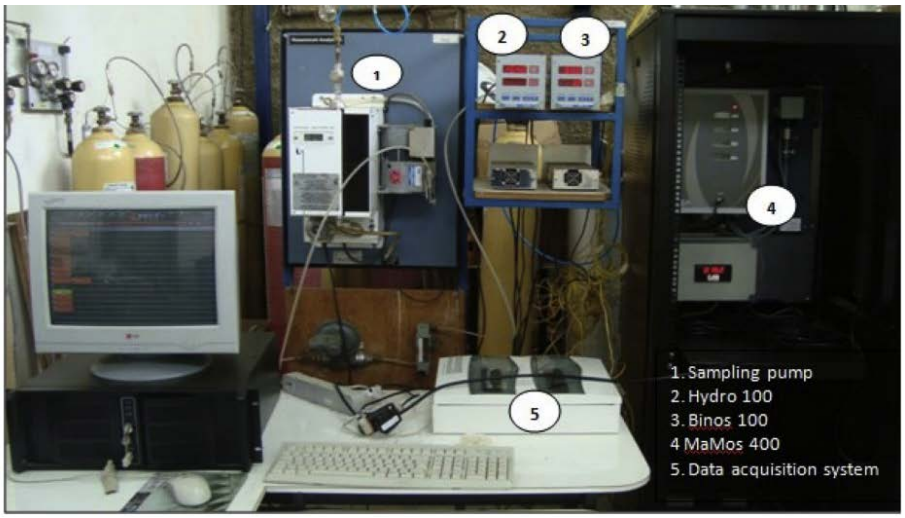

Figure 3.15: Equipment used to determined syngas compositions

Setup and procedure

Biomass gasification starts with preheating the bed by using an external burner. The reactor is heated up to 250 °C (temperature at the combustion zone in the inner wall of the reactor). Once this temperature is attained, air is fed into the gasifier. Quasi-stoichiometric combustion conditions (around 4 Nm^3/kg) are adjusted, reaching a bed temperature (in the combustion zone) of around 800–850 °C. Airflow values are obtained through flow measurement by an orifice plate and a control valve for each stage. The total desired air flow was obtained using a combination of air entering in both the first stage and second stage. The average total air flow was 24 $Nm^3\ h^{-1}$. Once a steady state is attained, the operating conditions and outputs are recorded. The resulting biochar and tar are then collected. Once steady state is attained, the operating conditions and data are recorded. The resulting biochar and tar are then collected.

The total air flow and the air ratio (AR) between the primary and secondary stages were controlled in this experiment. The following variables were measured:

- The temperature in the different gasifier zones.

- CO, CH_4, and H_2 concentrations of the producer gas using the gas analyzer systems: BINOS 100, and HYDROS 100 (Emerson Process Management, Hasselroth, Germany). The uncertainty of BINOS 100 is ±0.2%, while that of HYDROS 100 is ±0.01%
- The syngas content for equivalence ratio between 0.2 to 0.45
- The biochar surface area was analyzed using a Nova 4200 instrument and a Hitachi S-4800 SEM instrument (Emerson Process Management, Hasselroth, Germany).
- Tar was collected using a set of six impingers, five of which contain isopropanol at a temperature of less than 0 °C. The average tar collected at steady state and content is obtained in mg/Nm^3

Material used

The material used here is Miscanthus. The University of Iowa power plant which has been testing different types of biomasses to produce electricity, and have been particularly interested in using Miscanthus as a potential fuel source. According to the studies done by Wildom et al., high yielding Miscanthus could require 87% less land to produce the same amount of yield as other low input biomasses [53]. This biomass has low water and nutritional requirements and can grow on barren land with little fertilization needed [54]. Studies also show that Miscanthus has a higher yield of up to 40 Mg/ha, compared to other similar grass, such as P.virgatum (switchgrass), which was found to produce 20 Mg/ha [55].

For the experiment in this section, Miscanthus briquettes were obtained from Bripell, a local biomass supplier located in Ipassu, Brazil. The biomass briquettes, as seen in Figure 18, had a diameter of 3 X 2 cm. These were tested in the double-stage downdraft gasifier. The biomass

moisture and heating value were measured in the NEST laboratory, using a calorimeter pump IKA, Series C2000, which operated at 25 °C for seven minutes. The proximate and ultimate analyses of Miscanthus were determined by a CHNSO analyzer from Perkin Elmer, Series II 2400 (using the ASTM D5373-08 standard), and a thermogravimetric analysis from LECO Systems, ref. LECO 701 (using the ASTM D 317x standard). The results of the proximate and ultimate analyses can be seen in Table 9.

Figure 3.16: Miscanthus Briquettes

Table 3.3: Proximate and ultimate analyses of Miscanthus (wt. %)

Proximate analysis		Ultimate analysis	
Moisture	11.56 %	Carbon	48.6 %
Volatile Matter	67.15%	Hydrogen	6 %
Fixed Carbon	16.88%	Nitrogen	0.27 %
Ash	4.41	Sulfur	0.07%
Total	100.00%	Oxygen	45.06 %
HV[MJ/kg]	16.257	Total	100%

4. SINGLE STAGE SYNGAS RESULTS

Syngas results used from a one stage gasifier were analyzed. The fuel tested were corn, wood pellets and refused derived waste (RDF). Corn grains were used due to their high availability, while wood pellets were used because of their uniformity. Refused derived waste pellets where tested due their increased interest by the University of power plant to replace coal.

Temperature profile

Previous results from showed the temperature profile obtained from the downdraft gasifier system as seen below:

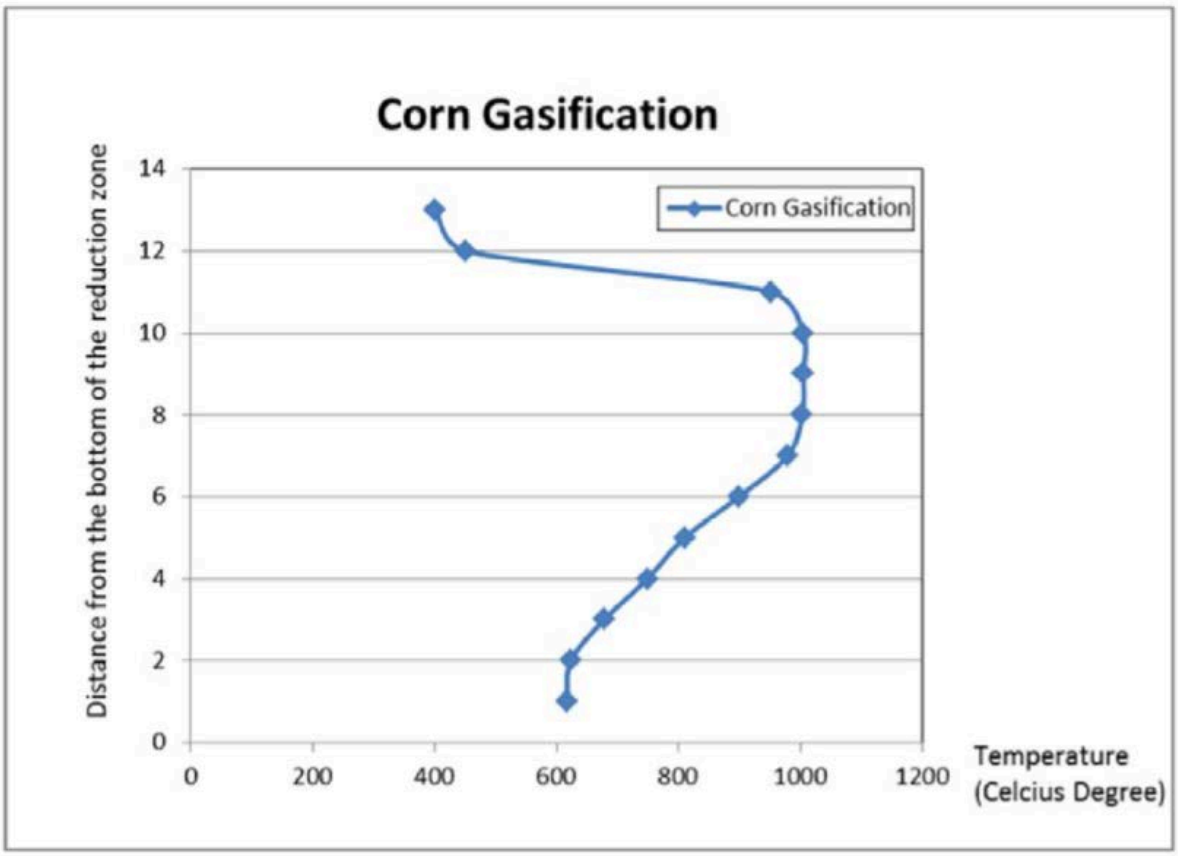

Figure 4.1: Temperature profile in a downdraft gasifier

The data was obtained approximately between an equivalence ratio of 0.25 to 0.3 with an approximate airflow rate of $0.1m^3/s$. The approximate temperature in the combustion zone was about 1000 degrees Celsius. The average fuel feeding rate was 50 – 75 lbs. / hour.

Coated seed corn is used as the initial fuel to build up char in the gasifier. Once steady state has been achieved and the gas for the fuel has been obtained, woodchip is inserted into the system followed by refused derived waste pellets.

The syngas output can be seen in Table 4.1

Table 4.1: Syngas content from different fuel

Fuel	CO%	H%	CO_2%	CH_4	C_2H_4
Corn	5.01	2.18	6.87	1.21	0.45
Wood Chips	8.21	2.56	10.53	1.89	0.34
Refused Derived Waste	8.4	3.85	11.3	2.14	0.3

From the data observed, it is seen the highest CO and H_2 content was obtained from Refused derived waste pellets, followed by woodchips and corn. One of the possible reasons for the high CO and H content from the RDF is the plastic coating of the fuel which burn quickly and hotter than the other fuels. This would also explain the high CO_2 content from RDF when compared to the fuels.

Table 4.2: Biomass components of different fuel.

	Hemicellulose	Cellulose	Lignin	ash
Waste Material	29.2	50.60	24.70	4.50
Hardwood	31.30	45.30	21.70	2.7
Corn grain	5.5	2.4	0.2	1.4

It appears that the fuel material with the highest amount of cellulose led to the highest amount of CO as some previous of having shown, however, the waste material RDF which also has the highest amount of lignin also led to a relatively higher amount of Hydrogen content. This is consistent with the study done by Yang et al [36].

We see that the Hemicellulose, cellulose and lignin content of waste material (RDF) is similar to that of hardwood. Although physical, both fuels may look different, the similarity of these three major components (hemicellulose, cellulose and lignin) may explain where resulting Hydrogen and Carbon monoxide results are close to one another.

5. SINGLE STAGE BIOCHAR RESULTS

Ultimate and proximate analysis, the Brunauer-Emmett-Teller (BET) surface area and scanning electron microscopy (SEM including X-ray) surface area studies were carried on corn, soybean, wood and refused derived waste pellets. This section discusses the findings.

5.1 Ultimate and proximate analysis

The ultimate and proximate analysis of the biochar were done in a lab called keystone material testing in Newton, Iowa. The used ASTM standards D291 AND D7582 to carry the analysis on these chars. Tables 5.1 and 5.2 show the ultimate and proximate analysis of all biochar fuel. It can be seen that biochar from corn, soybean, and wood all had high fixed carbon content while the char from RDF was very little. The highest carbon content observed was in wood with 91% fixed carbon. Part of the reason for the low content carbon content comes from the original fuel as shown on table 5.1. The original fuel just contained 7% fixed carbon to begin with. The original RDF pellet fuel is known to be made up of 35% plastic and the rest of it is cardboard and paper. Most of the paper and plastic is believed to have combusted leaving traces of plastic and this may explain why there is such as a little amount of carbon present in the biochar output from RDF fuel. This can visually be seen from the SEM microscope in section 5.3. The amount of Sulphur obtained from the biochar appears from the different fuels are under 0.05%.

Table 5.1: Proximate analysis of biochar and RDF pellet

	Corn grain Char	Soybeans Char	Wood pellets Char	Refused derived waste (RDF) Char	Refused derived waste (RDF) Pellet
Volatile Matter	5.37	32.41	6.00	0%	63.71
Fixed Carbon	73.39	49.79	91.53	0.10	7.53
Ash	21.23	17.85	2.47	<100	28.71
Total	100%	100%	100%	100%	100%
High heat s	10620 btu/lb	11250 btu/lb	13900 btu/lb	N/A	8759 btu/lb

Table 5.2: Ultimate analysis of biochar and RDF pellet

	Corn grain Char	Soybeans Char	Wood pellets Char	Refused derived waste (RDF) Char	Refused derived waste (RDF) Pellet
Carbon	71.54	65.67	89.43	0.42	43.28
Hydrogen	<0.50	5.97	<0.50	0.79	14.40
Nitrogen	2.31	4.33	0.71	< 0.2	1.09
Sulfur	0.04	0.15	0.04	0.13	0.19
Oxygen	5.17	15.87	7.49	< 0.10	12.32
Total	100%	100%	100%	100%	100%

5.2 Bet surface analyses

A Brunauer-Emmert-Teller (BET) analysis provides a precise, specific, surface evaluation of materials by gas multilayer adsorption. A Nova 4200 instrument was used to calculate the specific area of the biochar. In a Nova 4200, a nitrogen adsorption method was used. The degassing temperature of 150 °C and degassing time of 10 hours were set. Table 5.3 shows the summary of all the surface areas produced. We see that the largest surface area that was found was that of wood biochar at 92 m^2/g while the lowest surface area after was for refused derived waste. The surface area of corn and soybean were similar. This test shows that the refused derived waste biochar is much less porous. Typical biochar surface area from gasification systems have ranged between 0 – 64 m^2/g [19].

Table 5.3: Surface area analysis results

Biochar	**Surface area (m^2/g)**
Corn Biochar	22.8
Soybean Biochar	22.4
Wood Biochar	92.4
Refused derived waste biochar	0.75

5.3 Scanning electron Microscope and electron dispersive X-ray analysis

Scanning electron microscopy and an electron dispersive X-ray analysis was on all four biochar. Using the scanning election microscope, the pore areas and structure was analyzed and using the X-ray analysis, mineral content of biochar was analyzed. This is important as these are the first mineral analysis obtained from our downdraft gasifier. There are not many studies that examine the surface morphology from a one stage downdraft gasifier, and examine the metal and mineral presence and dispersion within the char.

In the following paragraphs, the surface structure and its mineral content is examined on corn, soybeans (inner and outer surface), wood char (inner and outer surface) and refused derived biochar. As mentioned earlier, the refused derive waste fuel contains 35% plastic which as a binder. This will further be examined below.

As shown in figure 5.1, Corn biochar from our downdraft gasifier has a wide range of pores opening. These openings range between 20 – 200 Micrometers. The first round of X-ray analysis as shown below showed traces of elements other than carbon. Potassium (K) and phosphorus mineral were found on the surface area of the char of 31.7% and 9.6% respectively. To understand where these particular mineral were located, different regions where examined. As seen in figure 5.1 it was observed that these mineral were located next to the pores. Figure 5.2 and 5.3 show a mineral content deposit next to the pore with high concentration of potassium and phosphorus at 67.4% and 13.4 %. An initial Scan was of porous areas on the corn surface was taken and mineral next to the pores were analyzed.

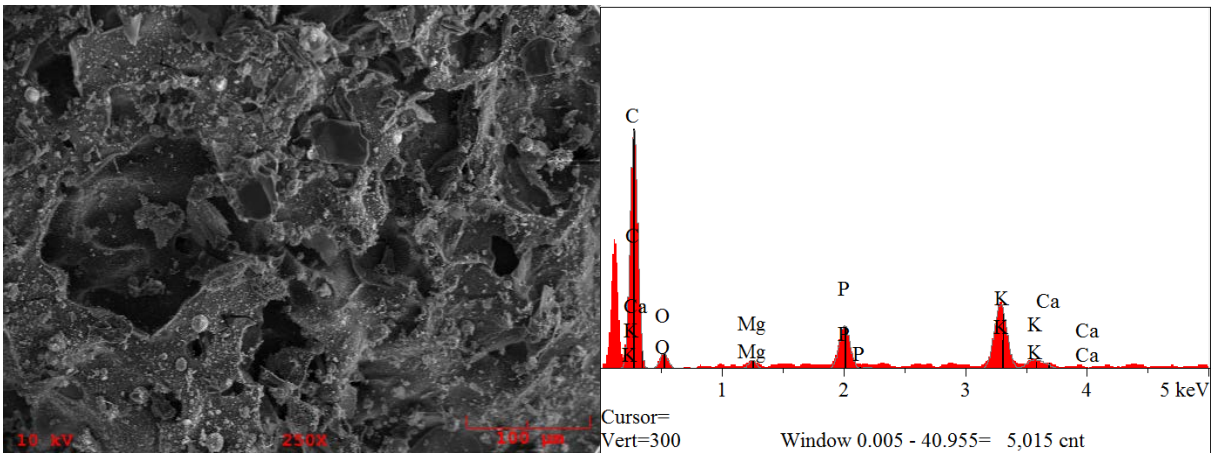

Figure 5.1: Surface area analysis from Corn biochar

Table 5.4: Surface area analysis from Corn biochar

Elt.	Line	Intensity (c/s)	Atomic %	Conc	Units	Error 2-sig	MDL 3-sig	
C	Ka	1,574.05	69.683	46.901	wt.%	0.100	0.053	
O	Ka	112.04	7.865	7.052	wt.%	0.218	0.026	
Mg	Ka	60.49	0.855	1.164	wt.%	0.065	0.006	
P	Ka	392.49	5.543	9.621	wt.%	0.096	0.021	
K	Ka	684.00	14.495	31.761	wt.%	0.195	0.051	
Ca	Ka	60.45	1.559	3.502	wt.%	0.258	0.022	
			100.000	100.000	wt.%			Total

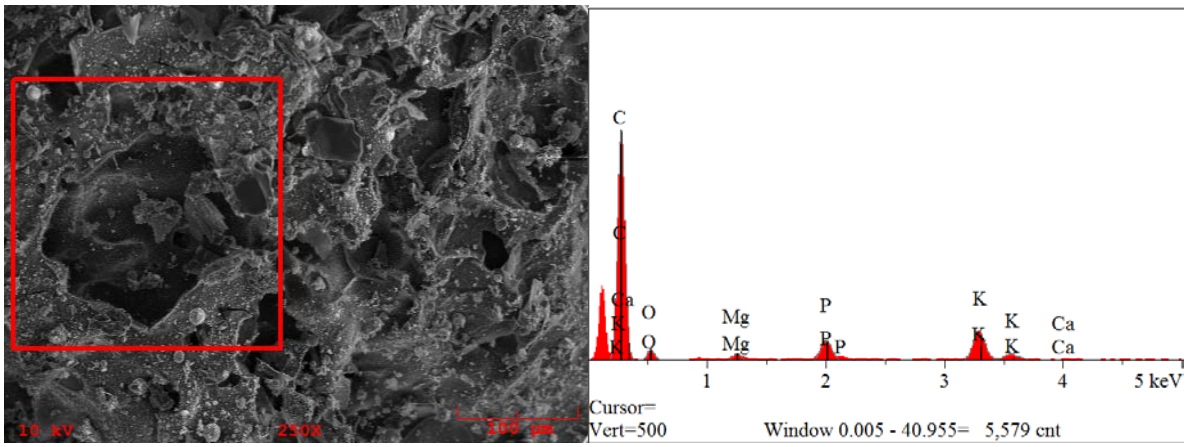

Figure 5.2: Surface area analysis from Corn biochar (Pore region)

Table 5.5: Surface area analysis from Corn biochar (Pore region)

Elt.	Line	Intensity (c/s)	Atomic %	Conc	Units	Error 2-sig	MDL 3-sig	
C	Ka	2,498.81	78.820	60.062	wt.%	0.084	0.054	
O	Ka	122.45	6.734	6.835	wt.%	0.184	0.025	
Mg	Ka	89.34	0.991	1.528	wt.%	0.060	0.007	
P	Ka	323.28	3.632	7.137	wt.%	0.089	0.017	
K	Ka	518.93	8.737	21.675	wt.%	0.174	0.041	
Ca	Ka	53.75	1.086	2.762	wt.%	0.233	0.016	
			100.000	100.000	wt.%			Total

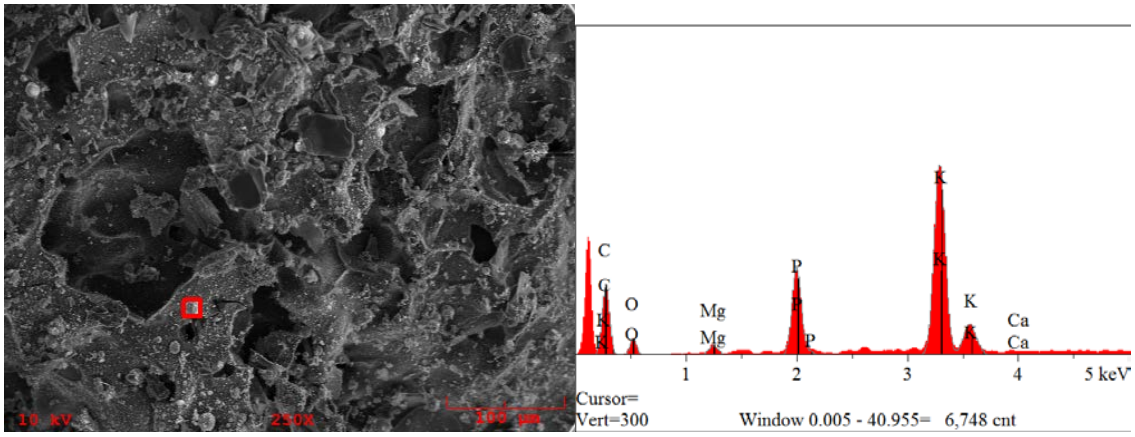

Figure 5.3: Surface area analysis from Corn biochar (Mineral spot)

Table 5.6 Surface area analysis from Corn biochar (mineral spot)

Elt.	Line	Intensity (c/s)	Atomic %	Conc	Units	Error 2-sig	MDL 3-sig	
C	Ka	507.83	28.270	12.058	wt.%	0.080	0.024	
O	Ka	112.10	9.015	5.122	wt.%	0.148	0.020	
Mg	Ka	92.23	1.436	1.240	wt.%	0.052	0.005	
P	Ka	810.11	12.224	13.446	wt.%	0.063	0.021	
K	Ka	2,143.28	48.556	67.424	wt.%	0.130	0.063	
Ca	Ka	17.32	0.500	0.711	wt.%	0.147	0.018	
			100.000	100.000	wt.%			Total

Other corn surface areas were examined, and traces of magnesium, aluminum and silicon were found. As shown in the figure below, high contents of potassium and phosphorus where found at 41.2% and 16.95%. The traces of magnesium, aluminum and silicon were under 4%. Other regions as shown in figure 5.4 and figure 5.5 also showed a similar trend with 21.8% K and 14% Phosphorus. It appears that major concentration of phosphorus and potassium is located next to pore openings.

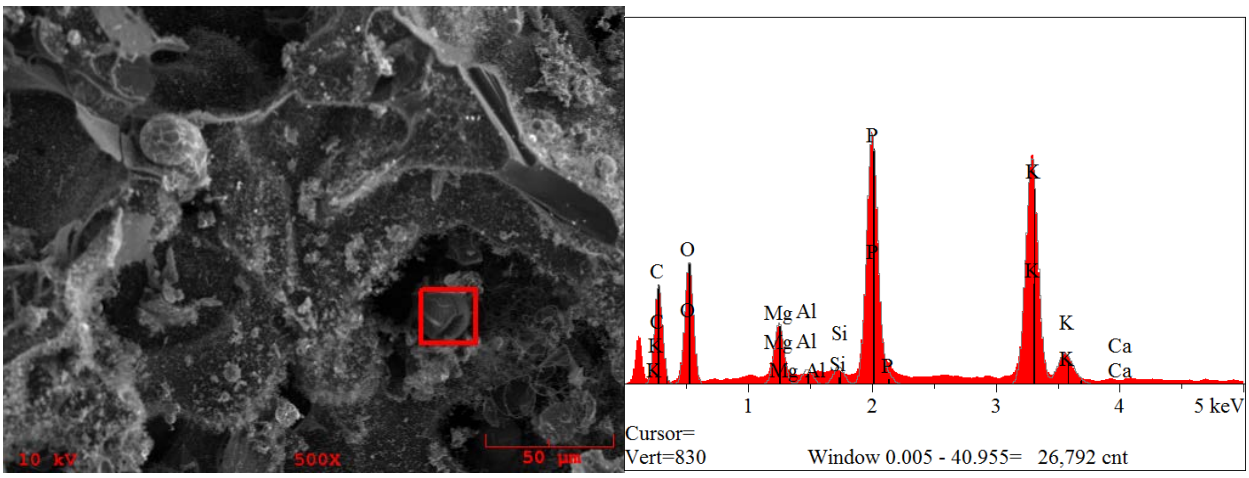

Figure 5.4: Surface area analysis from Corn biochar (Mineral analysis -2)

By testing different regions on the corn biochar analysis, it is seen that concentration of Potassium is higher than that of Phosphorus in different regions. We also see the mineral deposit such as phosphorus and potassium to be located closer to the porous region of the char. Potassium and phosphorus are known to be in fertilizers. Figure 5.5 examines a specific area on the biochar pore which showed traces of aluminum and silicon but had a high concentration of phosphorus and potassium.

Table 5.7: Surface area analysis from Corn biochar (Mineral analysis -2)

Elt.	Line	Intensity (c/s)	Atomic %	Conc	Units	Error 2-sig	MDL 3-sig	
C	Ka	1,783.33	24.599	12.233	wt.%	0.025	0.013	
O	Ka	2,326.63	26.643	17.649	wt.%	0.026	0.015	
Mg	Ka	1,323.89	3.575	3.598	wt.%	0.010	0.004	
Al	Ka	358.98	0.916	1.023	wt.%	0.011	0.002	
Si	Ka	424.02	1.088	1.265	wt.%	0.012	0.002	
P	Ka	6,236.03	16.950	21.737	wt.%	0.014	0.012	
K	Ka	6,264.27	25.476	41.245	wt.%	0.027	0.022	
Ca	Ka	151.64	0.753	1.249	wt.%	0.038	0.006	
			100.000	100.000	wt.%			Total

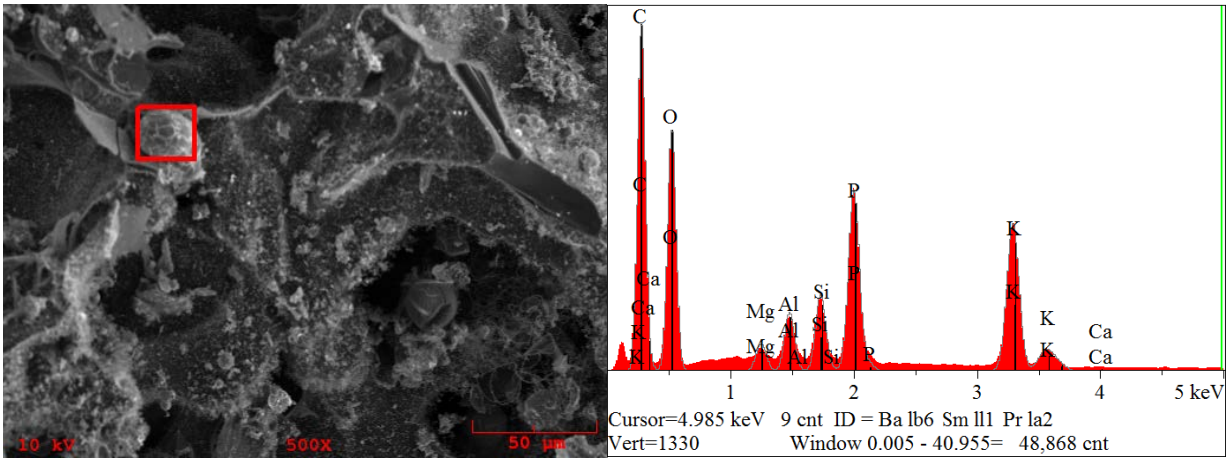

Figure 5.5: Surface area analysis from Corn biochar (Mineral analysis -3)

Table 5.8 Surface area analysis from Corn biochar (Mineral analysis -3)

Elt.	Line	Intensity (c/s)	Atomic %	Conc	Units	Error 2-sig	MDL 3-sig	
C	Ka	9,904.51	45.463	29.397	wt.%	0.011	0.013	
O	Ka	7,589.27	29.782	25.652	wt.%	0.012	0.012	
Mg	Ka	1,011.09	1.048	1.372	wt.%	0.005	0.002	
Al	Ka	2,127.72	2.060	2.992	wt.%	0.005	0.003	
Si	Ka	2,780.90	2.765	4.181	wt.%	0.006	0.003	
P	Ka	7,250.13	7.728	12.886	wt.%	0.007	0.006	
K	Ka	6,643.11	10.364	21.817	wt.%	0.014	0.011	
Ca	Ka	424.77	0.789	1.702	wt.%	0.019	0.004	
			100.000	100.000	wt.%			Total

Soy outside

A similar trend as that of corn was also observed on soybean biochar. The areas next to the pores contained higher amount of minerals as shown below. However, in contrast to corn biochar, traces of iron were found on the outer shell of soybeans. The concentration of potassium and phosphorus was found to be 17.1% and 14.48%. The concentration of iron was found to be 9.315%. A detailed examination x ray analysis of the minerals can be seen in figure 5.7 and 5.8. We see that the phosphorus deposits on the char closely matches that of potassium and oxygen. Figure 5.6 shows a mineral deposit next to various pores.

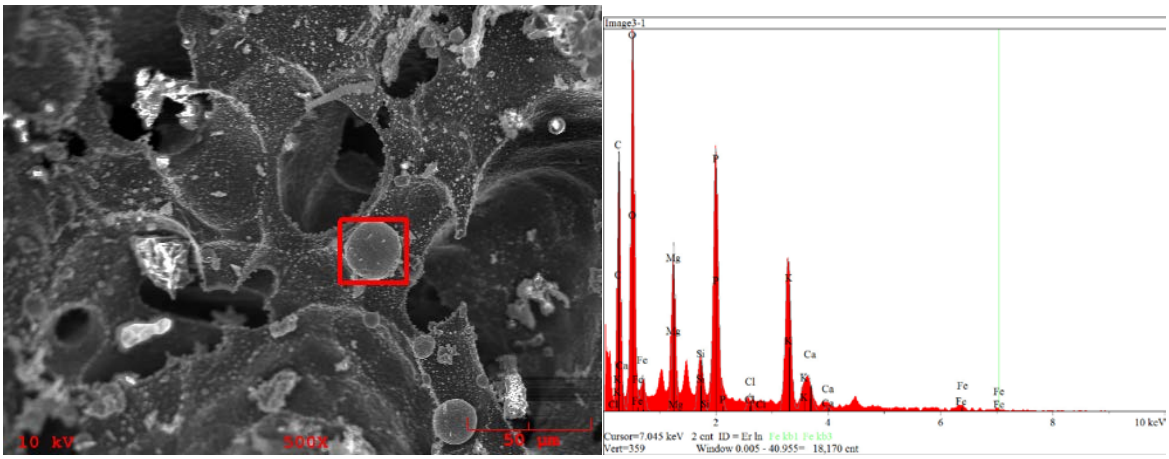

Figure 5.6 Surface area analysis from Outer soybean biochar

Table: 5.9 Surface area analysis from Outer soybean biochar

Elt.	Line	Intensity (c/s)	Atomic %	Conc	Units	Error 2-sig	MDL 3-sig	
C	Ka	1,881.21	31.634	17.921	wt.%	0.034	0.037	
O	Ka	3,078.13	35.496	26.787	wt.%	0.030	0.038	
Mg	Ka	1,273.89	4.631	5.311	wt.%	0.014	0.013	
Si	Ka	626.98	2.126	2.816	wt.%	0.017	0.009	
P	Ka	2,754.13	9.849	14.388	wt.%	0.021	0.023	
Cl	Ka	186.41	0.771	1.290	wt.%	0.027	0.008	
K	Ka	1,806.03	9.317	17.183	wt.%	0.040	0.034	
Ca	Ka	433.15	2.639	4.989	wt.%	0.052	0.021	
Fe	La	301.09	3.536	9.315	wt.%	0.127	0.045	
			100.000	100.000	wt.%			Total

Figure 5.7 and figure 5.8 shows in details the location of different minerals across the biochar surface. It is observed that the high amounts of carbon are present as it is would expected from a charcoal surface. However, we also observed nodules of mineral spread along the char surface. In figure 5.7 and 5.8, site A and site B represents the mineral deposits on the char. Site B shows the corresponding silicon nodule as show in figure 5.7. We see that potassium, phosphorus and oxygen appear in similar regions by comparing site A Site B it is observed that the location of silicon doesn't match with other elements. The two-nodule created on the surface of the biochar (site A) is consistent with oxygen, potassium and phosphorus concentrations. Chlorine and silicon appear to be randomly distributed but appear to have similar trend in concentration.

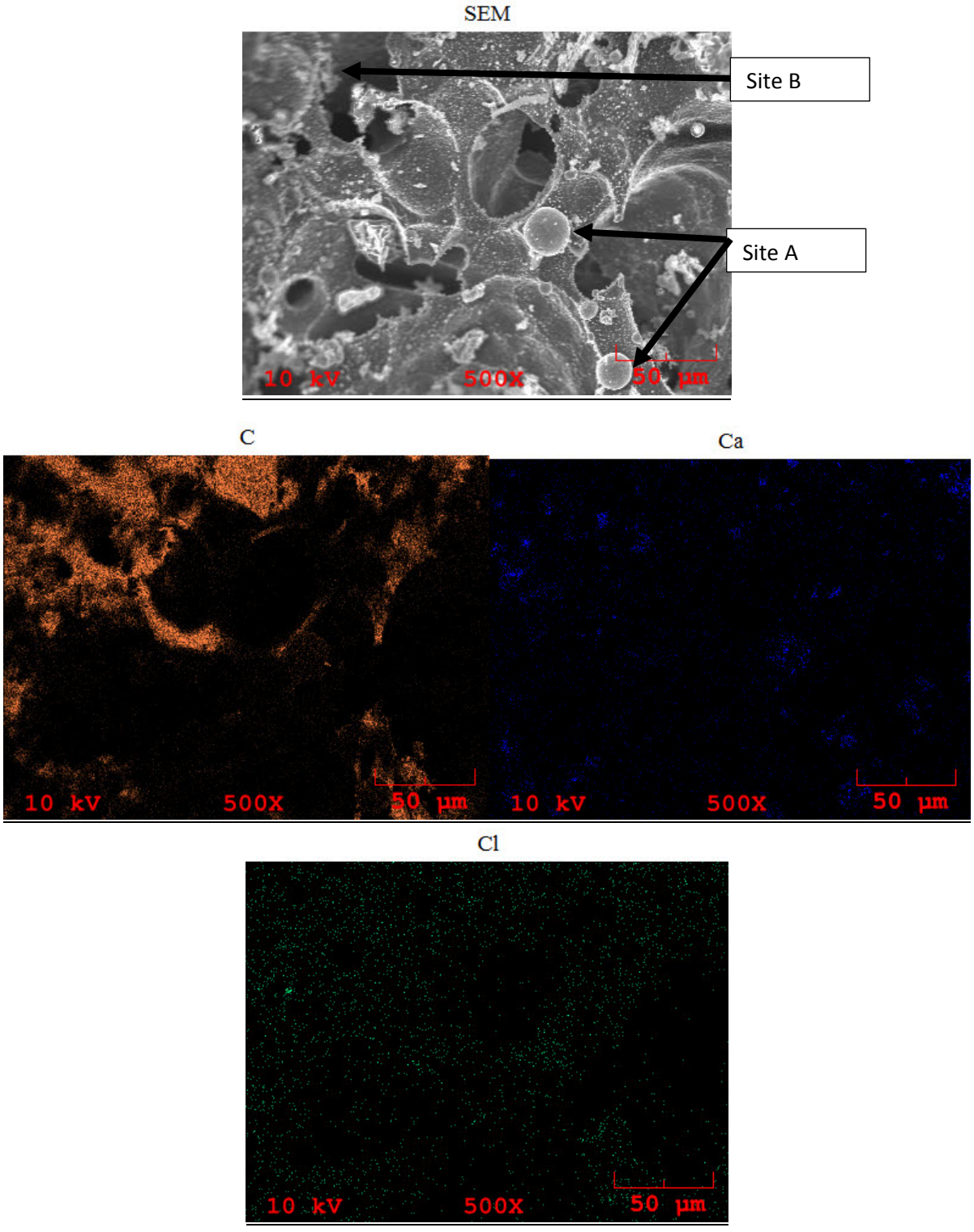

Figure 5.7 XRAY Surface area analysis from Outer soybean biochar – 1 (SEM, C, Ca and CL)

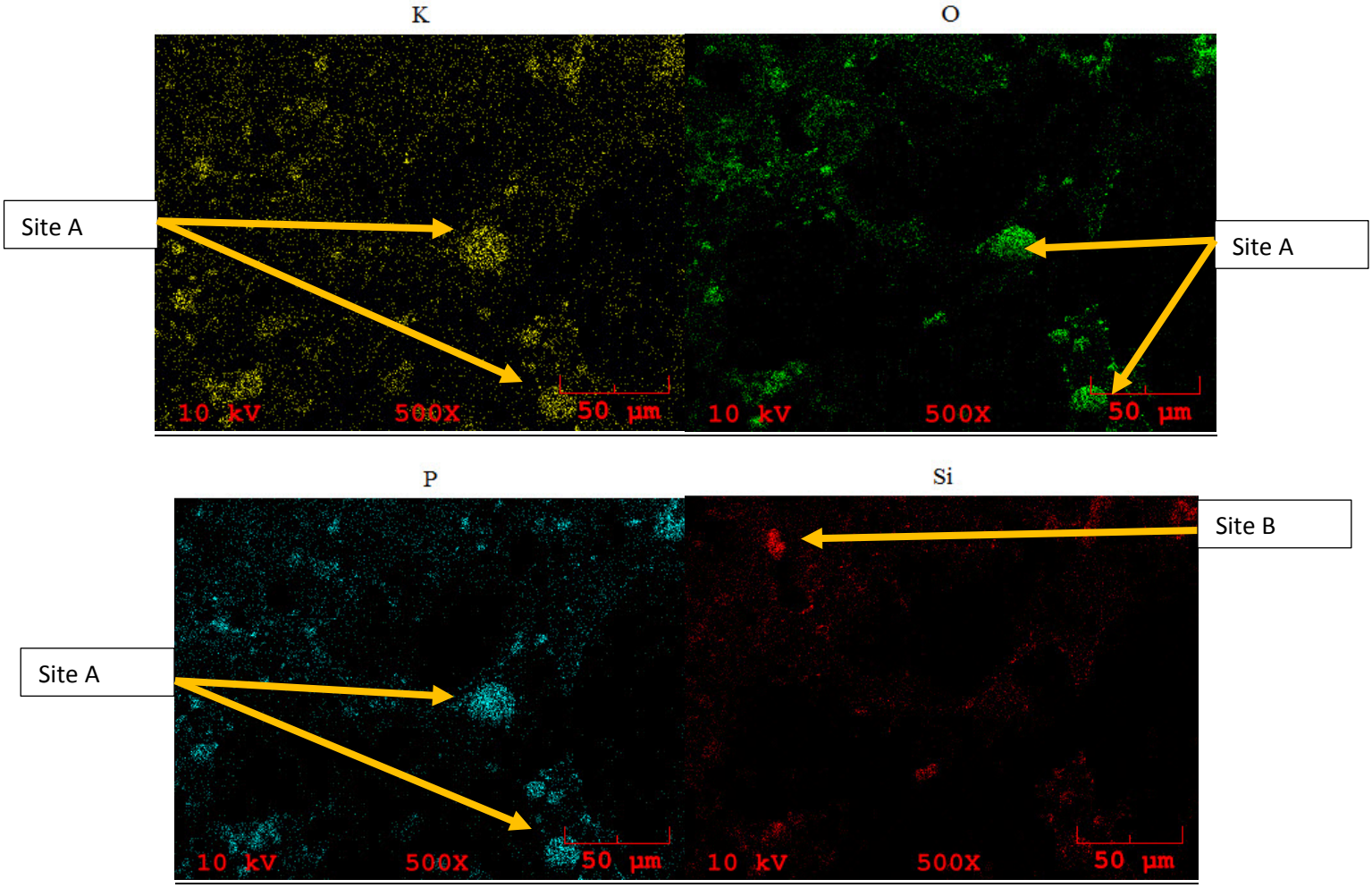

Figure 5.8 Surface area analysis from Outer soybean biochar - 2 (K, O, P, and Si)

Soy inside

The figure below shows the surface structure of soybeans. It appears to be similar to that of corn with pores spread over the surface. However, a closer look as seen in figure 5.9 shows a much wider range of minerals present compared to that of corn. Figure 5.10 – 5.13 shows that different mineral present in different locations of soybean char. High amount of calcium of up to 10% was found in soybean char. In a specific region as shown in figure 5.10, a location next to a pore showed potassium concentrations of 52.4%. Traces of Iron and nickel were also found in the inner of core of soybean biochar. Since these mineral appeared to be random and not as even when compared to corn, an additional step to detect the location of these mineral was taken as seen in figure 5.14. The x-ray analysis, traces of different minerals where located on the surface area. The highest content appeared to be carbon and calcium.

In figure 5.13 and 5.14, a similar trend to that of outer biochar is observed. We see that minerals such as Calcium, oxygen and phosphorus tend to be clustered in one area, shown as site A. Similar to the outer soy biochar, chlorine appeared to be located in a different pattern. In the inner biochar, potassium seems to spread out randomly throughout the char and doesn't appear to be concentrated in a particular region as seen in the outer biochar area figure.

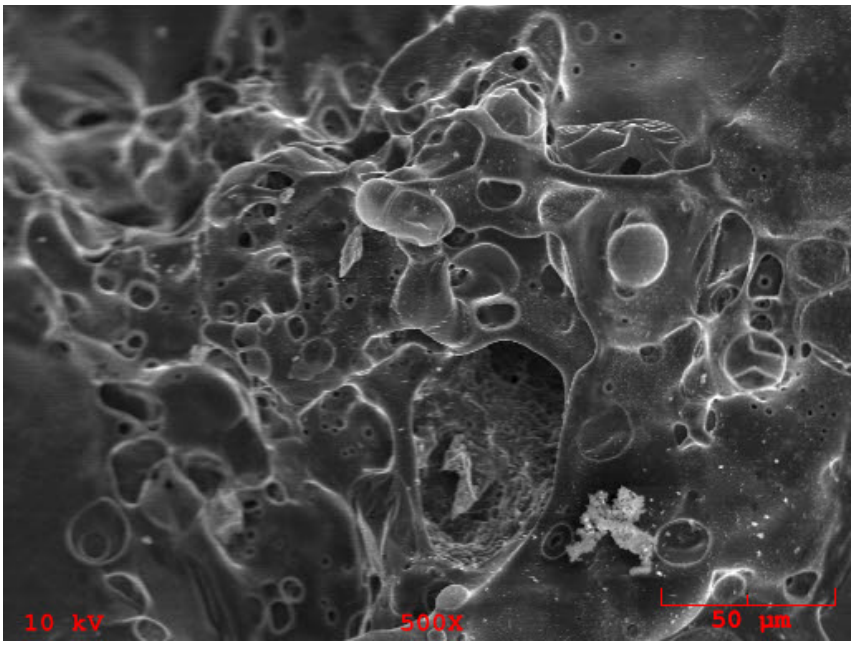

Figure 5.9 Surface area analysis from inner soybean biochar

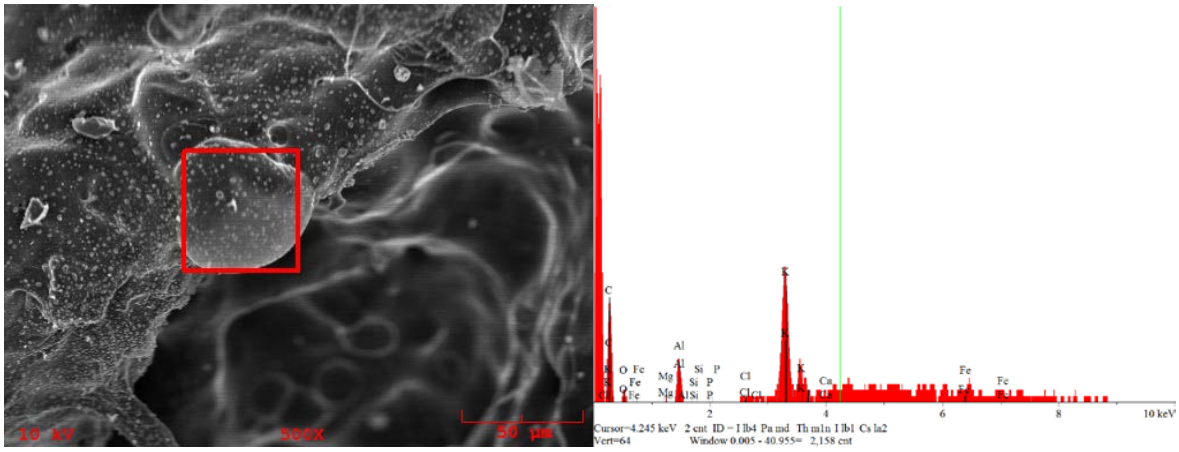

Figure 5.10 Surface area analysis from inner soybean biochar (Mineral analysis - 1)

Table 5.10 Surface area analysis from inner soybean biochar (Mineral analysis - 1)

Elt.	Line	Intensity (c/s)	Atomic %	Conc	Units	Error 2-sig	MDL 3-sig	
C	Ka	134.28	35.515	15.705	wt.%	0.388	0.121	
O	Ka	19.52	8.039	4.735	wt.%	0.912	0.077	
Mg	Ka	11.50	0.995	0.890	wt.%	0.263	0.011	
Al	Ka	64.94	5.148	5.114	wt.%	0.286	0.054	
Si	Ka	15.38	1.249	1.292	wt.%	0.328	0.000	
P	Ka	12.62	1.061	1.210	wt.%	0.336	0.000	
Cl	Ka	15.97	1.466	1.914	wt.%	0.467	0.040	
K	Ka	303.94	36.416	52.425	wt.%	0.757	0.250	
Ca	Ka	46.62	7.015	10.351	wt.%	0.992	0.129	
Fe	La	10.58	3.095	6.364	wt.%	1.901	0.000	
			100.000	100.000	wt.%			Total

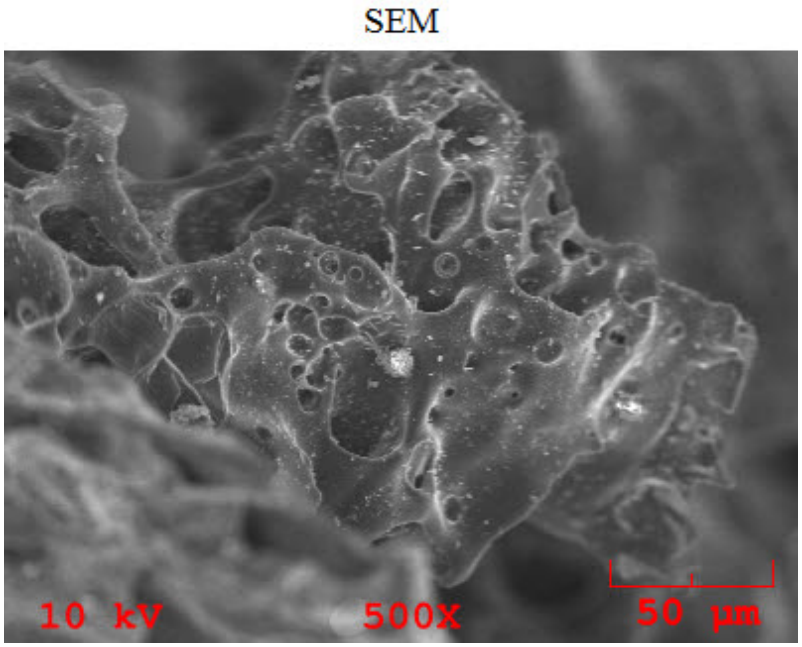

Figure 5.11 Surface area analysis from inner soybean biochar (Mineral analysis - 2)

Table 5.11 Surface area analysis from inner soybean biochar (Mineral analysis - 2)

Elt.	Line	Intensity (c/s)	Conc	Units	Error 2-sig	MDL 3-sig	
C	Ka	333,421.25	74.477	wt.%	0.001	0.000	
O	Ka	11,332.28	5.363	wt.%	0.002	0.000	
Na	Ka	5,265.36	0.901	wt.%	0.001	0.000	
Mg	Ka	5,184.96	0.801	wt.%	0.001	0.000	
Al	Ka	5,900.31	0.934	wt.%	0.001	0.000	
Si	Ka	3,836.65	0.643	wt.%	0.001	0.000	
P	Ka	9,034.55	1.761	wt.%	0.001	0.000	
Cl	Ka	3,589.63	0.912	wt.%	0.001	0.000	
K	Ka	12,958.25	4.631	wt.%	0.002	0.000	
Ca	Ka	2,003.51	0.856	wt.%	0.002	0.000	
Mn	Ka	907.94	1.693	wt.%	0.008	0.000	
Fe	Ka	772.30	2.174	wt.%	0.013	0.000	
Ni	Ka	492.44	4.853	wt.%	0.045	0.001	
			100.000	wt.%			Total

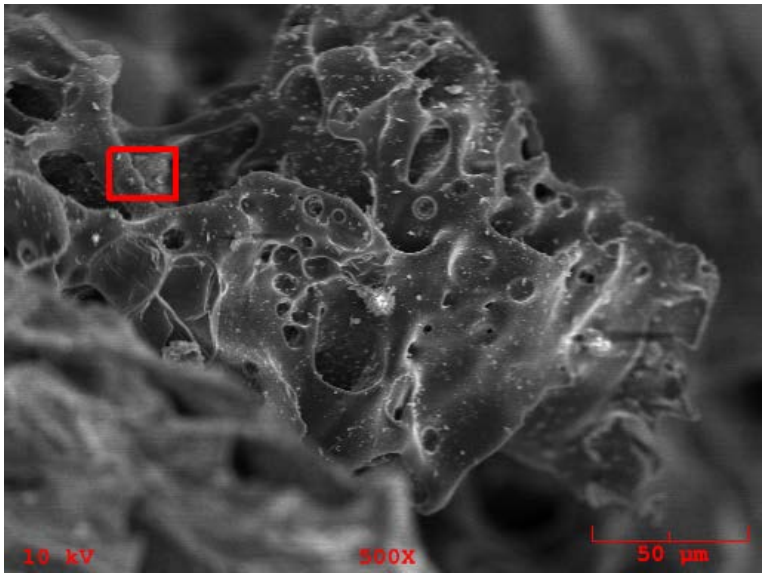

Figure 5.12 Surface area analysis from inner soybean biochar (Mineral analysis - 3)

Table 5.12: Surface area analysis from inner soybean biochar (Mineral analysis - 3)

Elt.	Line	Intensity (c/s)	Atomic %	Conc	Units	Error 2-sig	MDL 3-sig	
C	Ka	8,018.14	73.034	53.665	wt.%	0.024	0.054	
O	Ka	1,176.43	13.181	12.901	wt.%	0.040	0.029	
Mg	Ka	193.09	0.571	0.850	wt.%	0.015	0.005	
Al	Ka	300.57	0.817	1.348	wt.%	0.015	0.007	
Si	Ka	374.06	1.027	1.764	wt.%	0.018	0.007	
P	Ka	799.63	2.308	4.374	wt.%	0.021	0.013	
Cl	Ka	148.39	0.488	1.059	wt.%	0.030	0.007	
K	Ka	378.41	1.553	3.714	wt.%	0.043	0.016	
Ca	Ka	850.23	4.110	10.077	wt.%	0.052	0.030	
Mn	Ka	34.99	0.538	1.808	wt.%	0.259	0.024	
Fe	Ka	20.95	0.478	1.633	wt.%	0.350	0.026	
Ni	Ka	24.76	1.895	6.806	wt.%	1.279	0.055	
			100.000	100.000	wt.%			Total

In figures 5.13 and 5.14, the dispersion of the mineral present appears to be random, however, we see nodules of minerals that appear in the same region as seen through site A. Calcium, oxygen, potassium and silicon have a denser concentration in particular regions. These regions could either contain the elements in a singular form or be existent as a compound. Traces of potassium, phosphorus appear to have a denser concentration on the biochar surface while concentration of Iron and Nickel appear to be spread out.

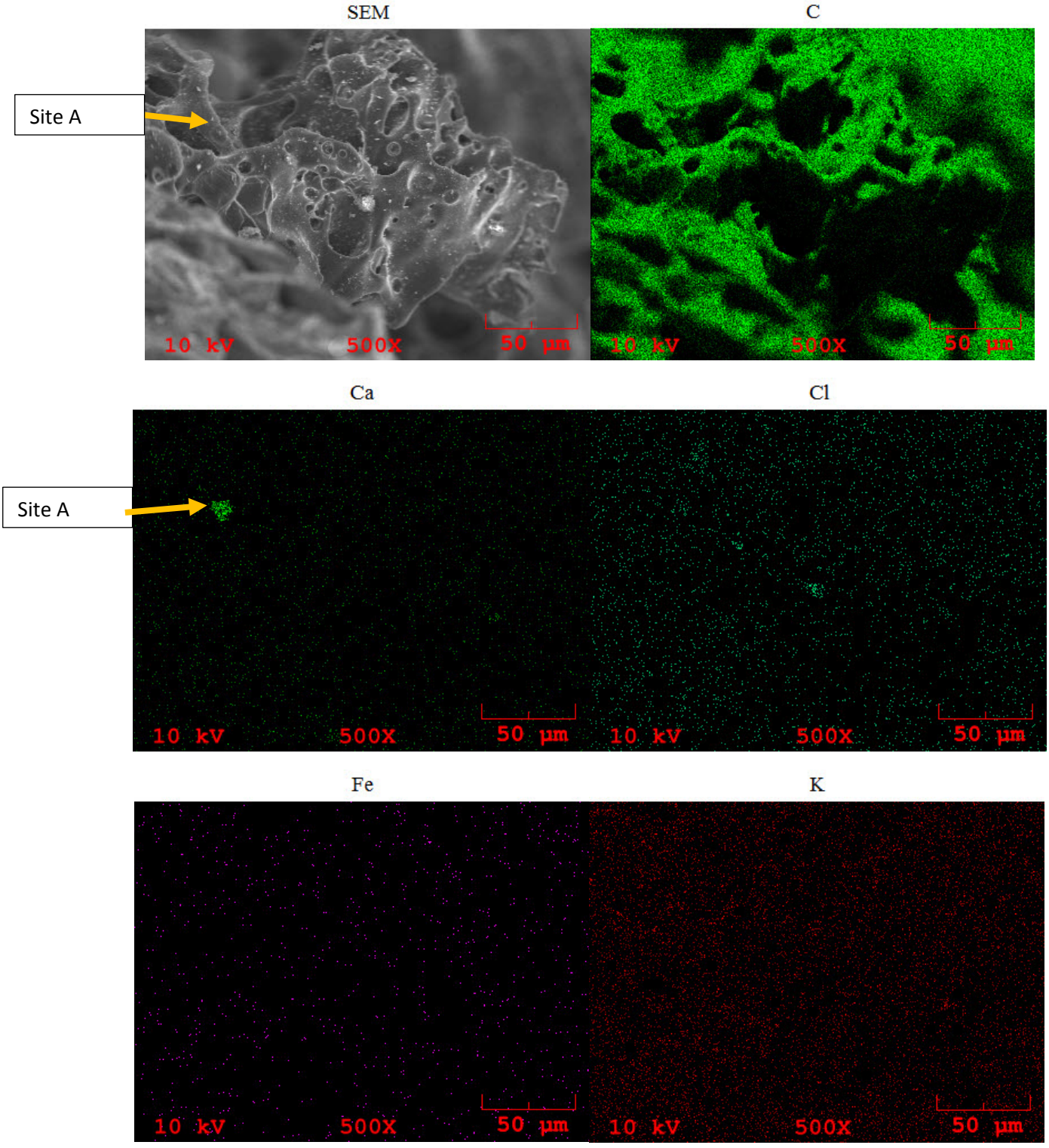

Figure 5.13 X- RAY Surface area analysis from inner soybean biochar-1 (SEM, C, Ca, Cl, Fe and K)

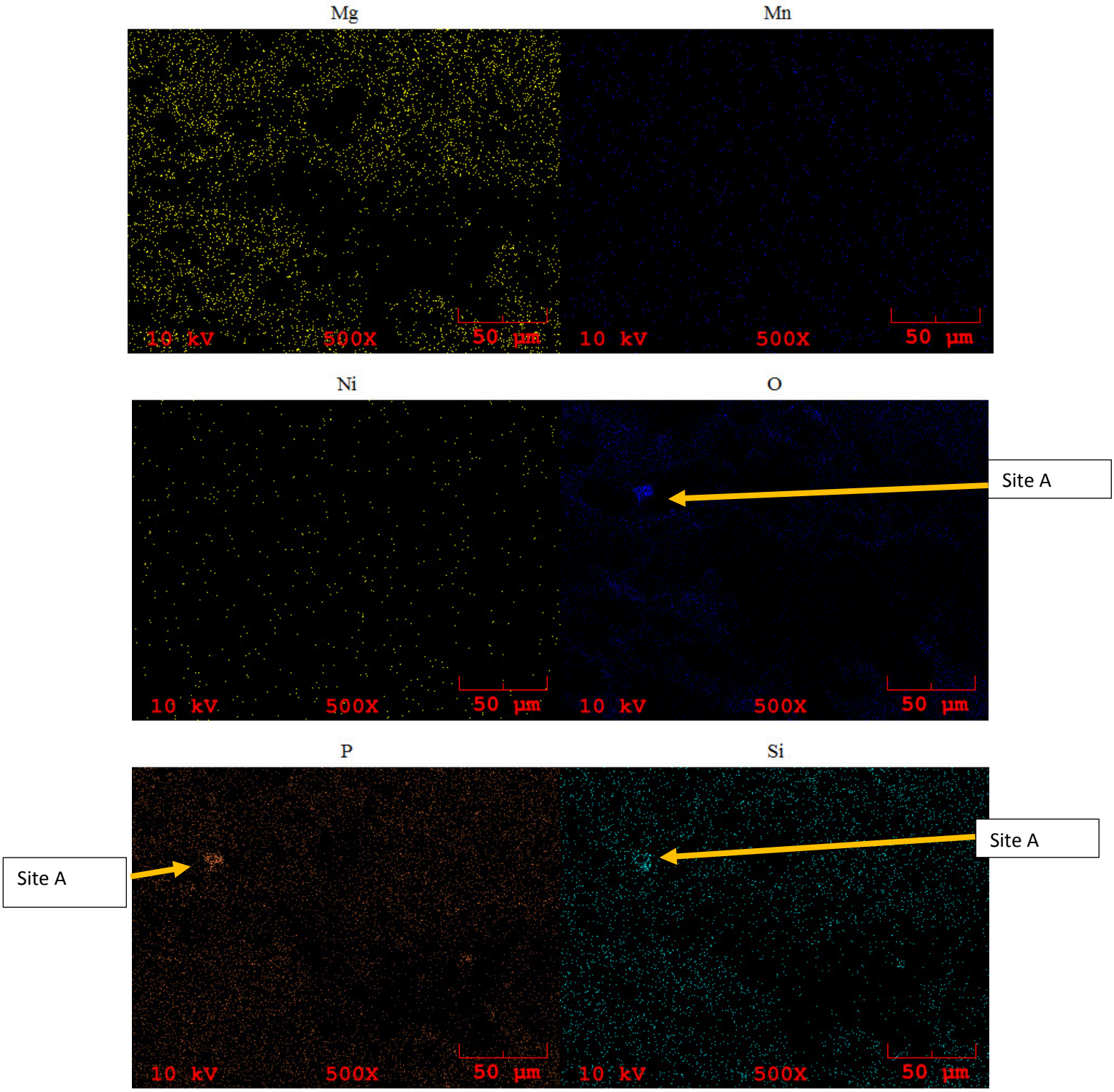

5.14 X- RAY Surface area analysis from inner soybean biochar -2(Mg, Mn, Ni, O, P and Si)

Wood outside

A similar approach was done for the wood biochar both inside and outside where their mineral content was analyzed. As seen below a wide range of elements including nickel, iron and silicon traces where found on the outer region of wood biochar. However, these traces were all under 5%. This dispersion of different minerals can closely be seen through the X-ray analysis. This dispersion of different minerals can closely be seen through the X-ray analysis. From figure 5.16 and 5.17, small traces and trend between phosphorus, potassium and oxygen can be observed. Although their traces do not match in some areas, areas such as site A show some similarity as to how the minerals are dispersed.

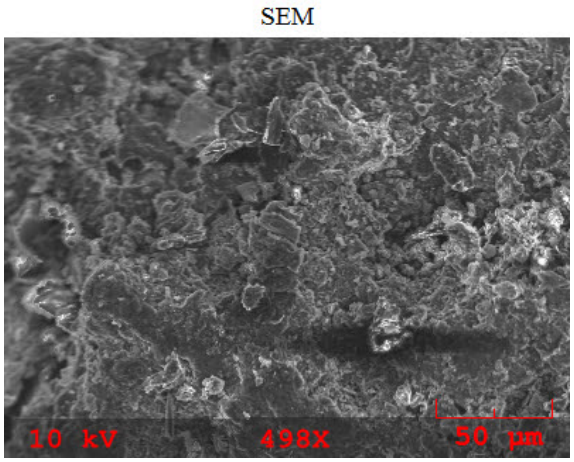

Figure 5.15 (a): SEM of Outer wood biochar analysis

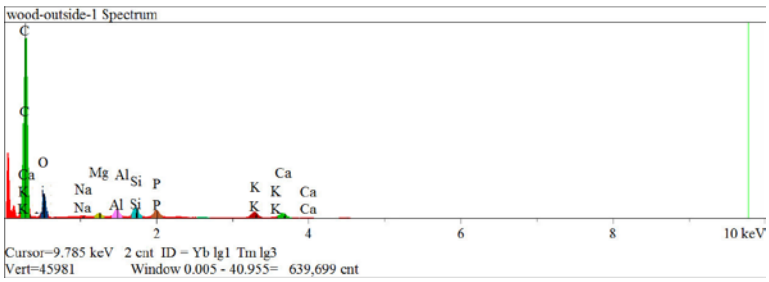

Figure 5.15 (b) Mineral concentration on outer wood-bottom

Table 5.13: Outer wood biochar analysis

Elt.	Line	Intensity (c/s)	Conc	Units	Error 2-sig	MDL 3-sig	
C	Ka	284,712.72	57.258	wt.%	0.001	0.000	
O	Ka	43,012.80	13.215	wt.%	0.001	0.000	
Mg	Ka	13,522.12	1.486	wt.%	0.000	0.000	
Al	Ka	22,502.81	2.536	wt.%	0.000	0.000	
Si	Ka	26,802.25	3.218	wt.%	0.000	0.000	
P	Ka	22,731.29	3.195	wt.%	0.001	0.000	
Cl	Ka	5,419.44	0.984	wt.%	0.001	0.000	
K	Ka	19,255.95	4.850	wt.%	0.001	0.000	
Ca	Ka	16,328.94	4.939	wt.%	0.001	0.000	
Mn	Ka	1,240.72	1.634	wt.%	0.006	0.000	
Fe	Ka	1,027.39	2.044	wt.%	0.009	0.000	
Ni	Ka	670.00	4.639	wt.%	0.032	0.000	
			100.000	wt.%			Total

As seen in figure 5.16 and figure 5.17, Nickel and Iron appear to be more widely spread out while minerals such as potassium, phosphorus and silicon appear to have dense regions. There is also a similar mineral deposit pattern among different minerals. Potassium, Phosphorus and oxygen have a similar trend in mineral deposit as shown in site A. These regions could either contain these minerals as elements or as compounds.

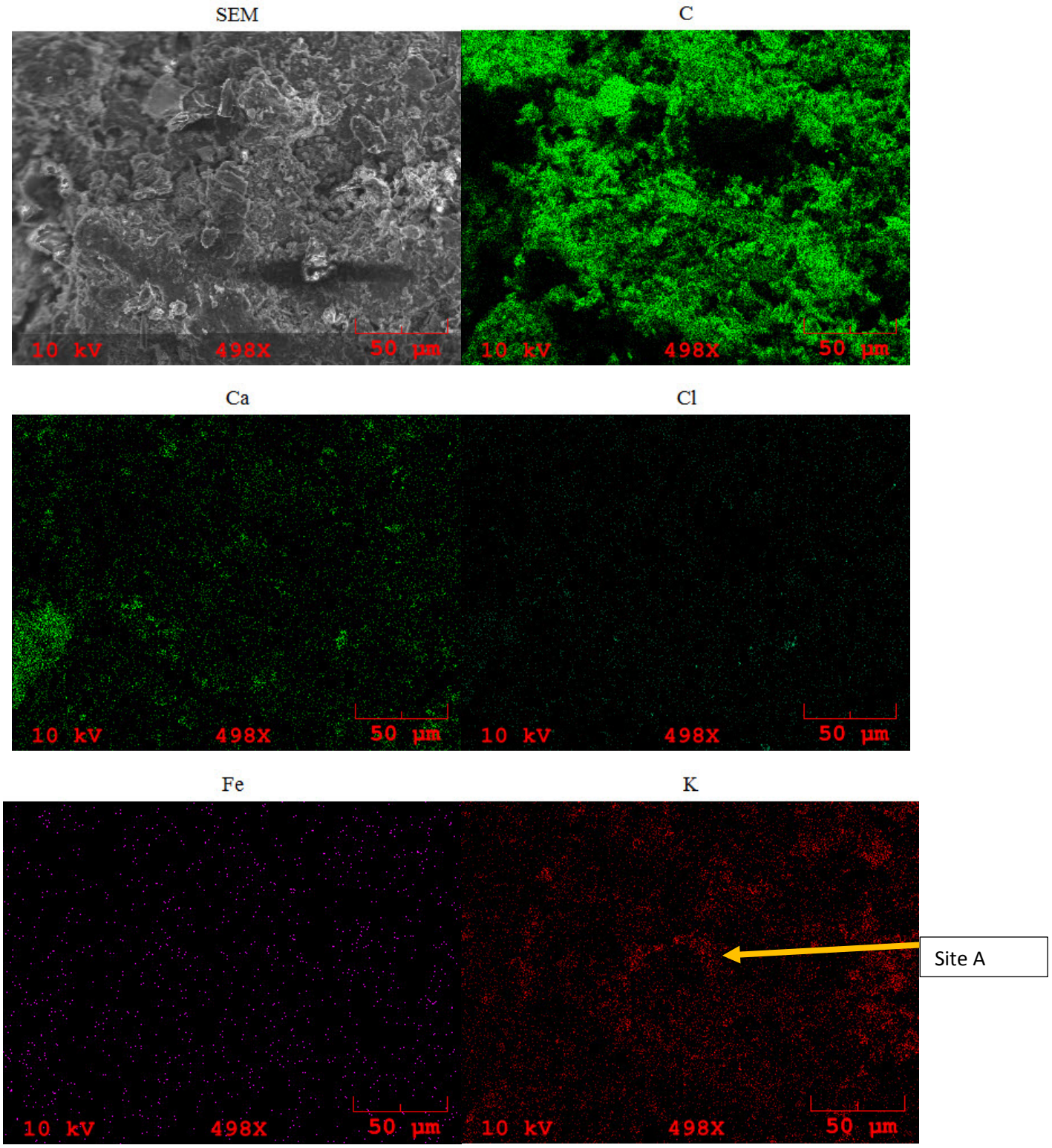

Figure 5.16 X-ray Surface area analysis from outer wood biochar – 1(SEM, C, Ca, Cl, Fe, and K)

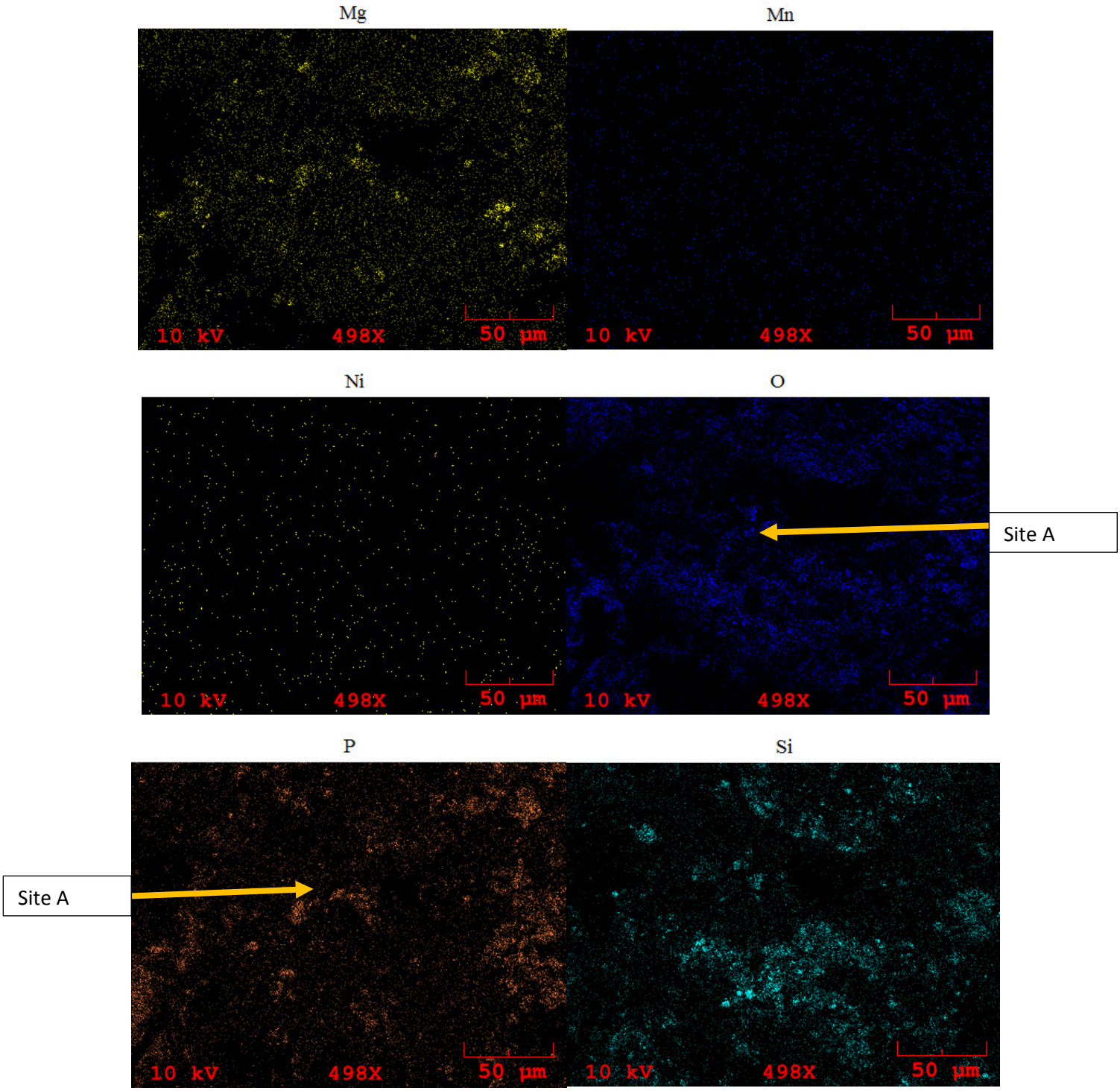

Figure 5.17 X- RAY Surface area analysis from outer wood biochar -2 (Mg, Mn, Ni, O, P, and Si)

Wood inside

When looking into the inside of the wood biochar, some of the regions showed high traces of potassium and calcium presence. A high calcium presence of up to 54% was found while up to 36% potassium concentration was found in other areas. The metal in wood biochar were all observed to be under 2%. Figures 5.18-5.21 show the different mineral concentration in different region of wood biochar. Wood inside showed a mixture of results. Some regions of wood showed a high concentration of potassium and phosphorus with little or no metal concentration, while other regions such as that shown in figure 5.21 showed high concentrations of potassium and phosphorus with traces of manganese, iron, aluminum and silicon. Figures 5.18 – 5.20 show the mineral content concentration in porous regions.

The SEM x-ray analysis shows the concertation and location of minerals at the surface of the char. A similar pattern of minerals can be seen on the char surface. Aluminum, Silicon, iron, magnesium, oxygen, and phosphorous appear to have a similar trend pattern as seen in figure 5.22.

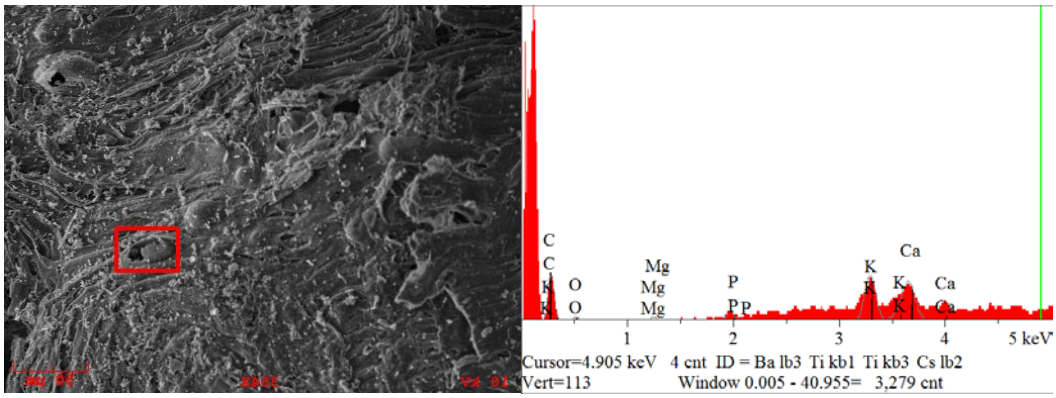

Figure 5.18 Surface area analysis from inner wood biochar (Mineral analysis - 1)

Table 5.14 Surface area analysis from inner wood biochar (Mineral analysis - 1)

Elt.	Line	Intensity (c/s)	Atomic %	Conc	Units	Error 2-sig	MDL 3-sig	
C	Ka	118.28	29.359	11.901	wt.%	0.318	0.050	
O	Ka	11.23	6.109	3.299	wt.%	0.985	0.021	
Mg	Ka	11.23	1.095	0.899	wt.%	0.268	0.000	
P	Ka	35.84	3.287	3.436	wt.%	0.375	0.022	
K	Ka	212.74	27.241	35.950	wt.%	0.710	0.101	
Ca	Ka	202.00	32.909	44.515	wt.%	1.020	0.131	
			100.000	100.000	wt.%			Total

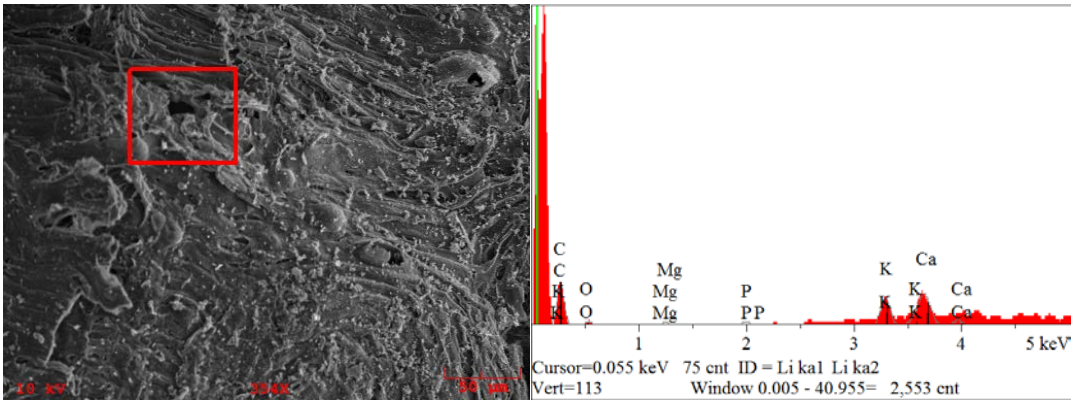

Figure 5.19 Surface area analysis from inner wood biochar (Mineral analysis - 2)

Table 5.15 Surface area analysis from inner wood biochar (Mineral analysis - 2)

Elt.	Line	Intensity (c/s)	Atomic %	Conc	Units	Error 2-sig	MDL 3-sig	
C	Ka	131.10	33.999	14.382	wt.%	0.357	0.056	
O	Ka	11.23	6.864	3.868	wt.%	1.155	0.000	
Mg	Ka	11.23	1.226	1.050	wt.%	0.314	0.000	
P	Ka	13.27	1.358	1.481	wt.%	0.402	0.012	
K	Ka	128.03	17.788	24.497	wt.%	0.841	0.086	
Ca	Ka	218.12	38.766	54.722	wt.%	1.124	0.154	
			100.000	100.000	wt.%			Total

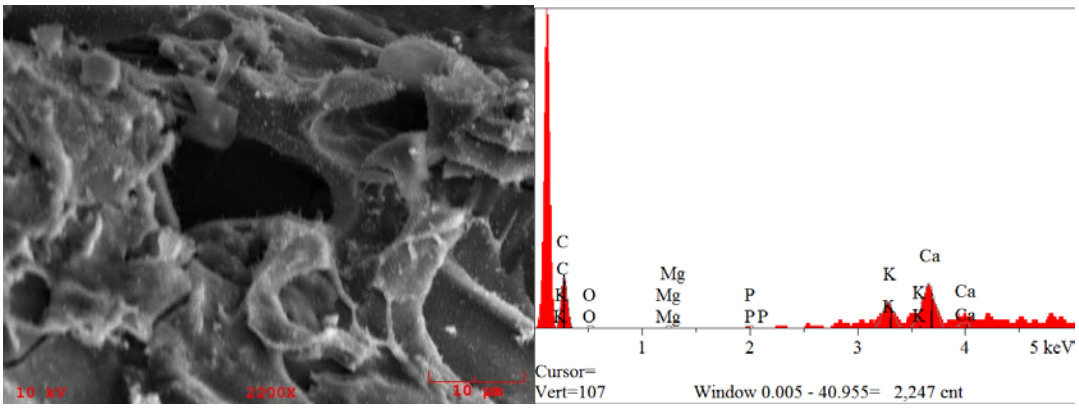

Figure 5.20 Surface area analysis from inner wood biochar (Mineral analysis - 3)

Table 5.16 Surface area analysis from inner wood biochar (Mineral analysis - 3)

Elt.	Line	Intensity (c/s)	Atomic %	Conc	Units	Error 2-sig	MDL 3-sig	
C	Ka	122.03	37.009	16.433	wt.%	0.461	0.066	
O	Ka	12.60	8.724	5.160	wt.%	1.373	0.050	
Mg	Ka	11.23	1.415	1.272	wt.%	0.380	0.000	
P	Ka	13.27	1.575	1.803	wt.%	0.489	0.000	
K	Ka	109.77	17.848	25.799	wt.%	0.916	0.108	
Ca	Ka	161.56	33.430	49.533	wt.%	1.369	0.159	
			100.000	100.000	wt.%			Total

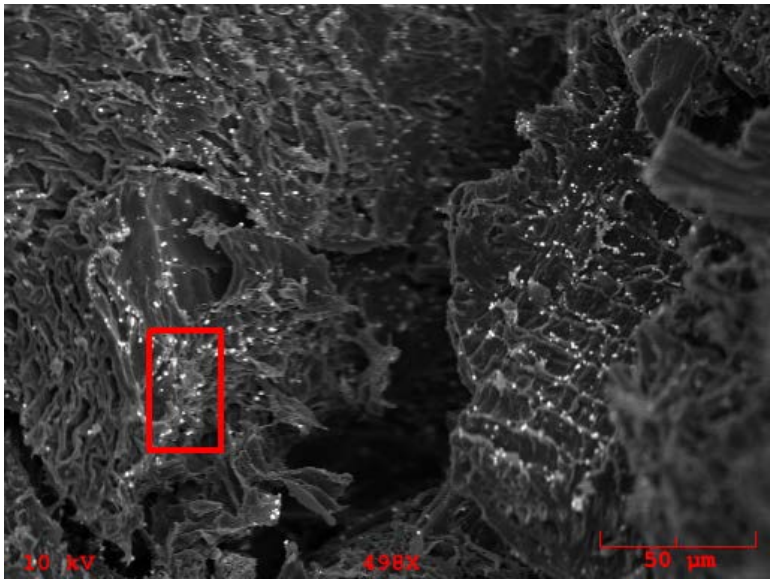

Figure 5.21 Surface area analysis from inner wood biochar (Mineral analysis - 4)

Table 5.17 Surface area analysis from inner wood biochar (Mineral analysis - 4)

Elt.	Line	Intensity (c/s)	Atomic %	Conc	Units	Error 2-sig	MDL 3-sig	
C	Ka	7,394.04	86.172	70.924	wt.%	0.034	0.074	
O	Ka	269.63	4.649	5.097	wt.%	0.071	0.023	
Mg	Ka	112.32	0.416	0.692	wt.%	0.021	0.006	
Al	Ka	108.07	0.375	0.693	wt.%	0.021	0.006	
Si	Ka	111.37	0.395	0.759	wt.%	0.023	0.006	
P	Ka	104.61	0.391	0.831	wt.%	0.028	0.007	
Cl	Ka	616.96	2.660	6.463	wt.%	0.043	0.022	
K	Ka	581.61	3.260	8.734	wt.%	0.064	0.031	
Ca	Ka	85.00	0.558	1.533	wt.%	0.082	0.016	
Mn	Ka	21.86	0.457	1.720	wt.%	0.347	0.024	
Fe	Ka	21.33	0.667	2.553	wt.%	0.538	0.029	
			100.000	100.000	wt.%			Total

As seen in Figures 5.22 and 5.23, there is a similar mineral deposit trend as shown in site A. The carbon mineral trend appears to match the mineral trends of Aluminum, magnesium, oxygen, silicon, phosphorus, oxygen and Silicon. Iron and Manganese however do not appear to be following the same trend and appear to more dispersed across the biochar surface region.

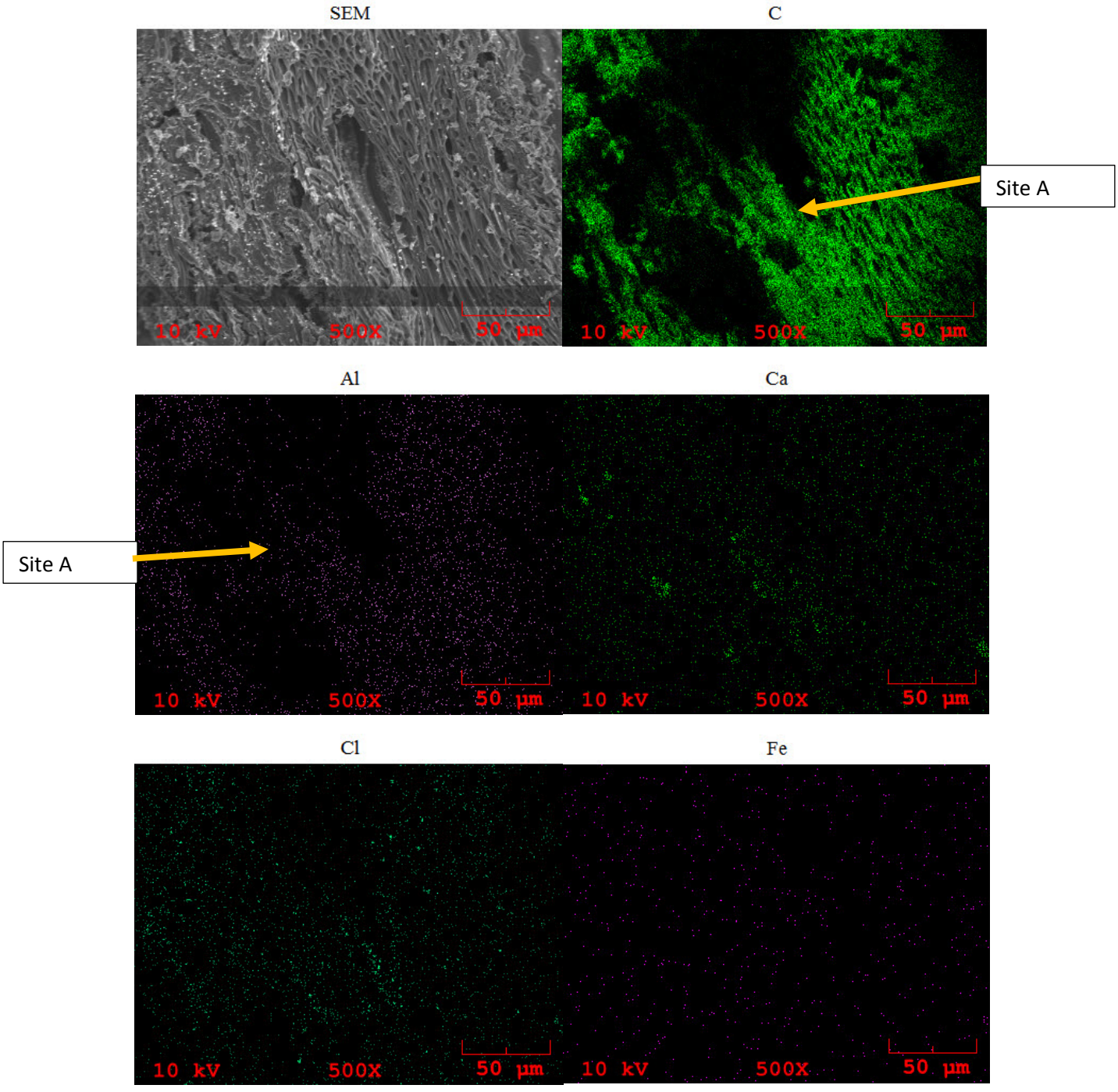

Figure 5.22 X-ray Surface area analysis from inner wood biochar -1 (SEM, C, Al, Ca, Cl and Fe)

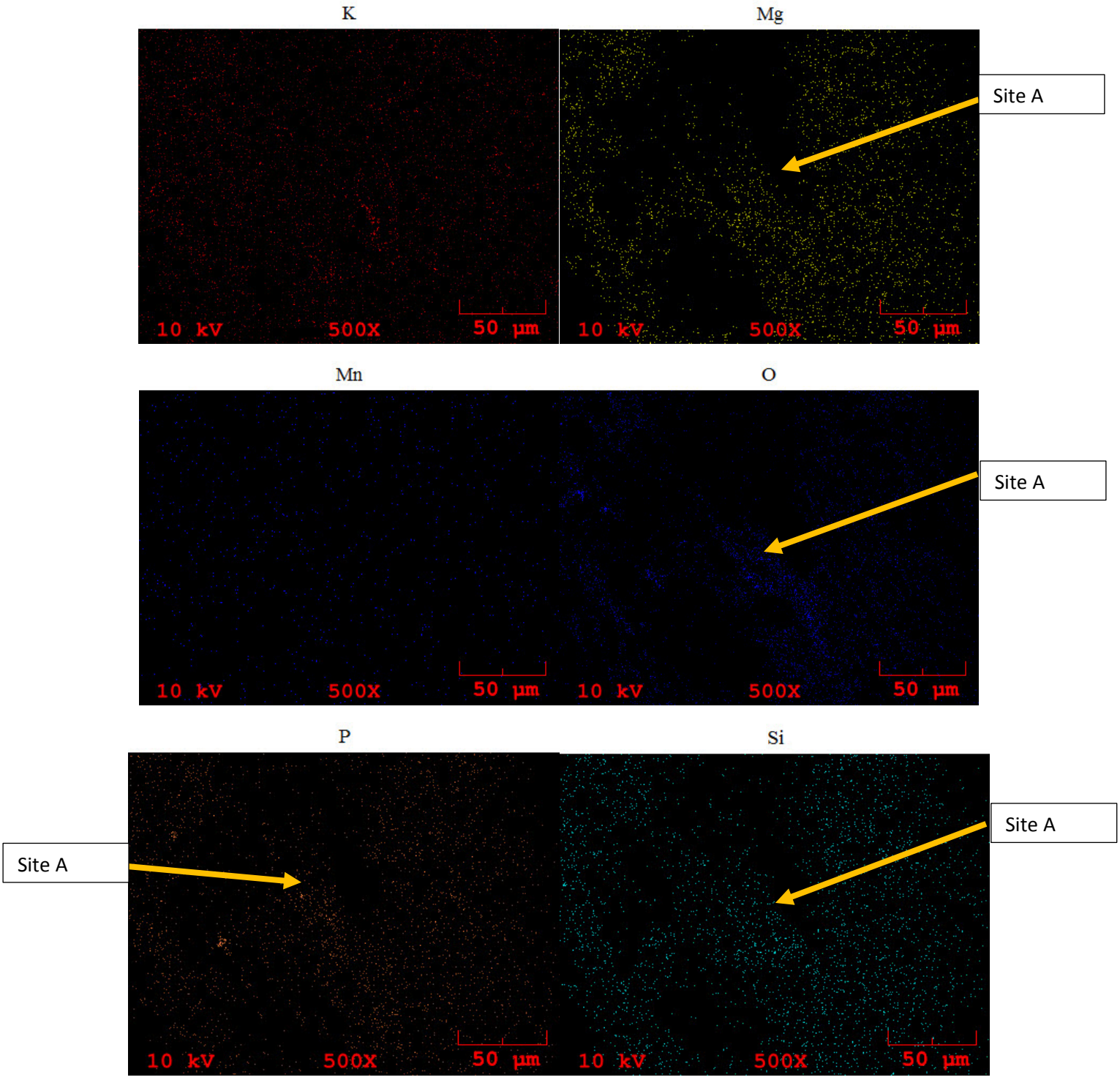

Figure 5.23 X-ray Surface area analysis from inner wood biochar (K, Mg, Mn, O, P and Si)

Refused derived waste (RDF, fuel and plastic)

Unlike the previous biochar where there was a high concentration of potassium and phosphorus, refused derived waste char had lowest concentrations. Several different sections of the RDF biochar was examined. Refused derived waste biochar was seen to have a higher percentage of nickel and aluminum. As seen in the figure below, the right hand portion of the char appears to be different. This region as shown in figure 5.24 carried a high concentration of Nickel and iron. It suspected that this region is the plastic remains from the original RDF fuel.

Other regions of the char showed a high concentration of aluminum. This high concentration of aluminum unlike other biochar was surprising. Due to the different minerals that were found on the biochar, the main uncooked RDF fuel was also tested where we saw similar trends of aluminum concentration. This suggests that the role of minerals found in the original fuel affects the biochar residue left. Figures 5.24 -5.38 look into the minerals from RDF. From figure 2.25 and 2.26, the local deposit pattern of calcium, aluminum, chlorine, potassium, oxygen and silicon matches as shown in site A.

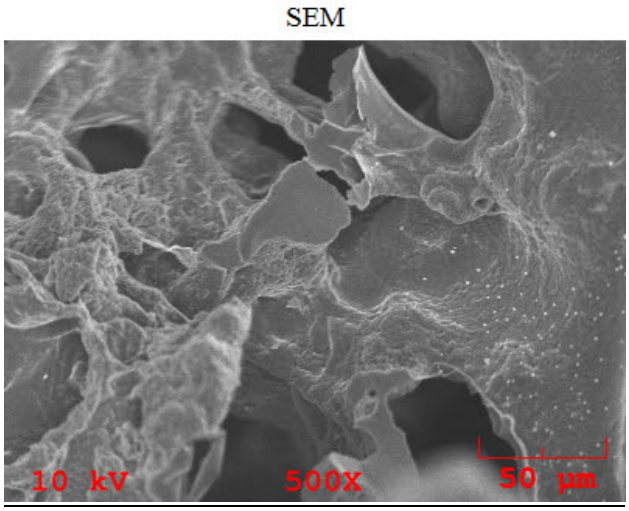

5.24 RDF biochar Surface area analysis

5.18 RDF biochar Surface area analysis

Elt.	Line	Intensity (c/s)	Conc	Units	Error 2-sig	MDL 3-sig	
C	Ka	254,622.72	78.164	wt.%	0.001	0.000	
O	Ka	3,983.06	2.716	wt.%	0.003	0.000	
Al	Ka	3,398.99	0.769	wt.%	0.001	0.000	
Si	Ka	2,420.29	0.579	wt.%	0.001	0.000	
P	Ka	3,323.61	0.923	wt.%	0.001	0.000	
Cl	Ka	3,196.65	1.156	wt.%	0.001	0.000	
K	Ka	6,319.90	3.210	wt.%	0.002	0.000	
Ca	Ka	1,917.21	1.162	wt.%	0.002	0.000	
Fe	Ka	887.25	3.511	wt.%	0.018	0.000	
Ni	Ka	557.61	7.810	wt.%	0.064	0.001	
			100.000	wt.%			Total

As seen in figure 5.25 and figure 5.26 there is a dense concentration of minerals throughout the biochar's surface. Aluminum, calcium, chlorine, potassium, phosphorus, oxygen and silicon show a similar pattern as seen in Site A. Iron and Nickel however appear to follow random pattern and more spread out on the biochar surface.

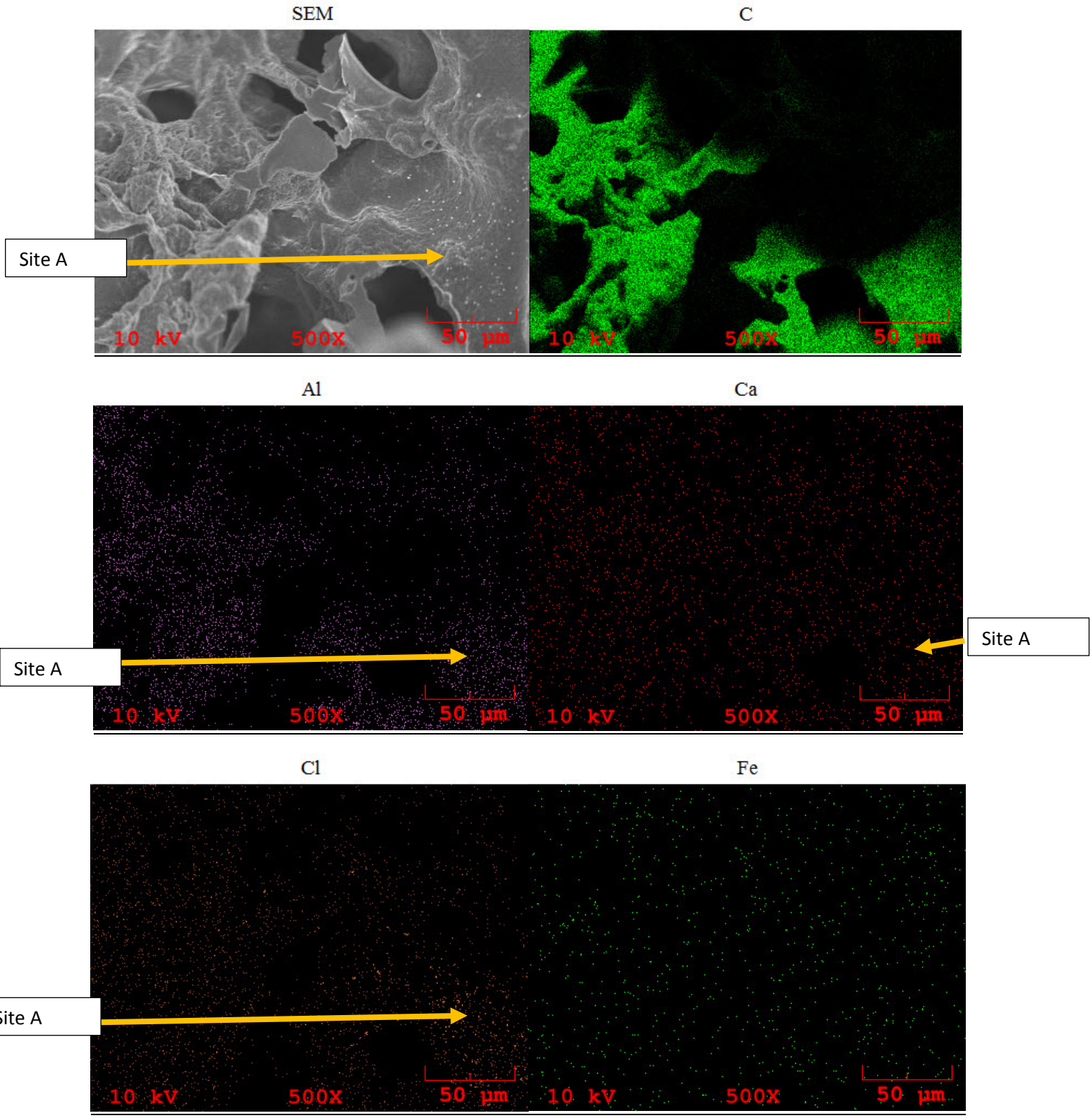

Figure 5.25 X-ray surface area analysis of RDF biochar -1 (SEM, C, Al, Ca, Cl and Fe)

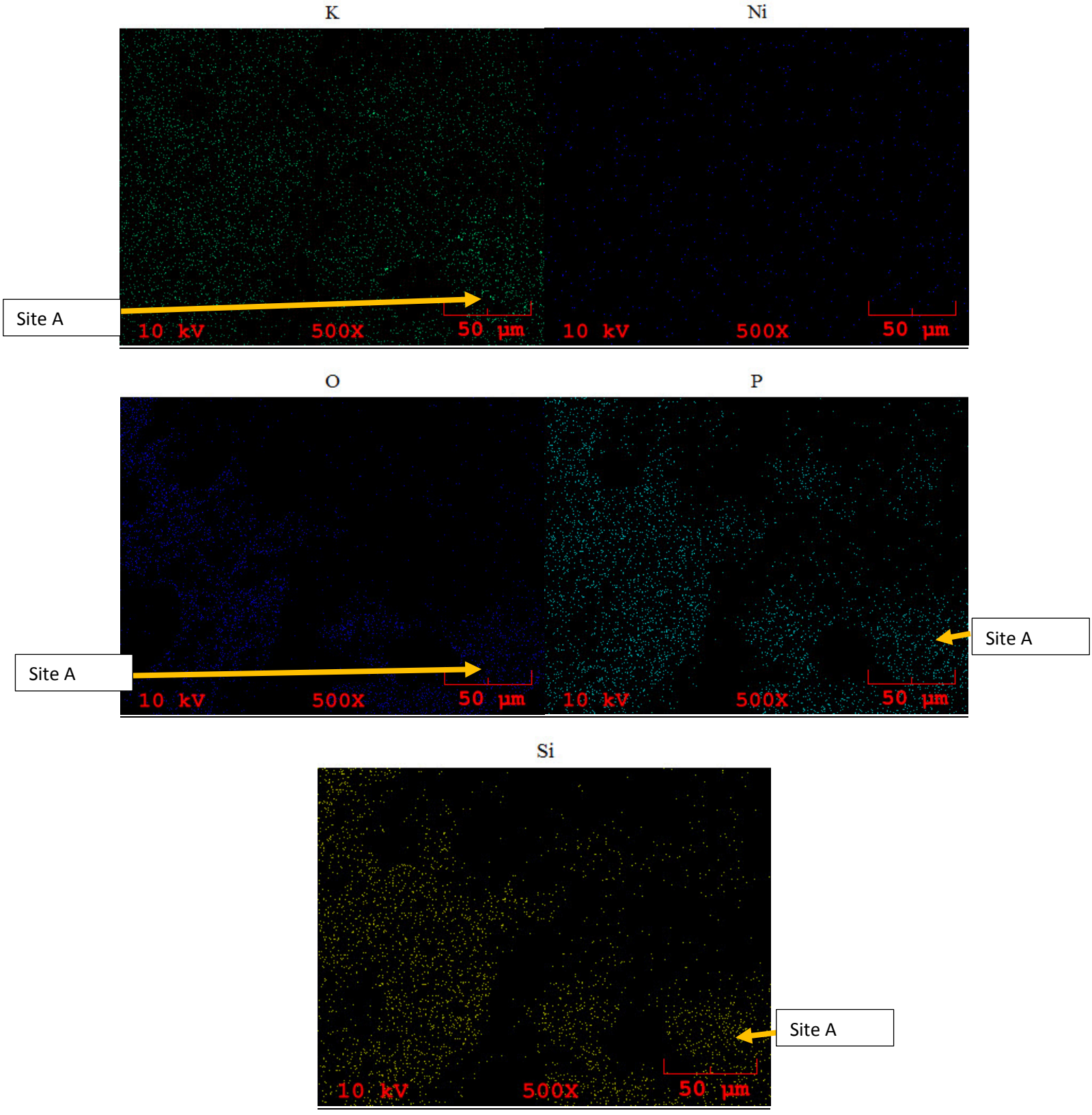

Figure 5.26: X-ray surface area analysis of RDF biochar -2 (K, Ni, O, P, and Si)

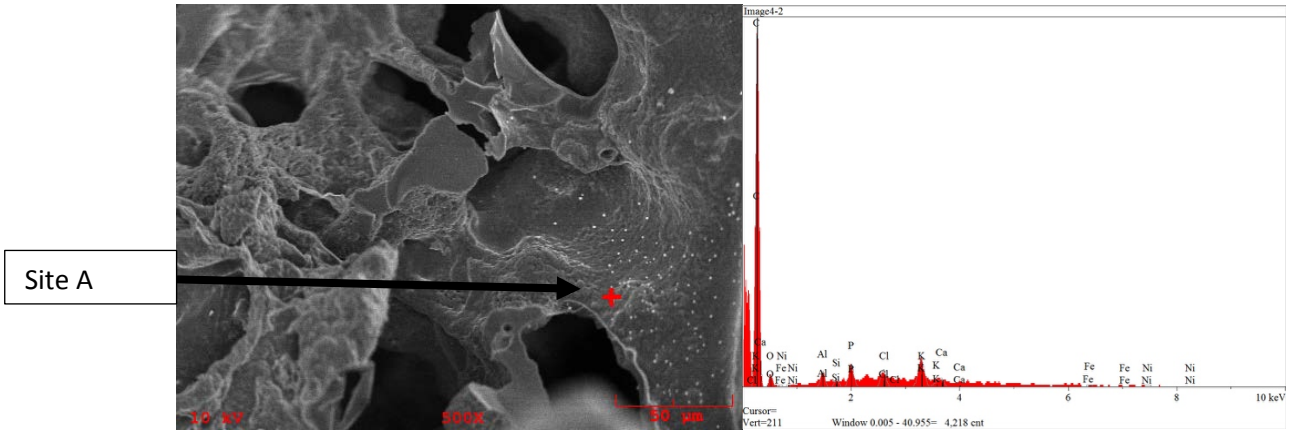

Figure 5.27 Surface area analysis from refused derived waste biochar (Mineral analysis - 1)

Table 5.19 Surface area analysis from refused derived waste biochar (Mineral analysis - 1)

Elt.	Line	Intensity (c/s)	Atomic %	Conc	Units	Error 2-sig	MDL 3-sig	
C	Ka	1,630.99	76.488	47.775	wt.%	0.103	0.106	
O	Ka	63.66	2.748	2.286	wt.%	0.128	0.022	
Al	Ka	92.83	1.174	1.647	wt.%	0.067	0.014	
Si	Ka	48.45	0.605	0.884	wt.%	0.069	0.010	
P	Ka	149.40	1.919	3.090	wt.%	0.084	0.021	
Cl	Ka	122.68	1.756	3.238	wt.%	0.109	0.024	
K	Ka	233.73	4.200	8.539	wt.%	0.163	0.045	
Ca	Ka	52.42	1.095	2.283	wt.%	0.174	0.032	
Fe	Ka	23.00	2.149	6.241	wt.%	1.216	0.086	
Ni	Ka	24.76	7.866	24.015	wt.%	4.513	0.168	
			100.000	100.000	wt.%			Total

Zoomed in

Other areas showed a much higher concentration of aluminum as shown below. Several regions were analyzed to understand the chemical and metal content of the biochar as seen below. Among all these results a high concentration of aluminum and nickel is observed in the biochar. Figures 5.28 (a and b) – 5.30 show the mineral analysis from site A. From figure 29 and figure 30, the dense particles of Chlorine and potassium are laid on the surface of the char, while minerals such as aluminum, iron, potassium and silicon are widely spread throughout the surface and are not as densely concentrated.

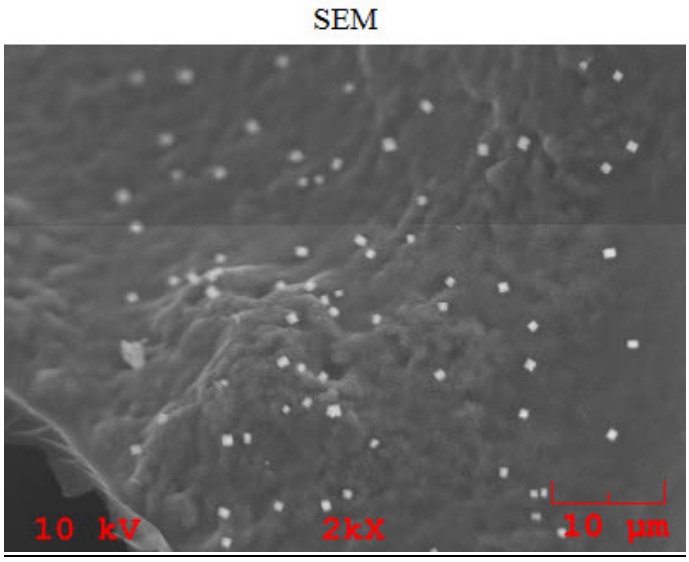

Figure 5.28(a): SEM image of RDF Biochar

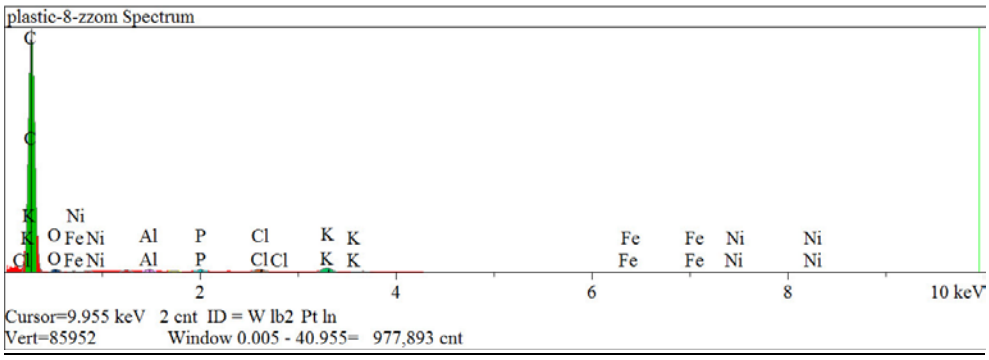

Figure 5.28(b): Mineral analysis from RDF biochar (zoomed in)

Table 5.20: Mineral analysis from RDF biochar (zoomed in)

Elt.	Line	Intensity (c/s)	Conc	Units	Error 2-sig	MDL 3-sig	
C	Ka	665,541.31	70.491	wt.%	0.000	0.000	
O	Ka	12,714.53	2.463	wt.%	0.001	0.000	
Al	Ka	11,020.13	0.818	wt.%	0.000	0.000	
Si	Ka	6,727.05	0.528	wt.%	0.000	0.000	
P	Ka	9,894.92	0.905	wt.%	0.000	0.000	
Cl	Ka	17,095.42	1.990	wt.%	0.000	0.000	
K	Ka	23,631.89	3.815	wt.%	0.001	0.000	
Ca	Ka	6,023.97	1.154	wt.%	0.001	0.000	
Fe	Ka	1,770.24	2.201	wt.%	0.007	0.000	
Ni	Ka	1,356.90	5.934	wt.%	0.023	0.000	
Tb	La	2,694.55	9.703	wt.%	0.015	0.000	
			100.000	wt.%			Total

As seen in figure 5.29 and Figure 5.30 there is high concentration of mineral deposit along the biochar surface. Chlorine and Potassium appear to have similar mineral concentration which appears on the SEM image as seen using site A and Site B. Oxygen, Aluminum and phosphorus appear to have a similar dispersion throughout the surface. A similar but different can be observed with Iron and nickel which appear to have similar trend.

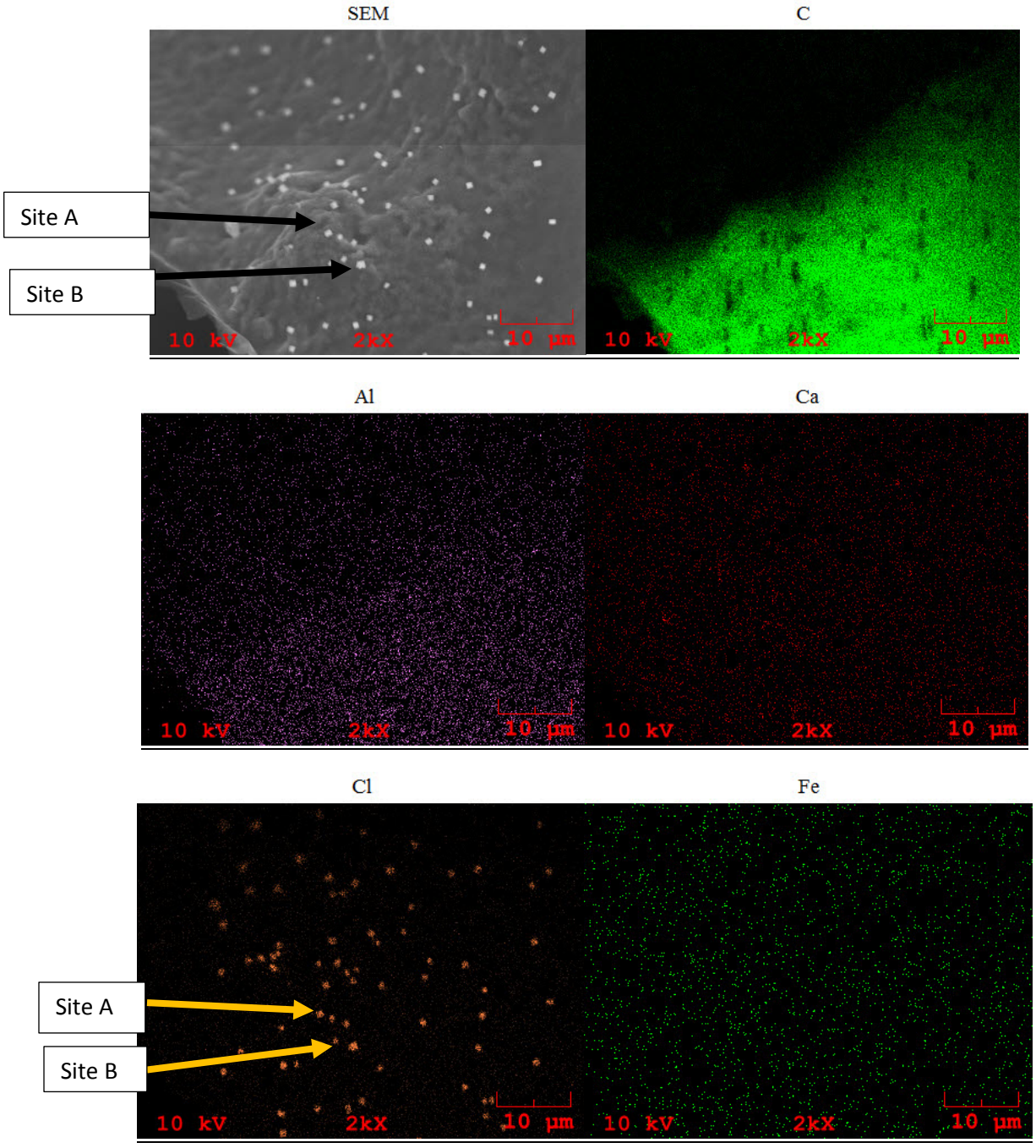

Figure 5.29 X-ray analysis from RDF biochar Zoomed -1 (SEM, C, Al, Ca, Cl and Fe)

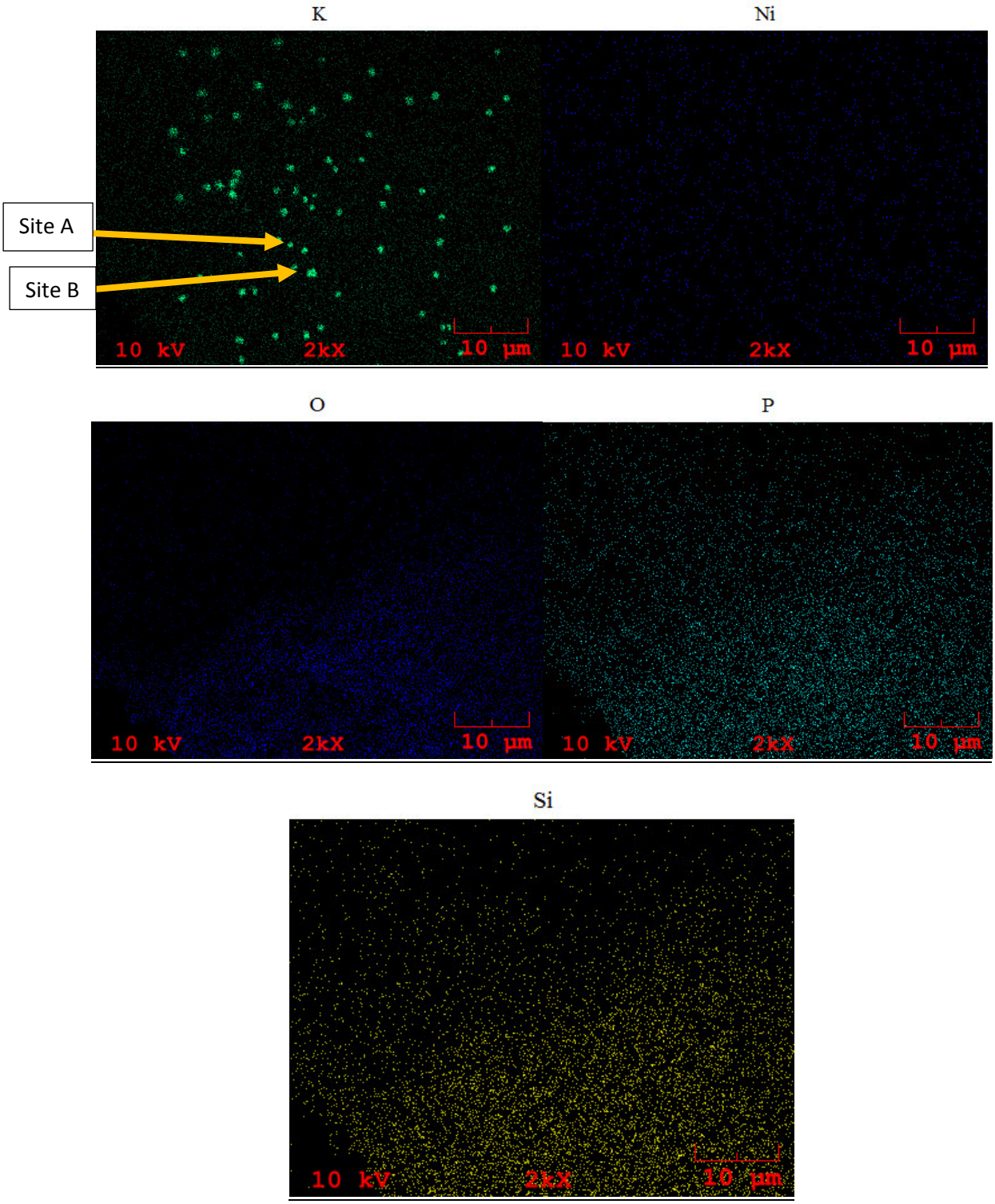

Figure 5.30: X-ray analysis from RDF biochar Zoomed -2 (SEM, C, Al, Ca, Cl and Fe)

From figure 5.31, it can be observed that the surface layer of RDF is much more different than that of corn, wood and soybeans. The surface doesn't show as many pores as observed with biochar from corn, wood and soybeans. Further examination show that a higher percentage of Nickel and aluminum of about 9% and 27% respectively are present in the RDF biochar.

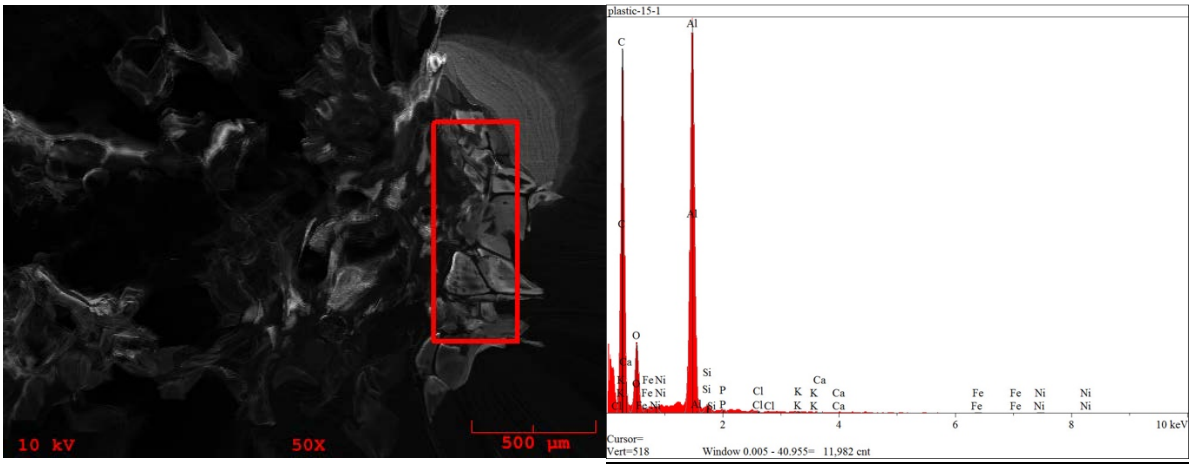

Figure 5.31: XRAY analysis from 'plastic region' of the RDF biochar

Table 5.21: XRAY analysis from 'plastic region' of the RDF biochar

Elt.	Line	Intensity (c/s)	Atomic %	Conc	Units	Error 2-sig	MDL 3-sig	
C	Ka	3,664.20	68.264	48.990	wt.%	0.047	0.073	
O	Ka	810.45	10.053	9.610	wt.%	0.042	0.026	
Al	Ka	4,893.39	17.100	27.568	wt.%	0.021	0.034	
Si	Ka	134.81	0.553	0.928	wt.%	0.027	0.006	
P	Ka	51.52	0.215	0.397	wt.%	0.027	0.005	
Cl	Ka	60.37	0.275	0.582	wt.%	0.041	0.005	
K	Ka	34.72	0.196	0.458	wt.%	0.051	0.007	
Ca	Ka	21.03	0.136	0.326	wt.%	0.061	0.006	
Fe	Ka	22.96	0.688	2.295	wt.%	0.448	0.000	
Ni	Ka	24.76	2.522	8.846	wt.%	1.663	0.000	
			100.000	100.000	wt.%			Total

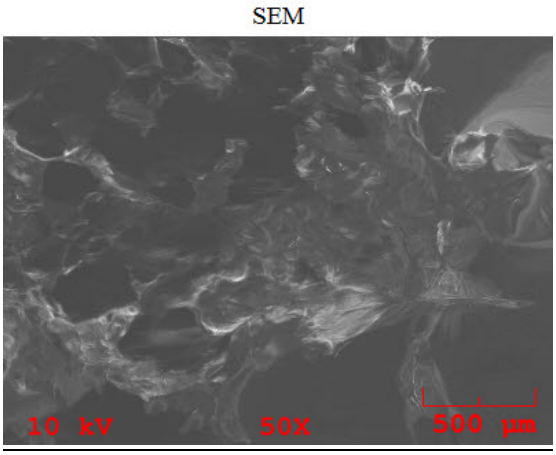

Figure 5.32: SEM image analysis from RDF biochar (Mineral analysis-2)

Table 5.22: SEM image analysis from RDF biochar (Mineral analysis-2)

Elt.	Line	Intensity (c/s)	Conc	Units	Error 2-sig	MDL 3-sig	
C	Ka	137,178.53	47.868	wt.%	0.001	0.000	
O	Ka	30,956.97	8.757	wt.%	0.001	0.000	
F	Ka	2,549.66	0.515	wt.%	0.001	0.000	
Na	Ka	6,469.68	0.762	wt.%	0.000	0.000	
Mg	Ka	8,805.76	0.953	wt.%	0.000	0.000	
Al	Ka	277,194.47	31.608	wt.%	0.000	0.000	
Si	Ka	6,278.20	0.904	wt.%	0.001	0.000	
P	Ka	3,567.76	0.575	wt.%	0.001	0.000	
Cl	Ka	3,361.38	0.673	wt.%	0.001	0.000	
K	Ka	2,596.69	0.710	wt.%	0.001	0.000	
Ca	Ka	2,593.08	0.835	wt.%	0.001	0.000	
Fe	Ka	917.04	1.930	wt.%	0.009	0.000	
Ni	Ka	533.57	3.911	wt.%	0.034	0.000	
			100.000	wt.%			Total

From the X-ray analysis in figure 5.33 and 5.34, we see a large concentration of aluminum minerals and observed that the local presence matches that of Chorine, potassium, phosphorus and silicon. Figures 5.35 to 5.37 show the different composition of minerals. Figure 5.37 also shows the presence of cadmium, which wasn't present in biochar results from corn, wood and soybeans. Using the SEM X-ray analysis, a large concentration of aluminum is observed in the RDF biochar. The patterns of mineral dispersion of aluminum matches other elements such as calcium, chlorine, iron, potassium, phosphorus and silicon as seen using site A and site B. Iron and nickel appear to

be more dispersed while mineral such as aluminum appear to be more densely concentrated on the char surface. The similar patterns among minerals such as Chlorine, potassium and phosphorus suggest that they may be present as a compound.

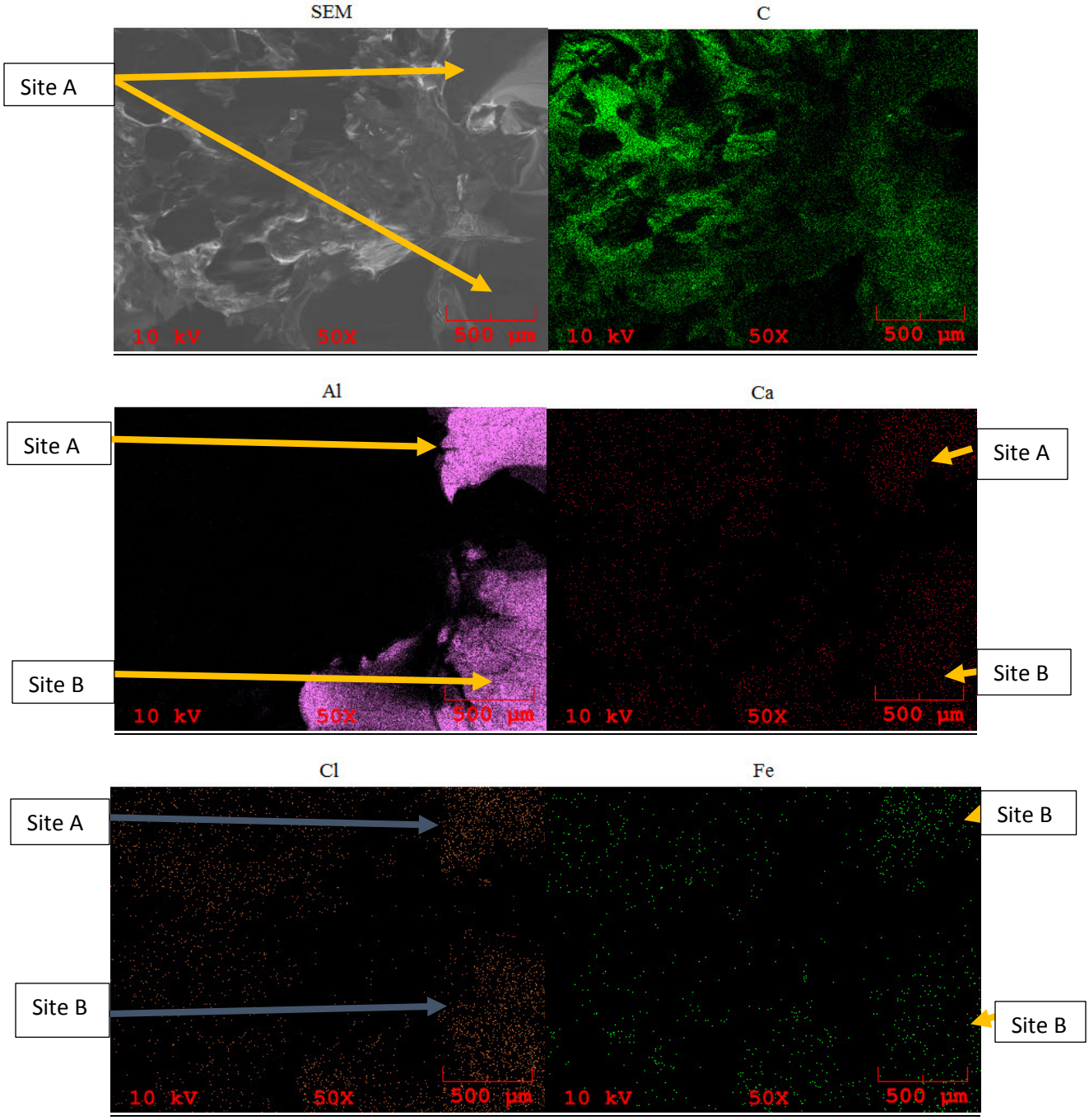

Figure 5.33 XRAY Surface area analysis from RDF biochar mineral analysis -2-1a (SEM, C, Al, Ca, Cl, Fe)

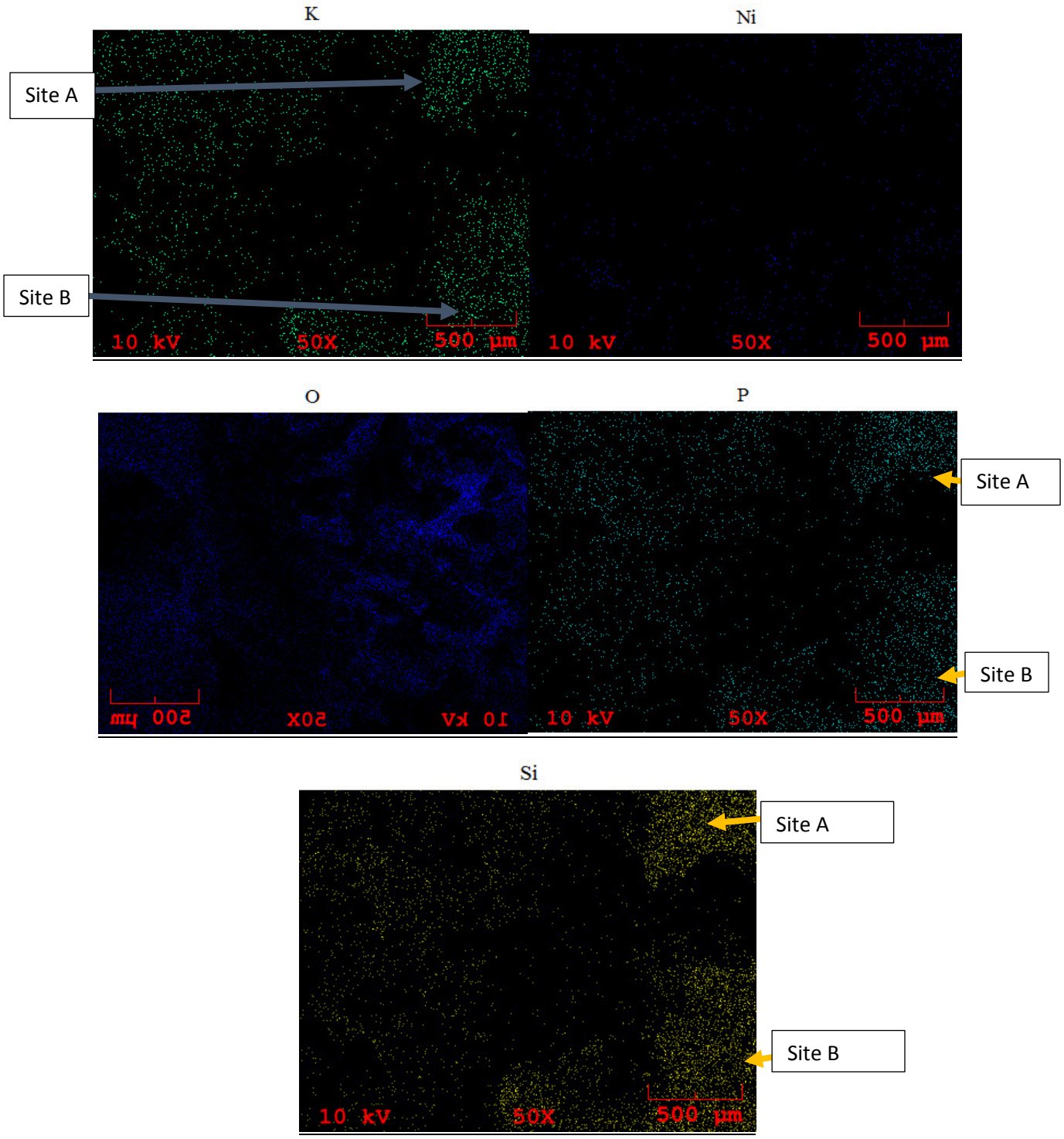

Figure 5.34 XRAY Surface area analysis from RDF biochar mineral analysis -2-1b(K, Ni, O, P and Si)

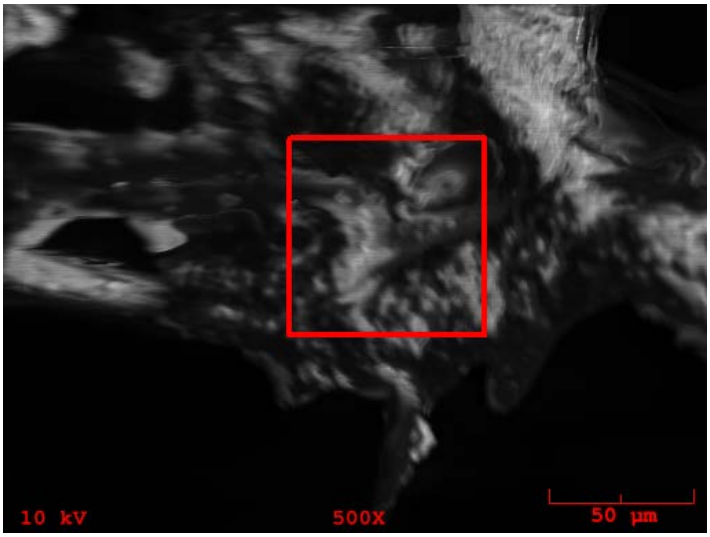

Figure 5.35 Surface area analysis from refused derived waste biochar- Plastic region (Mineral analysis – 3)

Table 5.23: Surface area analysis from refused derived waste biochar- Plastic region (Mineral analysis – 3)

Elt.	Line	Intensity (c/s)	Atomic %	Conc	Units	Error 2-sig	MDL 3-sig	
C	Ka	15,098.62	72.593	63.269	wt.%	0.015	0.046	
O	Ka	3,605.40	22.546	26.176	wt.%	0.026	0.034	
Al	Ka	2,343.90	3.780	7.402	wt.%	0.012	0.013	
Si	Ka	132.16	0.227	0.462	wt.%	0.012	0.004	
P	Ka	96.92	0.174	0.391	wt.%	0.014	0.004	
Cl	Ka	68.05	0.139	0.358	wt.%	0.022	0.003	
K	Ka	54.86	0.143	0.404	wt.%	0.032	0.004	
Ca	Ka	21.16	0.063	0.185	wt.%	0.034	0.003	
Fe	Ka	22.96	0.334	1.352	wt.%	0.264	0.000	
			100.000	100.000	wt.%			Total

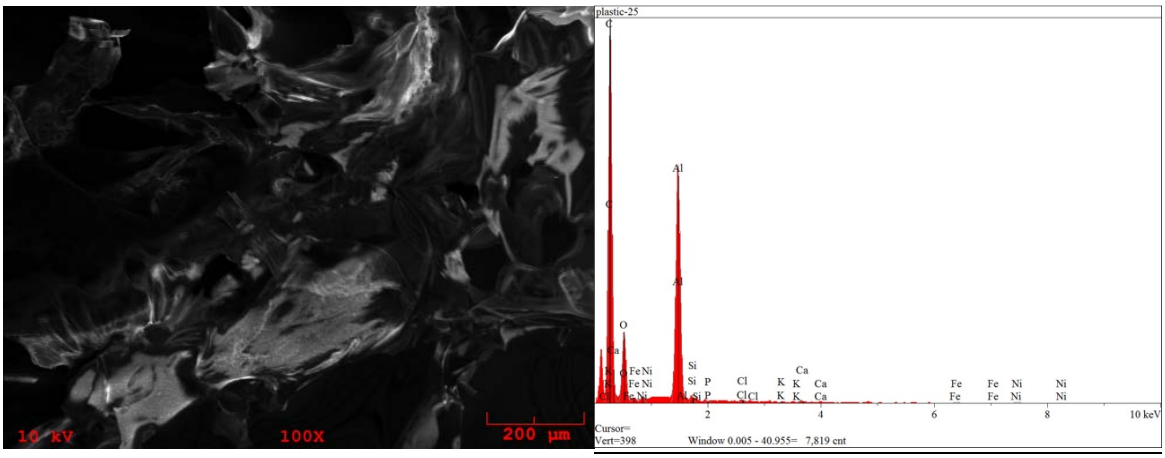

Figure 5.36: Surface area analysis from refused derived waste biochar- Plastic region (Mineral analysis – 4)

Table 5.24: Surface area analysis from refused derived waste biochar- Plastic region (Mineral analysis -4)

Elt.	Line	Intensity (c/s)	Atomic %	Conc	Units	Error 2-sig	MDL 3-sig
C	Ka	3,100.25	70.768	50.895	wt.%	0.058	0.082
O	Ka	630.42	11.001	10.539	wt.%	0.058	0.033
Al	Ka	2,383.13	12.132	19.601	wt.%	0.030	0.034
Si	Ka	77.36	0.438	0.737	wt.%	0.033	0.007
P	Ka	34.85	0.201	0.373	wt.%	0.038	0.006
Cl	Ka	49.30	0.313	0.665	wt.%	0.054	0.008
K	Ka	31.41	0.248	0.581	wt.%	0.081	0.008
Ca	Ka	43.98	0.399	0.957	wt.%	0.099	0.012
Fe	Ka	22.96	0.958	3.202	wt.%	0.625	0.000
Ni	Ka	24.76	3.542	12.450	wt.%	2.340	0.000

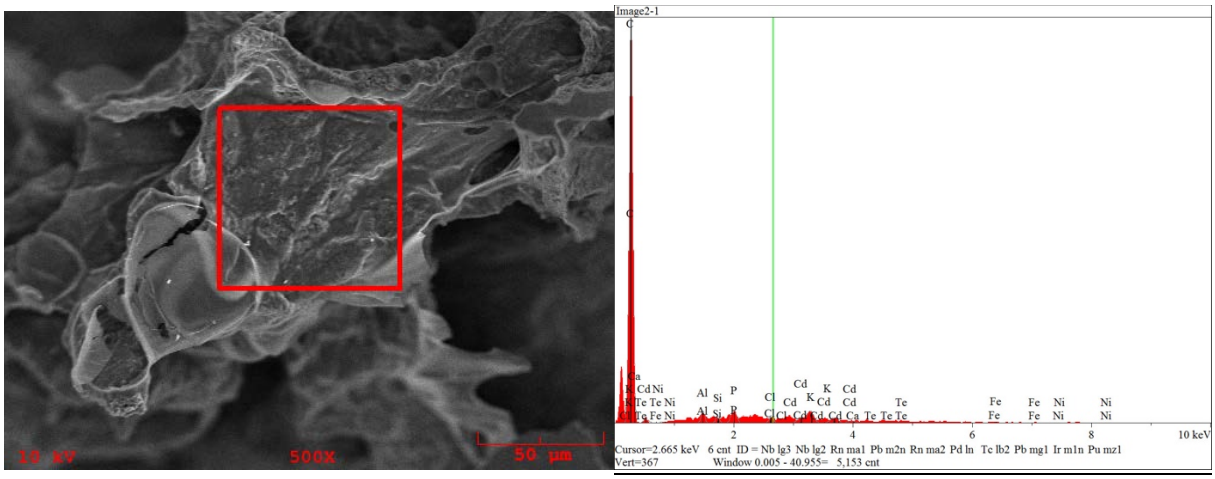

Figure 5.37: Surface area analysis from refused derived waste biochar- Plastic region (Mineral analysis – 5)

Table 5.25: Surface area analysis from refused derived waste biochar- Plastic region (Mineral analysis – 5)

Elt.	Line	Intensity (c/s)	Atomic %	Conc	Units	Error 2-sig	MDL 3-sig
C	Ka	2,822.89	90.827	69.413	wt.%	0.081	0.117
O	Ka	0.00	0.000	0.000	wt.%	0.000	0.000
Al	Ka	90.21	1.024	1.757	wt.%	0.065	0.017
Si	Ka	57.42	0.666	1.190	wt.%	0.071	0.014
P	Ka	144.35	1.764	3.477	wt.%	0.098	0.023
Cl	Ka	65.23	0.911	2.055	wt.%	0.117	0.023
K	Ka	106.19	1.880	4.677	wt.%	0.249	0.046
Ca	Ka	36.27	0.758	1.933	wt.%	0.288	0.040
Fe	La	0.00	0.000	0.000	wt.%	0.000	0.000
Ni	La	12.95	0.295	1.102	wt.%	0.285	0.023
Cd	La	74.12	0.859	6.142	wt.%	0.369	0.061

RDF FUEL *(RAW)

To understand the high concentration of the nickel and Aluminum, the raw RDF fuel was analyzed, and a trace of aluminum and nickel were found from the source fuel. This suggest that part or perhaps most of aluminum mineral found on the biochar may have been as a result of its presence in the original fuel.

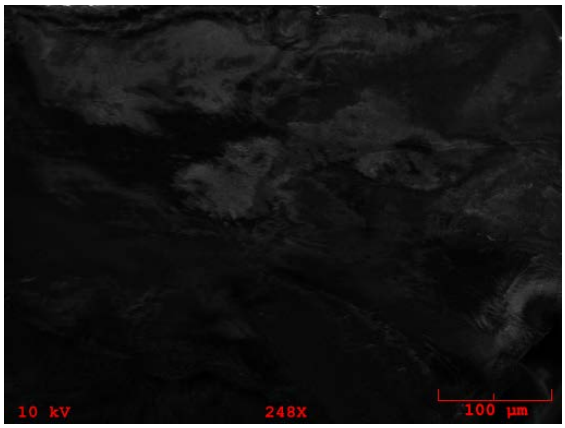

Figure 5.38 Surface area analysis from refused derived (raw) pellet

Table 5.26: Surface area analysis from refused derived (raw) pellet

Elt.	Line	Intensity (c/s)	Atomic %	Conc	Units	Error 2-sig	MDL 3-sig	
C	Ka	4,203.19	63.970	48.704	wt.%	0.041	0.067	
O	Ka	1,929.02	26.215	26.586	wt.%	0.048	0.047	
Al	Ka	996.03	4.442	7.597	wt.%	0.028	0.021	
Si	Ka	224.88	1.043	1.856	wt.%	0.031	0.010	
P	Ka	34.94	0.168	0.330	wt.%	0.038	0.004	
Cl	Ka	15.97	0.086	0.193	wt.%	0.047	0.004	
K	Ka	16.21	0.109	0.270	wt.%	0.064	0.003	
Ca	Ka	17.14	0.132	0.336	wt.%	0.078	0.000	
Fe	Ka	22.96	0.818	2.896	wt.%	0.565	0.000	
Ni	Ka	24.76	3.018	11.231	wt.%	2.111	0.000	
			100.000	100.000	wt.%			Total

6. DOUBLE STAGE SYNGAS AND BIOCHAR RESULTS

The purpose of testing in a two-stage downdraft gasifier is to understand the effect of the more extended thermal equilibrium zone on syngas, char, and tar and to understand whether this zone leads to better results when compared the first stage downdraft gasifier. In this test, miscanthus briquettes were tested, and the resulting syngas, tar, and char are analyzed.

Gas Composition and Analysis

The average syngas contents, obtained at equivalence ratios of 0.2, 0.35, and 0.45, can be seen in Table 6.1

Table 6.1. Syngas composition.

ER	H_2 %	CO%	CH_4 %
0.2	11.2	10.97	1.03
0.35	18.68	20.29	0.86
0.45	17.07	19.43	1.22

Figure 6.1 shows the CO, CH_4, and H_2 concentration content at the equivalence ratio of 0.35. The maximum average syngas content at 0.35 was found to be 20.29% CO, 18.68 % H_2, and 0.86% CH_4. These results agree with others from literature. The gas compositions obtained in the experiment are similar to those in the gasification of Eucalyptus: 19.2 % CO, 17.14 % H_2, and 1.3 % CH_4 [57]. Kallis et al. carried out Miscanthus gasification on a downdraft gasifier with ER values between 0.27 and 0.30, which yielded a syngas composition of 14.26 % CO, 11.29 % H_2, and 1.93 % CH_4 [58]. The results from Kallis et al. (obtained at ER = 0.28) show a smaller percentage in CO and H_2, but a higher CH_4 composition, when compared to our results. This difference could be due to the low ER used.

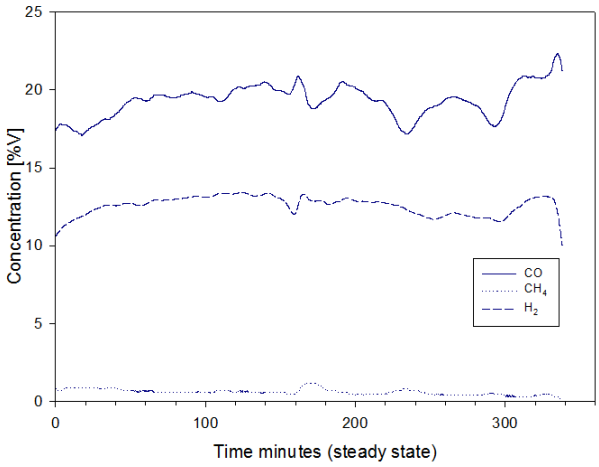

Figure 6.1. Syngas composition at ER 0.35.

Figure 6.2 shows the respective temperatures within the gasifier in a steady state. The measured temperatures may not be precise due to the location of the thermocouples along the gasifier wall. However, this gives a general idea of the temperatures in each zone. The drying and pyrolysis zones correspond (in location) to the primary air inlet, while the combustion and reduction zones correspond to the secondary air inlet.

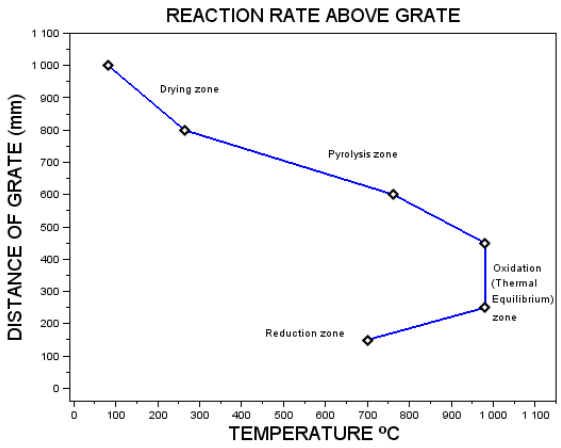

Figure 6.2. Temperature profile in double stage downdraft gasifier at steady state.

As seen in Figure 4, the thermal equilibrium zone is much wider than the temperature profiles obtained in a single stage gasifier such as those listed in [59,60], in which thermal equilibrium is

much smaller. Therefore, the thermal equilibrium zone in the second stage downdraft gasifier is wider and more stable than a single-stage downdraft gasifier.

The amount of biomass consumed in a system every hour is highly dependent on the equivalence ratio of the system [3]. The biomass consumption in this experiment was, on average, 14 kg/hr, with an average airflow of 24 Nm^3/hr.

Biochar analysis

The BET analysis provides a precise surface evaluation of a material by using a gas multilayer adsorption. A Nova 4200 instrument was used to calculate the surface area of the biochar using a nitrogen adsorption method. A degassing temperature of 150 °C was used for a time period of 10 hours. The surface area of Miscanthus biochar was 186.06 m^2/g. Experiments carried out by Cetin et al. [61] found that surface areas of other biochar, such as pine char, range from 236 to 296 m^2/g. Other studies also showed biochar with a surface area of 141 m^2/g to increase water retention and reduce toxic pollutants in fields, such as mines [62].

The Micro-pore volume of the Miscanthus biochar from the double stage downdraft gasifier was calculated using the Dubinin-Radushkevich equation [63]. The biochar was found to have a micro-pore volume of 0.07 cm^3/g. When comparing to other studies [64–58], as seen in Figure 6.3, we see that miscanthus biochar falls in the medium porous region. The biochar with a surface area between 0–100 m^2/g with a micro pore volume between 0–0.05 cm^3/g can be considered to be a low porous region, while those with a surface area of greater than 400 m^2/g (mostly activated carbon) with micro-pore greater than 0.15 can be considered to be in higher porosity region.

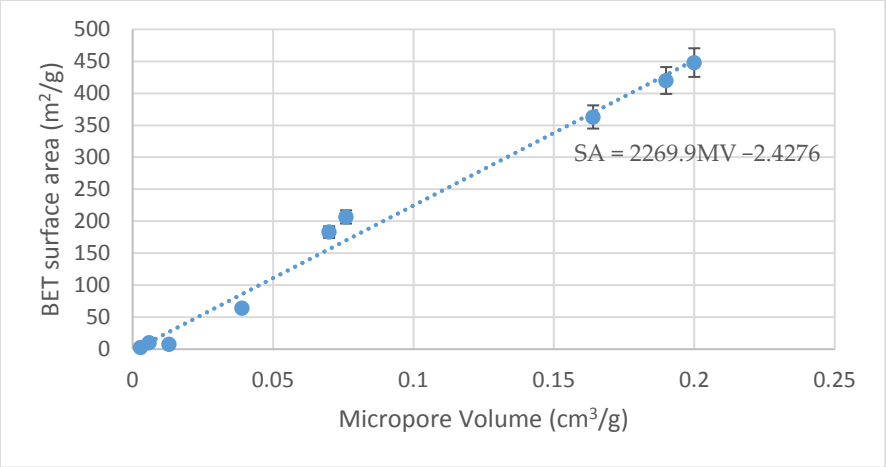

Figure 6.3. Relationship between Biochar surface area and Micropore volume.

Where SA = Surface Area and MV = Micro pore Volume.

Temperature is one of the parameters that affect the surface of the biochar. There are many studies done which look into the general behavior of temperature and biochar surface area. The general trends reported by Lehman et al. [69] as plotted in Figure 6.4a, show that in thermal pyrolysis conditions, the surface area peaks at around 400 m^2/g. For gasification studies in Figure 6.4b [70–72], where the air was used to provide significant heat to the system, the air significantly reduces the porosity at 700 degrees Celsius to a 100 m^2/g. Our data point fills the part of the gap where the biochar temperature is 800 degrees and the data at 950 has a higher porosity, as seen in Figure 6.4b. We see a keen sensitivity to temperature, and that there is a high porosity with significant oxygen and at high temperatures. What is surprising is that at 650 degrees, the amount of porosity reduces significantly.

Although these graphs do not fully contain data from all the studies, they show that a quantifiable relationship can be inferred to predict the surface area of biochar at varying temperatures.

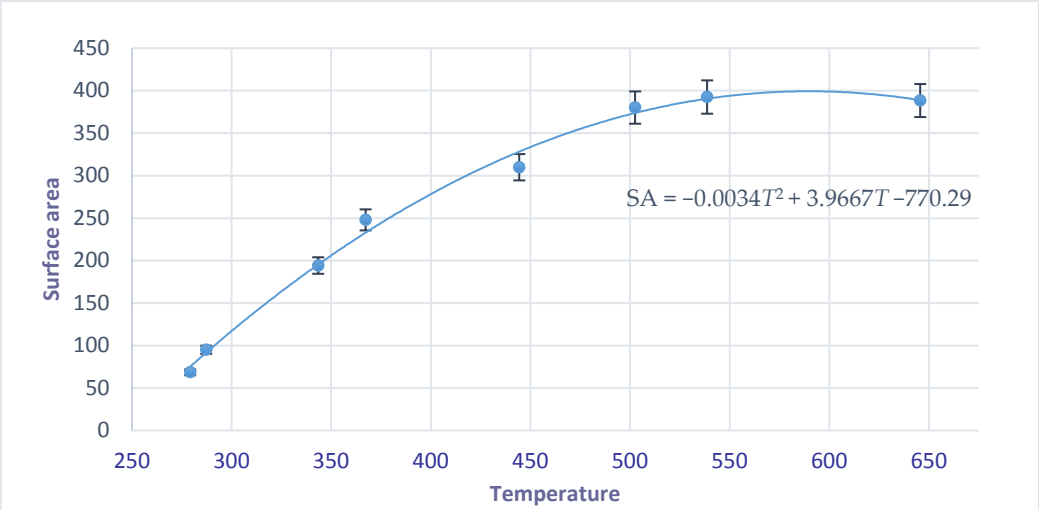

Figure 6.4 (a) Temperature versus surface area under 750 degrees Celsius.

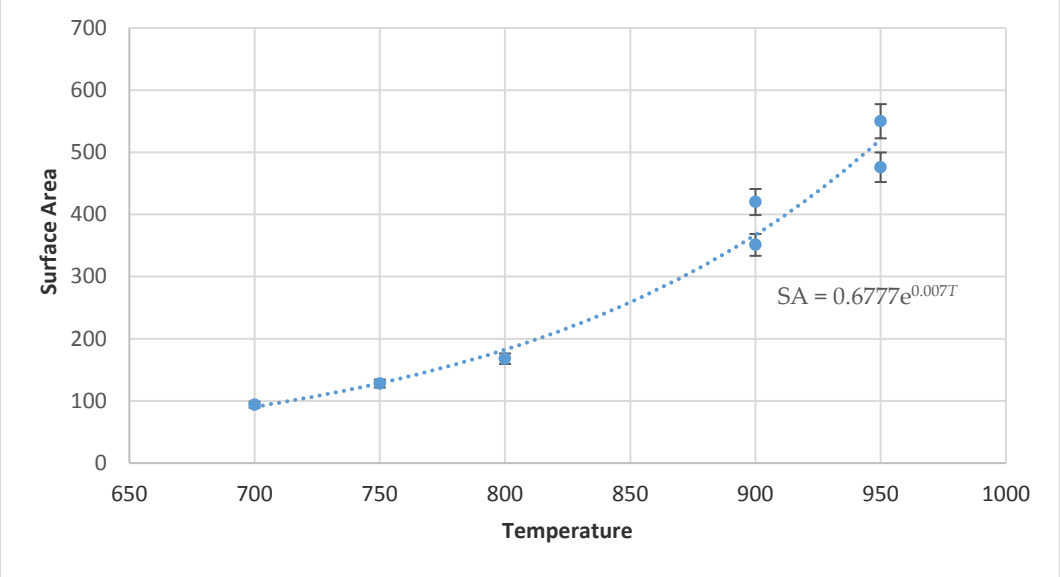

Figure 6.4 (b) Temperature versus surface area above 750 degrees Celsius.

where SA = Surface Area and T = Temperature

To better understand the outer surface structure of the char produced, a scanning electron microscope (SEM) (Hitachi S-4800) was used.

As seen in Figure 6.5, under a magnification of x500 (at 100 µm), little or no pores could be observed on fresh Miscanthus; rather, the biomass appeared to be made up of solid cells strongly bonded together. However, once the biomass underwent the process of gasification, different sizes of pore openings could be observed under the same magnification, as seen in Figure 6.6, where

the cells appeared to be loosely bound. These pores on the surface may be the result of high temperatures within the gasifier. The high temperature in the gasifier leads to the weakening of the cell structure of the biomass [73,74].

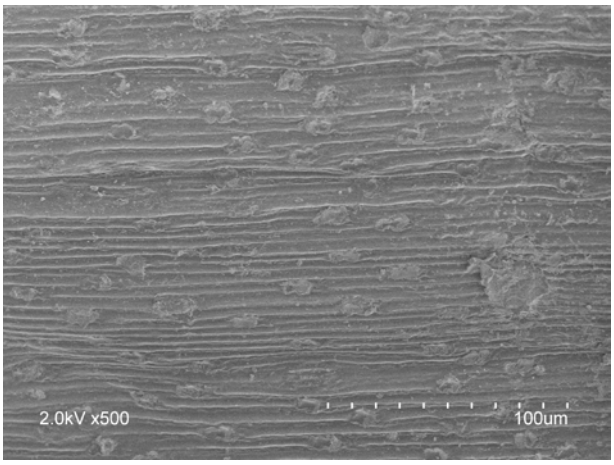

Figure 6.5. Fresh Miscanthus briquettes outer layer at a magnification of x500 (100 µm).

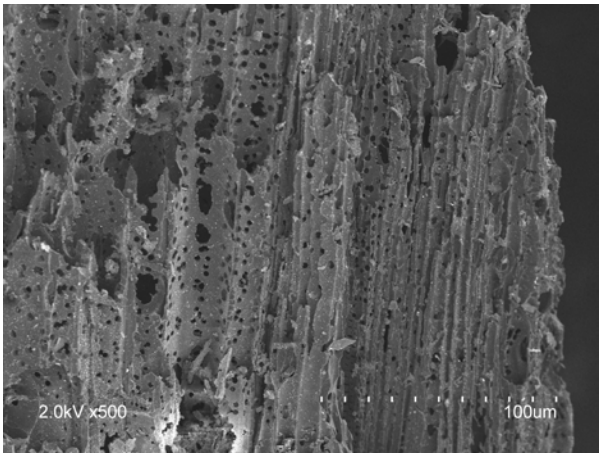

Figure 6.6. Miscanthus char outer layer at a magnification at x500 (100 µm).

Figures 6.7 and 6.8 represent the SEM images of Miscanthus biochar at different locations under a higher magnification of x1 k at 50 µm. It was observed that the pore sizes on the Miscanthus biochar ranged from 2 to 30 µm.

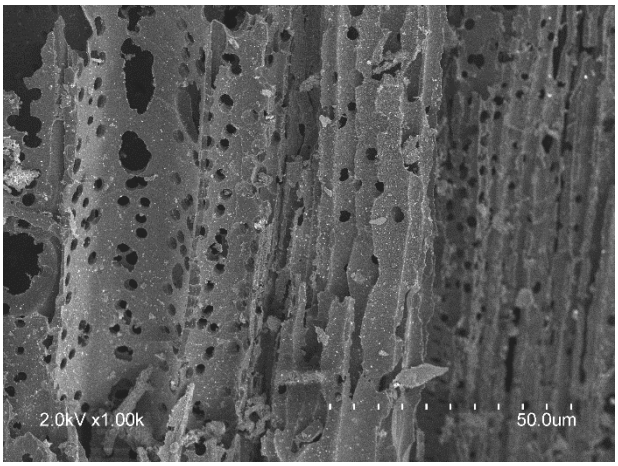

Figure 6.7 Biochar obtained from Miscanthus briquettes gasification at a magnification at x1000 (50 µm).

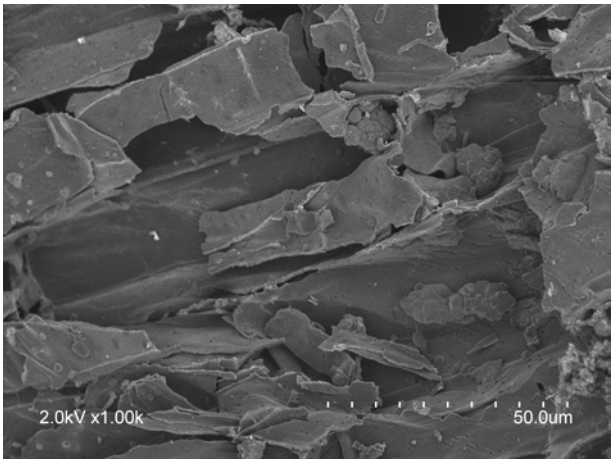

Figure 6.8 Miscanthus char at a magnification of x1000 (50 µm).

The pores on the surface may explain why biochar acts as a useful soil amendment. The pores on the surface of the biochar may enable an increase in nutrient absorption in the soil.

Tar Analysis

To capture the tar, the solid particles from the gas were filtered using a heated particulate filter at 300 °C (module 1), and tar was captured using five of the six impingers which contained isopropanol (module 2) as shown in Figure 6.9. A pump was used to extract the gas. The gas flow rate and temperature were monitored. The sample gas was passed through for an hour at a steady state. The temperature of the isopropanol was kept under 0 °C by using a mixture of salt and water. The cold temperature condensed the tar, which was present in vapor form in the producer gas. The

average amount of tar present after particulate filtering was calculated to be 14.95 mg/Nm^3. This is a popular method of capturing tar [75].

One of the key parameters that affect the amount of tar produced is temperature. In previous studies done by Galindo et al. [57], it was observed that an increase in temperature in the combustion zone leads to a significant decrease in tar content. Figure 6.10 shows a logarithmic relationship between temperature and tar production.

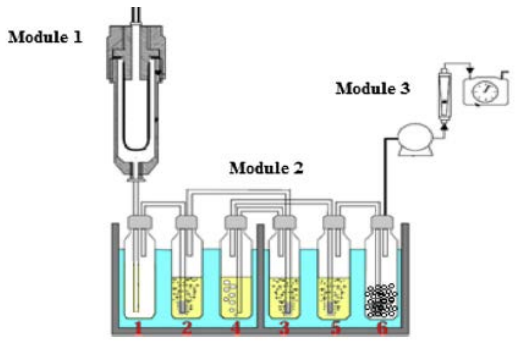

Figure 6.9 Tar collection system.

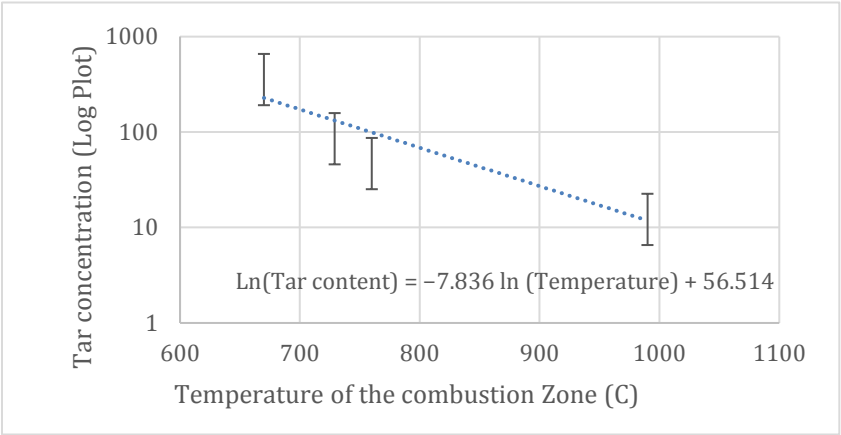

Figure 6.10. Output tar concentration vs. gasifier bed temperature.

The following equations can be obtained:

$$\text{Tar concentration } \left({}^{g}/_{Nm^3}\right) = e^{-7.836\ln(T)+56.14} \quad 6.1$$

which can be reduced to

$$\text{Tar concentration } (g/Nm^3) = \frac{3.49718 * 10^{24}}{T^{7.836}} \quad 6.2$$

where *T* is the temperature in °C in the combustion zone.

According to a study done by Basu, the limits of allowed tar content in producer gas for a gas turbine operation range from 0.05 to 5 mg/Nm^3 [3], while internal combustion engines are limited to 50–100 mg/Nm^3 [76]. Tars can condense in an internal combustion engine which can lead, in the long run, to damage in internal combustion engines [77-79]. The tar content from this study is relatively lower than the limits for a gas turbine and internal engine. As such, the syngas from the gasifier can go through minimal cleanup before been inserted to an internal combustion engine. This, in practice, could save some financial costs when converting syngas to other forms of energy.

From this study, it can be concluded the two-stage gasifier led to better syngas and higher biochar porosity. In the two-stage gasifier, there is a better ability to control oxygen entering the system. The syngas produced has a higher energy content, and the high biochar porosity is also a result of the broader thermal equilibrium zone present.

The optimum ER at which Miscanthus briquettes can be gasified in a double-stage downdraft gasifier is 0.35. This ER produced the highest content of CO and H_2 at 20.29% CO and 18.68% H_2, which yielded the maximum syngas heating value content of 5.5 MJ/Nm^3. The surface area of Miscanthus biochar from the double stage downdraft gasifier was found to be 186.06 m^2/g, and volume pore surface area was calculated to be 0.07 cm^3/g. We found that the biochar from the double stage gasifier could be considered to fall within a medium porosity area, while those with higher volume and surface area such as activated biochar may be categorized as having a high porosity area. The structure of the biochar was also studied and the pores were examined. These pores, once immersed in the soil, absorb nutrients which enables plants to grow. By comparing our biochar data with those of other authors, we find that the biochar's volume pore increases with an increase in surface area. A relationship between biochar properties and the temperature was also

found. With reference to other studies, a predictive model could be used to approximate the surface area of biochar. Further studies on a specific gasifier would have to be done to fully validate this model. The average amount of tar present after particulate filtering was calculated to be 14.95 mg/Nm^3. The amount of tar produced in a downdraft gasifier is much lower than the single stage gasifier. We see that a relationship between temperature and tar can be obtained, and can be used to predict the amount of tar formed.

7. SUMMARY AND CONCLUSION

An extensive analysis was carried out on syngas and biochar output from gasification under various conditions with various fuel. The syngas results were found to align well with results from previous studies. Material with a high amount of lignin led to higher hydrogen content whereas the feedstock with high amounts of cellulose led to a higher amount of carbon monoxide content.

For the biochar, we see that corn biochar had a high percentage of phosphorus and potassium elements with no metal content. Soy biochar followed a similar trend, but traces of iron and nickel were found. Wood biochar had mixed regions with some regions showing high potassium and calcium content with no iron or nickel traces while other areas showed traces of iron and nickel with concentrations lower than 3%. Refused derived waste showed greater differences. Some regions of the char showed a high concentration of aluminum with traces of potassium and phosphorus. A further test in the initial RDF (uncooked) sample also showed a similar trend with a significant percentage of aluminum present. Wood biochar was found to be the most porous biochar with the highest amount of carbon present while RDF had the lowest surface area with the lowest amount of carbon present in it.

For the two-stage gasification results, the surface area of Miscanthus biochar from the double stage downdraft gasifier was found to be 186.06 m^2/g, which is significantly higher than that of biochar from the single stage. Single stage downdraft gasifiers produce char with a surface area less than 64 m^2/g. The equilibrium condition in two-stage gasifier leads better char porosity which is essential for absorbing nutrients to enable plants to grow. By comparing our biochar data with those of other authors, we find that the biochar's volume pore increases with an increase in surface area. A relationship between biochar properties and the temperature was also found. Similarly, if

one could find a relationship between syngas content, biochar production, and tar, this would help to optimize the double-stage downdraft gasifier system.

8. FUTURE WORK

In this thesis, we observed several results involving the dispersion of mineral elements in biochar and its relationship to the pores surrounding it. The concentration of the minerals (both metal and nonmetal) appear to follow a pattern and the products are formed as nodules. The mineral elements in the biochar could open new avenues of research not only related to gasification but also in biochar field testing, and biochar mineral mining and extraction.

The minerals deposit on the char appears to be because of the condensation of tar present in the syngas on the biochar as it exits the gasifier. These minerals deposits vary from phosphorous, potassium, calcium to elements such as cadmium and aluminum. The finding leads to some future testing that could be carried out in a gasifier.

The amount of tar content produced from the gasification process could further be tested. The amount of tar produced by different fuels may vary, and although the amount of tar produced from a downdraft gasifier is the lowest among other types of gasifiers, quantifying the amount of tar produced from different fuels would help undermine issues such as clogging in a combustion engine. A next step would be to use isopropanol and impinger bottles to capture the amount of tar produced.

Another future area of research is regarding the mining and extraction of minerals present in the biochar. Minerals such as aluminum, calcium, Iron, and other elements found in the biochar could carefully be extracted from the biochar for further use. Such as extraction process may require grinding the biochar, and the remaining carbon present, in addition to potassium and phosphorous (which are known to present in fertilizers) could be used for further field and soil testing.

Fuel pellets which contain a higher percentage of plastic could also be tested. The RDF pellet used in this experiment only held 35% plastic. Further fuels pellets containing between 25 - 75% plastic

could be examined to understand and quantify the variation of mineral nodules produced on the resulting biochar.

In conclusion, some of the results observed in this thesis lead to further questions and possible research possibilities in other fields such as environmental engineering and sustainability. Further heating tests using a pyrolizer could also be done on the biochar to increase their surface area. An increased surface area could lead to applications such as in air filters and lead to an increase in the amount of nutrients held in the soil. The downdraft gasification process could also be applied to several real-life applications. If the percentage of plastic in pellets could be increased, it could lead to further studies such as testing plastics from the oceans and converting them into clean energy. In times of hurricanes, the biomass residue left could be converted to pellets and briquettes to be used for short term power supply utilizing the syngas and its combustion in a boiler. These real-life applications would not only lead to interdisciplinary collaboration but could also lead to bettering the lives of people.

Appendix A.1: Lignocellulosic constituents of some biomasses. [31]

Lignocellulosic residues	Hemicellulose (%)	Cellulose (%)	Lignin (%)	Ash (%)	Reference
Nut shells	25–30	25–30	30–40	NA	[31]
Corn Cobs	35	45	15	1.36	
Paper	0	85–99	0–15	1.1–3.9	
Rice Straw	24	32.1	18	NA	
Sorted Refuse	20	60	20	NA	
Leaves	80–85	15–20	0	NA	
Cotton seeds Hair	5–20	80–95	0	NA	
Waste paper from chemical pulps	10–20	60–70	5–10	NA	
Primary wastewater solids	NA	8–15	24–29	NA	
Sugar cane bagasse	27–32	32–44	19–24	4.5–9	
Barley straw	24–29	31–34	14–15	5–7	
Oat straw	27–38	31–37	16–19	6–8	
Rye straw	27–30	33–35	16–19	2–5	
Bamboo	15–26	26–43	21–31	1.7–5	
Rye grass (early leaf)	15.8	21.3	2.7	NA	
Rye grass (seed setting)	25.7	26.7	7.3	NA	
Orchard grass (medium maturity)	40	32	4.7	NA	
Esparto grass	27–32	33–38	17–19	6–8	
Sabai grass	23.9	NA	22.0	6.0	
Elephant grass	24	22	23.9	6	
Bast fiber seed flax	25	47	23	5	
Bast fiber Kenaf	22–23	31–39	15–19	2–5	

Lignocellulosic residues	Hemicellulose (%)	Cellulose (%)	Lignin (%)	Ash (%)	Reference
Bast fiber Jute	18–21	45–53	21–26	0.5–2	
Banana waste	14.8	13.2	14	11.4	
Hardwood stems	24–40	40–50	18–25	NA	
Softwood stems	25–35	45–50	25–35	NA	
Beech Wood	31.2	45.3	21.9	NA	
Spruce Wood	20.7	49.8	27.0	NA	
Walnut Shell	22.7	25.6	52.3	NA	
Almond Shell	28.9	50.7	20.4	NA	
Sunflower shell	34.6	48.4	17.0	NA	
Ailanthus wood	26.6	46.7	26.2	NA	
Hazelnut kernel husk	15.7	29.6	53.0	NA	
Corn Cob	32.32	52.49	15.19	NA	
Corn straw	30.88	51.53	17.59	NA	
Olive cake	21.63	23.08	55.29	NA	
Newspaper	25–40	40–55	18–30	NA	
Swine waste	28	6.0	NA	NA	
Solid cattle manure	1.4–3.3	1.6–4.7	2.7–5.7	NA	
Coastal Bermuda grass	35.7	25	6.4	NA	
Grasses	35–50	25–40	10–30	NA	
Hazelnut shell	29.9	25.9	42.5	1.3	
Hazelnut seedcoat	15.7	29.6	53.00	1.40	
Soft Wood	24.4	45.80	28.00	1.7	
Hardwood	31.30	45.30	21.70	2.7	
Waste Material	29.2	50.60	24.70	4.50	
Tea Waste	19.90	30.20	40.00	3.40	

Lignocellulosic residues	Hemicellulose (%)	Cellulose (%)	Lignin (%)	Ash (%)	Reference
Wood Bark	29.80	24.80	43.80	1.60	
Wheat Straw	39.10	28.80	18.60	13.50	
Corn Stover	30.70	51.20	14.40	3.70	
Tobacco stalk	28.20	42.40	27.00	2.40	
Tobacco Leaf	34.40	36.30	12.10	17.2	
Olive Husk	23.6	24.0	48.4	4.0	
Spruce Wood	21.20	50.80	27.50	0.5	
Beech Wood	31.80	45.80	21.90	0.4	
Ailanthus wood	26.60	46.70	26.20	0.5	
Biomass	20–40	40–60	10–25	NA	
Switchgrass	32.10	37.10	17.20	NA	
Birch wood	25.70	40.00	15.70	NA	
Switch grass	32.10	37.10	17.20	NA	

Appendix A.2: Equipment list (Iowa)

Details on the University of Iowa Pilot scale gasifier located at Oakdale Ag Bio-Power (ABP Model B2 - 2.5MM Btu, 45.5” dia. x 101.5” tall):

* Exterior canister (.25” mild steel, 44” dia. x 60” tall)
* Air/fuel intake cap (.25” mild steel, 24” dia x 15.5” tall)
* Instrument ports above reaction zone (four ½” NPT female)
* High-temp removable 3” sight glass (top-mounted)
* Four-leg stand (4x4x0.5 angle attached, 26” tall to canister)
* Shaft-mounted turntable (.37” stainless, 34.75 dia. x 6.5” wall)
* Vertical driveshaft (1.25” dia. x 74.5”)
* Turntable drive gear-motor (Dayton 2H618)
* Top-mounted adjustable firetube (refractory 24.5” idia – 28.5” odia.)
* Firetube mount shell (.25” mild steel x 47.5”)
* Ash/Char removal auger (4” x 120”) & tray
* Auger drive gear-motor (Dayton 2Z817)
* Airlock (Meyer 4x4 HDX)
* Spockets, chains, mounts, and idlers, as required
* Removable Insulating safety jacket w/embossed metal skin (max 130º OST)
* High-temp paint (basic machine gray)

Control Devices and Instrumentation:

* (1) Wall Mounted, NEMA 4, 36”T x 32”W x 10”D disconnect enclosure containing the following:
* (2) Allen Bradley PowerFlex 70 VFD’s with “Safe-Off” option & Line Reactors for the primary & secondary fuel to Gasifier Augers, with reversible drive capability.
* (4) Motor Starters for Gasifier Platter Drive, Char/Ash Auger, Primary Fuel Flexible Auger, & Secondary Fuel Flexible Auger.
* All terminals, fuses, and circuit breakers needed to control the enclosed devices.
* (1) Wall Mounted (2) Door, NEMA 4, 36”T x 60”W x 12”D enclosure containing the following:
* (1) Allen Bradley ControlLogix PLC(1)
* (1) Allen Bradley Panelview 1500 Color HMI
* (1) Mushroom head E-Stop button and flush E-Stop reset button.
* (1) Horn to indicate critical alarms
* All terminals and power supplies needed to control the Gasifier.
* (1) Remote Thermocouple Termination Enclosure for terminating Data Acquisition thermocouples.
* (2) Load Cell Summing enclosures for weighing of Primary and Secondary Metering Bins. To be located near Metering Bins.
* (1) ABM Guided Wave Radar Level Transmitter for Gasifier Chamber level control
* (1) Air Monitor (air flow) sensor for combustion air intake.
* (6) Allen Bradley Capacitive Proximity Switches for Metering Bin level control.
* (1) 8” Control Damper and Modulating Actuator for combustion air intake to Gasifier. Damper seals rated to 400 Deg F.

* (1) Johnson Gas (natural gas) adjustable power burner (#321) fuel igniter for gasifier (top mounted, 1” natural gas feed, electric flame ignition, fault monitor, Fireye brand flame safeguard)
* Pressure reduction valves, piping, and venting to reduce 120 psi natural gas delivered to the gasifier ignition system at maximum of ½ psi max, 100 CFM
* Electrically modulated air intake damper at gasifier air inlet – controlled by Ag Bio-Power’s Allen Bradley controller.
* Allen Bradley communications module to communicate with Oakdale control system
Syngas Handling Equipment
* Pipe from Ag Bio-Power gasifier to Hurst boiler (24 ga.,10” dia. stainless, 15’ maximum length)
* Removable insulation (max 130º OST, embossed metal)
* Instrument ports (two ½” NPT female)
* Couplings, sealant, supports, as required, up to Hurst-Boiler-provided shutoff valve.

REFERENCES

[1]Sen, S.; Ganguly, S. Opportunities, barriers and issues with renewable energy development—A discussion. *Renew. Sustain. Energy Rev.* **2017**, *69*, 1170–1181.

[2] Basu, P. *Biomass Gasification, Pyrolysis and Torrefaction: Practical Design and Theory*; Academic Press: Cambridge, CA, USA, 2013.

[3] Sharma, T., Yepes Maya, D., M Nascimento, F., Shi, Y., Ratner, A., Silva Lora, E., ... & Vieira Andrade, R. (2018). An Experimental and Theoretical Study of the Gasification of Miscanthus Briquettes in a Double-Stage Downdraft Gasifier: Syngas, Tar, and Biochar Characterization. *Energies*, *11*(11), 3225.

[4] Martinez, J.D.; Lora, E.E.S.; Andrade, R.V.; Jaén, R.L. Experimental study on biomass gasification in a double air stage downdraft reactor. *Biomass Bioenergy* **2011**, *35*, 3465–3480.

[5] Molino, A.; Larocca, V.; Chianese, S.; Musmarra, D. Biofuels production by biomass gasification: A review. *Energies* **2018**, *11*, 811.

[6] Reed, T.B.; Walt, R.; Ellis, S.; Das, A.; Deutch, S. Superficial velocity—The key to downdraft gasification. In *Biomass—A Growth Opportunity in Green Energy*; Overend, R., Chornet, E., Eds.; Pergamon Press: Pergamon, Turkey, 1999.

[7] Peterson, S.C.; Jackson, M.A.; Kim, S.; Palmquist, D.E. Increasing biochar surface area: Optimization of ball milling parameters. *Powder Technol.* **2012**, *228*, 115–120.

[8] Brewer, C.E.; Schmidt-Rohr, K.; Satrio, J.A.; Brown, R.C. Characterization of biochar from fast pyrolysis and gasification systems. *Environ. Prog. Sustain. Energy* **2009**, *28*, 386–396.

[9] Bhandari, P.N.; Kumar, A.; Bellmer, D.D.; Huhnke, R.L. Synthesis and evaluation of biochar-derived catalysts for removal of toluene (model tar) from biomass-generated producer gas. *Renew. Energy* **2014**, *66*, 346–353.

[10] Qian, K.; Kumar, A.; Patil, K.; Bellmer, D.; Wang, D.; Yuan, W.; Huhnke, R.L. Effects of biomass feedstocks and gasification conditions on the physiochemical properties of char. *Energies* **2013**, *6*, 3972–3986.

[11] Sikarwar, V.S.; Zhao, M.; Clough, P.; Yao, J.; Zhong, X.; Memon, M.Z.; Fennell, P.S. An overview of advances in biomass gasification. *Energy Environ. Sci.* **2016**, *9*, 2939–2977.

[12] Son, Y.I.; Yoon, S.J.; Kim, Y.K.; Lee, J.G. Gasification and power generation characteristics of woody biomass utilizing a downdraft gasifier. *Biomass Bioenergy* **2011**, *35*, 4215–4220.

[13] Ravikiran, A.; Renganathan, T.; Pushpavanam, S.; Voolapalli, R.K.; Cho, Y.S. Generalized analysis of gasifier performance using equilibrium modeling. *Ind. Eng. Chem. Res.* **2011**, *51*, 1601–1611.

[14]https://www.netl.doe.gov/research/coal/energy-systems/gasification/gasifipedia/history-gasification

[15] https://www.lowtechmagazine.com/2010/01/wood-gas-cars.html

[16] https://www.epa.gov/renewable-fuel-standard-program/overview-renewable-fuel-standard

[17] Sharma, T. (2015). Gasification and combustion of corn kernels in a pilot scale system.

[18] Sadaka, Samy. "Gasification, producer gas and syngas." (2009).

[19]Reed, T., Reed, T. B., Das, A., & Das, A. (1988). Handbook of biomass downdraft gasifier engine systems.

[20] projects, n. (n.d.). What do we mean by gasification. Retrieved March 22, 2015, from projects.nri: http://projects.nri.org/biomass/conference_papers/gasification_process.pdf

[21] De Cristofaro, E. R. (2009). Gas Evolution from Biomass Gasification and Pyrolysis.

[22]. Ulstad, J. S. (2010). Gas evolution of corn kernels, oat hulls, and paper sludge from biomass gasification.

[23]. Adlhoch, W., Sato, H., Wolff, J., & Radtke, K. (2000, October). Hightemperature Winkler gasification of municipal solid waste. In Gasification Technology Conference (Vol. 8, No. 11).

[24] Sethuraman, S. (2010). Performance of a pilot scale biomass gasification and producer gas combustion system using feedstock with controlled nitrogen content.

[25]. Zwart, R., van der Heijden, S., Emmen, R., Dall Bentzen, J., Ahrenfeldt, J., Stoholm, P., & Krogh, J. (2010). Tar removal from low-temperature gasifiers

[26]. Elder, T., & Groom, L. H. (2011). Pilot-scale gasification of woody biomass. biomass and bioenergy, 35(8), 3522-3528.

[27] Akudo, C. O. (2008). Quantification of Tars and Particulates from a Pilot Scale, Downdraft Biomass Gasifier

[28] Samy Sadaka, P. E., & Eng, P. 1. Gasification.

[29] Roberts, D. G., & Harris, D. J. (2000). Char gasification with O2, CO2, and H2O: Effects of pressure on intrinsic reaction kinetics. *Energy & Fuels*, *14*(2), 483-489.

[30] Phillips, J. (2006). Different types of gasifiers and their integration with gas turbines. *The gas turbine handbook*, *1*.

[31]Saidur, R., Abdelaziz, E. A., Demirbas, A., Hossain, M. S., & Mekhilef, S. (2011). A review on biomass as a fuel for boilers. *Renewable and sustainable energy reviews*, *15*(5), 2262-2289.

[32] Shen, D. K., & Gu, S. (2009). The mechanism for thermal decomposition of cellulose and its main products. *Bioresource Technology*, *100*(24), 6496-6504.

[33] Osada, M., Sato, T., Watanabe, M., Adschiri, T., & Arai, K. (2004). Low-temperature catalytic gasification of lignin and cellulose with a ruthenium catalyst in supercritical water. *Energy & Fuels*, *18*(2), 327-333.

[34] Shen, D. K., Gu, S., & Bridgwater, A. V. (2010). Study on the pyrolytic behaviour of xylan-based hemicellulose using TG–FTIR and Py–GC–FTIR. *Journal of analytical and applied pyrolysis*, *87*(2), 199-206.

[35]Shen, D. K., Gu, S., Luo, K. H., Wang, S. R., & Fang, M. X. (2010). The pyrolytic degradation of wood-derived lignin from pulping process. *Bioresource technology*, *101*(15), 6136-6146.

[36] Yang, H., Yan, R., Chen, H., Lee, D. H., & Zheng, C. (2007). Characteristics of hemicellulose, cellulose and lignin pyrolysis. *Fuel*, *86*(12), 1781-1788.

[37] Hanaoka, T., Inoue, S., Uno, S., Ogi, T., & Minowa, T. (2005). Effect of woody biomass components on air-steam gasification. *Biomass and bioenergy*, *28*(1), 69-76.

[38] Koelsch, R. K., Fabian, E. E., Guest, R. W., & Campbell, J. K. (2001). Anaerobic digesters for dairy farms, agricultural and biological engineering extension bulletin 458. Ithaca, NY: Cornell University, 14853.

[39] Hurst boiler series 200 from- https://www.hurstboiler.com/boilers/scotch_marine/series_200

[40] Energy, c. (2014). clarck energy. Retrieved March 20, 2015, from clarke-energy: http://www.clarke-energy.com/gas-engines/type-2-gas-engine/

[41] electric, G. (2014). GE Power generation. Retrieved March 15, 2015, from https://powergen.gepower.com/plan-build/products/gas-turbines/index.html

[42]. Orr, D., & Maxwell, D. A Comparison of Gasification and Incineration of Hazardous Wastes. Rep. no. DCN 99.803931. 02. Austin, Texas: Radian International LLC, 2000. Web. 9 May 2012.

[43]. Allsopp, M., Costner, P., & Johnston, P. (2001). Incineration and human health. Environmental Science and Pollution Research, 8(2), 141-145

[44]. Arsova, L. (2010). Anaerobic digestion of food waste: Current status, problems and an alternative product.

[45] Koelsch, R. K., Fabian, E. E., Guest, R. W., & Campbell, J. K. (2001). Anaerobic digesters for dairy farms, agricultural and biological engineering extension bulletin 458. Ithaca, NY: Cornell University, 14853.

[46]. Parsons, R. A. (1984). NRAES-20: On-Farm Biogas Production. Natural Resource, Agricultural and Engineering Service. Ithaca, NY.

[47]. Phothilangka, P., Schoen, M. A., & Wett, B. (2008). Benefits and drawbacks of thermal pre-hydrolysis for operational performance of wastewater treatment plants. Water Science and Technology, 58(8), 1547.

[48] Lehmann, J., & Joseph, S. (Eds.). (2015). *Biochar for environmental management: science, technology and implementation*. Routledge.

[49]BIO, A. (n.d.). AG BIO-Power gasification system, model B2-250(R).

[50] Termoquip Energia Alternativa Ltd. *Gaseificador Tipo Co-Corrente com Dois Estágios*; Protocolo de Venda do Equipamento; Termoquip Energia Alternativa Ltd.: São Paulo, Brazil, 2007.

[51] https://www.agmrc.org/renewable-energy/biofuelsbiorefining-general/biochar-a-multitude-of-benefits

[52] Martinez, J.D.; Lora, E.E.S.; Andrade, R.V.; Jaén, R.L. Experimental study on biomass gasification in a double air stage downdraft reactor. *Biomass Bioenergy* **2011**, *35*, 3465–3480.

[53]Burcat, A. *Third Millennium Ideal Gas and Condensed Phase Thermochemical Database for Combustion with Updates from Active Thermochemical Tables*; Argonne National Lab.: Argonne, IL, USA, 2005.

[54]Balu, E.; Lee, U.; Chung, J.N. High temperature steam gasification of woody biomass—A combined experimental and mathematical modeling approach. *Int. J. Hydrog. Energy* **2015**, *40*, 14101–14115.

[55] Diyoke, C.; Gao, N.; Aneke, M.; Wang, M.; Wu, C. Modelling of down-draft gasification of biomass—An integrated pyrolysis, combustion and reduction process. *Appl. Therm. Eng.***2018**, *142*, 444–456.

[56] Han, J., & Kim, H. (2008). The reduction and control technology of tar during biomass gasification/pyrolysis: an overview. *Renewable and sustainable energy reviews*, *12*(2), 397-416.

[57] Galindo, A.L.; Lora, E.S.; Andrade, R.V.; Giraldo, S.Y.; Jaén, R.L.; Cobas, V.M. Biomass gasification in a downdraft gasifier with a two-stage air supply: Effect of operating conditions on gas quality. *Biomass Bioenergy* **2014**, *61*, 236–244.

[58] Kallis, K.X.; Susini, G.A.; Oakey, J.E. A comparison between Miscanthus and bioethanol waste pellets and their performance in a downdraft gasifier. *Appl. Energy* **2013**, *101*, 333–340.

[59]Dogru, M.; Howarth, C.R.; Akay, G.; Keskinler, B.; Malik, A.A. Gasification of hazelnut shells in a downdraft gasifier. *Energy* **2002**, *27*, 415–427.

[60]Guo, F.; Dong, Y.; Dong, L.; Guo, C. Effect of design and operating parameters on the gasification process of biomass in a downdraft fixed bed: An experimental study. *Int. J. Hydrog. Energy* **2014**, *39*, 5625–5633.

[61] Cetin, E.; Moghtaderi, B.; Gupta, R.; Wall, T.F. Influence of pyrolysis conditions on the structure and gasification reactivity of biomass chars. *Fuel* **2004**, *83*, 2139–2150.

[62]Fellet, G.; Marchiol, L.; Delle Vedove, G.; Peressotti, A. Application of biochar on mine tailings: Effects and perspectives for land reclamation. *Chemosphere* **2011**, *83*, 1262–1267.

[63]Nguyen, C.; Do, D.D. The Dubinin–Radushkevich equation and the underlying microscopic adsorption description. *Carbon* **2001**, *39*, 1327–1336.

[64]Sun, L.; Wan, S.; Luo, W. Biochars prepared from anaerobic digestion residue, palm bark, and eucalyptus for adsorption of cationic methylene blue dye: Characterization, equilibrium, and kinetic studies. *Bioresour. Technol.* **2013**, *140*, 406–413.

[65]Cha, J.S.; Park, S.H.; Jung, S.C.; Ryu, C.; Jeon, J.K.; Shin, M.C.; Park, Y.K. Production and utilization of biochar: A review. *J. Ind. Eng. Chem.* **2016**, *40*, 1–15.

[66]Ahmad, M.; Lee, S.S.; Dou, X.; Mohan, D.; Sung, J.K.; Yang, J.E.; Ok, Y.S. Effects of pyrolysis temperature on soybean stover-and peanut shell-derived biochar properties and TCE adsorption water. *Bioresour. Technol.* **2012**, *118*, 536–544.

[67]Chen, B.; Zhou, D.; Zhu, L. Transitional adsorption and partition of nonpolar and polar aromatic contaminants by biochars of pine needles with different pyrolytic temperatures. *Environ. Sci. Technol.* **2008**, *42*, 5137–5143.

[68]Yang, K.; Peng, J.; Srinivasakannan, C.; Zhang, L.; Xia, H.; Duan, X. Preparation of high surface area activated carbon from coconut shells using microwave heating. *Bioresour. Technol.* **2010**, *101*, 6163–6169.

[69] Lehmann, J.; Joseph, S. (Eds.) *Biochar for Environmental Management: Science, Technology and Implementation*; Routledge: Abingdon, UK, 2015.

[70]. Guerrero, M.; Ruiz, M.P.; Millera, Á.; Alzueta, M.U.; Bilbao, R. Characterization of biomass chars formed under different devolatilization conditions: Differences between rice husk and eucalyptus. *Energy Fuels* **2008**, *22*, 1275–1284.

[71] Macias-García, A.; García, M.B.; Díaz-Díez, M.A.; Jiménez, A.H. Preparation of active carbons from a commercial holm-oak charcoal: Study of micro-and meso-porosity. *Wood Sci. Technol.* **2004**, *37*, 385–394.

[72] Ronsse, F.; Van Hecke, S.; Dickinson, D.; Prins, W. Production and characterization of slow pyrolysis biochar: Influence of feedstock type and pyrolysis conditions. *GCB Bioenergy* **2013**, *5*, 104–115.

*[*73]Porbatzki, D.; Stemmler, M.; Müller, M. Release of inorganic trace elements during gasificationof wood, straw, and miscanthus. *Biomass Bioenergy* **2011**, *35*, S79–S86.

[74]. Cetin, E.; Moghtaderi, B.; Gupta, R.; Wall, T.F. Influence of pyrolysis conditions on the structure and gasification reactivity of biomass chars. *Fuel* **2004**, *83*, 2139–2150.

[75] LI, C.; SUZUKI, K. Tar property, analysis, reforming mechanism and model for biomass gasification-An overview. Renewable and Sustainable Energy Reviews, v. 13, n. 3, p. 594–604, 2009

[76]Devi, L.; Ptasinski, K.J.; Janssen, F.J. A review of the primary measures for tar elimination in biomass gasification processes. *Biomass Bioenergy* **2003**, *24*, 125–140.

[77] Huang, J.; Schmidt, K.G.; Bian, Z. Removal and conversion of tar in syngas from woody biomass gasification for power utilization using catalytic hydrocracking. *Energies* **2011**, *4*, 1163–1177.

[78] Han, J., & Kim, H. (2008). The reduction and control technology of tar during biomass gasification/pyrolysis: an overview. *Renewable and sustainable energy reviews*, *12*(2), 397-416.

[79] Bhaduri, S., Contino, F., Jeanmart, H., & Breuer, E. (2015). The effects of biomass syngas composition, moisture, tar loading and operating conditions on the combustion of a tar-tolerant HCCI (Homogeneous Charge Compression Ignition) engine. *Energy*, *87*, 289-302.